

University of Pardubice

Faculty of Transport Engineering

Determination of fouling level change in the railway ballast layer during machine cleaning process by measuring changes of relative permittivity using GPR technology

Borkovcová Anna

Bachelor Thesis

2019

ZADÁNÍ BAKALÁŘSKÉ PRÁCE

(PROJEKTU, UMĚLECKÉHO DÍLA, UMĚLECKÉHO VÝKONU)

Jméno a příjmení: **Anna Borkovcová**
Osobní číslo: **D15562**
Studijní program: **B3607 Stavební inženýrství**
Studijní obor: **Dopravní stavitelství**
Název tématu: **Stanovení změny míry znečištění železničního štěrkového lože při procesu strojního čištění pomocí měření změn relativní permitivity materiálu zařízením GPR**
Zadávající katedra: **Katedra dopravního stavitelství**

Z á s a d y p r o v y p r a c o v á n í :

Na základě opakovaného GPR měření na vybraném železničním traťovém úseku stanovte změnu míry znečištění štěrkového lože před a po procesu strojního čištění. Popište metody měření a vyhodnocení získaných dat. V teoretické části práce popište a zhodnoťte využití GPR pro tyto účely v současné době. Dále uveďte základní principy fungování GPR technologie, popište používaná zařízení a programové vybavení. Práci vypracujte v anglickém jazyce v rozsahu stanoveném vedoucím práce.

Práce bude strukturována přibližně ve smyslu následujícího dělení:

1. Úvod
2. Teorie GPR, způsoby využití GPR na železnici
3. Rešerše literatury se zaměřením na využívání GPR pro diagnostiku stavu štěrkového lože
4. Popis použitého HW a SW
5. Vlastní měření pomocí GPR sestavy KDS
6. Zpracování naměřených dat, tvorba výstupů
7. Doporučení a závěr

Rozsah grafických prací:

Rozsah pracovní zprávy:

Forma zpracování bakalářské práce: **tištěná**

Seznam odborné literatury: **viz příloha**

Vedoucí bakalářské práce:

Ing. Vladislav Borecký, Ph.D.

Katedra dopravního stavitelství

Datum zadání bakalářské práce: **26. října 2018**

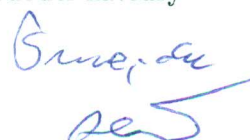
Termín odevzdání bakalářské práce: **21. května 2019**



doc. Ing. Libor Švadlenka, Ph.D.
děkan

L.S.

Ing. Aleš Šmejda, Ph.D.
vedoucí katedry



V Pardubicích dne 29. října 2018

Příloha zadání bakalářské práce

Seznam odborné literatury:

- [1] TILLARD, Sylvie. Analysis of GPR data: wave propagation velocity determination. *Journal of applied geophysics* [online]. 1995, 33(13), 7791. ISSN 0926-9851. Dostupné z: doi:10.1016/0926-9851(95)90031-4
- [2] NURMIKOLU, A a M SILVAST. An inspection of railway ballast quality using ground penetrating radar in Finland. *Proceedings of the Institution of Mechanical Engineers. Part F, Journal of rail and rapid transit* [online]. 2010, 224(5), 345351. ISSN 0954-4097. Dostupné z: doi:10.1243/09544097JRRT367
- [3] HYSLIP, James P., Stanley S. SMITH, Gary R. OLHOEFT a Ernest T. SELIG. Assessment of railway track substructure condition using ground penetrating radar. In: 2003 Annual Conference of AREMA [online]. 2003 [vid. 2014-04-27]. Dostupné z: http://205.252.224.180/files/library/2003_Conference_Proceedings/0010.pdf
- [4] CLARK, M.R. Electromagnetic properties of railway ballast. *NDT & E international: independent nondestructive testing and evaluation* [online]. 2001, 34(5), 305311. ISSN 0963-8695. Dostupné z: doi:10.1016/S0963-8695(00)00006-2
- [5] OLHOEFT, Gray R. a Ernest T. SELIG. Ground penetrating radar: Evaluation of railway track substructure conditions. In: *Proceedings, 9th International Conference on Ground Penetrating Radar* [online]. 2002, s. 4853 [vid. 2014-04-06]. Dostupné z: <http://geo.polymtl.ca/giroux/cours/gml6201a/articles/olhoeft02.pdf>
- [6] INNOTRACK TIP5. Methodology of geophysical investigation of railway track defects - D 2.1.5 GL [online]. Integrated Project (IP). Project No. TIP5-CT-2006-031415. 2006. Dostupné z: <http://www.gimpuls.cz/publikace.html>
- [7] DE BOLD, Robert Paul. Non-destructive evaluation of railway trackbed ballast [online]. Edinburgh, 2011 [vid. 2014-04-05]. School of Engineering University of Edinburgh. Dostupné z: <http://www.era.lib.ed.ac.uk/handle/1842/5027>
- [8] SPRÁVA ŽELEZNIČNÍ DOPRAVNÍ CESTY, S. O. Pokyny pro použití nedestruktivních geofyzikálních metod v diagnostice a průzkumu tělesa železničního spodku. B.m.: G IMPULS Praha spol. s r. o. 2006
- [9] SUSSMANN, Theodore R. Railway track condition indicators from ground penetrating radar. *NDT & E international: independent nondestructive testing and evaluation* [online]. 2003, 36(3), 157167. ISSN 0963-8695. Dostupné z: doi:10.1016/S0963-8695(02)00054-3
- [10] HUGENSCHMIDT, J. Railway track inspection using GPR. *Journal of Applied Geophysics*. 2000, 43(2), 147155.

Další literatura dle doporučení vedoucího práce

Prohlašuji:

Tuto práci jsem vypracovala samostatně. Veškeré literární prameny a informace, které jsem v práci využila, jsou uvedeny v seznamu použité literatury. Byla jsem seznámena s tím, že se na moji práci vztahují práva a povinnosti vyplývající ze zákona č. 121/2000 Sb., autorský zákon, zejména se skutečností, že Univerzita Pardubice má právo na uzavření licenční smlouvy o užití této práce jako školního díla podle § 60 odst. 1 autorského zákona, a s tím, že pokud dojde k užití této práce mnou nebo bude poskytnuta licence o užití jinému subjektu, je Univerzita Pardubice oprávněna ode mne požadovat přiměřený příspěvek na úhradu nákladů, které na vytvoření díla vynaložila, a to podle okolností až do jejich skutečné výše.

Beru na vědomí, že v souladu s § 47 b zákona č. 111/1998 Sb., o vysokých školách a o změně a doplnění dalších zákonů (zákon o vysokých školách), ve znění pozdějších předpisů, a směrnicí Univerzity Pardubice č. 9/2012, bude práce zveřejněna v Univerzitní knihovně a prostřednictvím Digitální knihovny Univerzity Pardubice.

V Pardubicích dne 17.5.2019



Anna Borkovcová

Poděkování:

Mé srdečné poděkování patří panu Ing. Vladislavu Boreckému, Ph.D. za odborné vedení, ochotu, pomoc, cenné rady a trpělivost v průběhu měření, vyhodnocování a zpracování mé bakalářské práce.

ANNOTATION

The bachelor thesis deals with the determination of the fouling level of the ballast layer using GPR technology in dependence on the change in the relative permittivity of the material, before and after the mechanical cleaning process. Repeated GPR measurements of the ballast layer were performed on selected sections of the railway line. After data processing, permittivity changes were determined on selected sections between each survey steps. In conclusion, the relation of the fouling level with the relative permittivity values of railway ballast is described.

KEYWORDS

Ground Penetrating Radar, GPR, signal velocity, relative permittivity, railway ballast fouling

ANOTACE

Bakalářská práce se zabývá stanovením míry znečištění štěrkového lože pomocí georadaru v závislosti na změně relativní permitivity materiálu před a po procesu strojního čištění na vybraném železničním traťovém úseku. Bylo provedeno opakované GPR měření štěrkového lože na vybraných úsecích železniční trati. Po zpracování dat byly určeny změny permitivity na vybraných úsecích mezi jednotlivými fázemi měření. V závěru práce je popsán vztah míry znečištění štěrkového lože s hodnotami relativní permitivity materiálu železničního štěrkového lože.

KLÍČOVÁ SLOVA

Georadar, GPR, rychlost šíření signálu, relativní permitivita, znečištění štěrkového lože

TITLE

Determination of fouling level change in the railway ballast layer during machine cleaning process by measuring changes of relative permittivity using GPR technology

Table of Contents

0. Introduction.....	13
1. Aims of the thesis and methods used.....	14
2. Machine cleaning process on railways	16
3. Ground Penetrating Radar	22
3.1. The principle of GPR	22
3.2. EM characteristics of materials	25
3.3. GPR assembly	30
3.4. GPR data acquisition.....	33
3.5. GPR applications.....	35
3.6. The use of GPR for railway diagnostics	37
4. State of the art research on railway ballast assessment by GPR.....	44
4.1. Ballast fouling mechanism and quantification.....	45
4.2. Fouling assessment of railway ballast using GPR	47
5. Equipment used.....	54
5.1. Hardware	54
5.2. Software	56
6. Experimental Survey.....	59
6.1. Site description.....	59
6.2. In-situ survey.....	65
6.3. Laboratory tests	69
7. Data processing and outputs	77
7.1. Data post-processing	77
7.2. Data interpretation and outputs	80
8. Results and Discussion	83
9. Conclusion	92

Bibliography	97
Annex.....	108

SEZNAM ILUSTRACÍ / LIST OF FIGURES

Figure 1 - RM 79	19
Figure 2 – RM 900 VB	19
Figure 3 - The schematic view of undercutter unit	21
Figure 4 - The basic principle of GPR technology	24
Figure 5 - Emitted and detected radio wave signals by GPR.	25
Figure 6 - Block diagram of the main components of a typical GPR.....	30
Figure 7 - GPR assembly used in this bachelor thesis	31
Figure 8 - Examples of dipole antennas.....	32
Figure 9 - Configuration and representation of an A-scan	34
Figure 10 - Multiple A-scans forming a B-scan	34
Figure 11 - Multiple parallel B-scans forming a C-scan	34
Figure 12 - GPR equipment on railroad track.....	38
Figure 13 - Antenna position in front of the locomotive	38
Figure 14 - Conventional permanent way structure.....	40
Figure 15 - The generation of a GPR profile with an air-coupled antenna over track bed.....	41
Figure 16 - Composite picture showing the survey area and the data	42
Figure 17 - Scheme of effective maintenance using GPR	43
Figure 18 - Track structure components	44
Figure 19 - Ballast with different degree of fouling	46
Figure 20 - GPR test results concerning ballast fouling in revenue service	48
Figure 21 – Description of GPR assembly components	55
Figure 22 - DAD Fast Wave	56
Figure 23 - Interface of K2 FAST WAVE software.....	57
Figure 24 - Interface of ReflexW software	58
Figure 25 - Marking the measured rail crossings on the map.....	60
Figure 26 – Marking of survey sections in the area of railway crossing number 2.....	61
Figure 27 - The railway crossing number 2	61
Figure 28 - Marking of survey sections in the area of railway crossing number 3	62
Figure 29 - The railway crossing number 3	62
Figure 30 - Marking of survey sections in the area of railway crossing number 6	63
Figure 31 - The railway crossing number 6	63
Figure 32 - Marking of survey sections in the area of railway crossing number 8	64
Figure 33 - The railway crossing number 8	64

Figure 34 – Extracting of the probe 1 material (P6U1)	67
Figure 35 – Excavating of the probe 2 material (P2U2).....	68
Figure 36 - Antenna orientation.....	69
Figure 37 - Aggregate sample of fraction 31,5 - 63 from P6U1 section.	70
Figure 38 - Electro-mechanical sieve shakers AS 200 basic	72
Figure 39 - Grain curve for the sample from P6U1 section.....	73
Figure 40 – Aggregate sample of fraction 31,5 - 63 from P2U2 section.....	74
Figure 41 - Grain curve for the sample from P2U2 section.....	76
Figure 42 - Point Mode display in ReflexW	80
Figure 43 - Wiggle Mode display in ReflexW	81
Figure 44 - The change of velocity during lifecycle of the railway track on section P2	85
Figure 45 - The change of velocity during lifecycle of the railway track on section P3	86
Figure 46 - The change of velocity during lifecycle of the railway track on section P6	87
Figure 47 - The change of velocity during lifecycle of the railway track on section P8	87
Figure 48 - Comparison of signal velocity in each section of the first phase	88
Figure 49 - Comparison of signal velocity in each section of the second phase	89
Figure 50 - Comparison of signal velocity in each section of the third phase.....	89
Figure 51 - Comparison of signal velocity in each section of the fourth phase	90
Figure 52 - Comparison of signal velocity in each section of the fifth phase	90
Figure 53 – Comparing individual section of phase 1, 3, 5.....	93
Figure 54 – Velocity (a) and RDP (b) change over depth variation	94
Figure 55 - The grain curve of the railway crossing n. 2 - sample 1	110
Figure 56 - The grain curve of the railway crossing n. 2 - sample 2	110
Figure 57 - The grain curve of the railway crossing n. 2 - sample 3	111
Figure 58 - The grain curve of the railway crossing n. 6 - sample 1	111
Figure 59 - The grain curve of the railway crossing n. 6 - sample 2	112
Figure 60 - The grain curve of the railway crossing n. 6 - sample 3	112

SEZNAM TABULEK / LIST OF TABLES

Table 1 - Conductivity, relative permittivity, and velocity of EM signal.....	26
Table 2 - Categories of Fouling	46
Table 3 - Modeled Ballast Pulse propagation Velocity at Radar Frequencies	49
Table 4 - Published RDP values of ballast	50
Table 5 - RDP values variation with the fouling index	51
Table 6 - Laboratory Estimates of RDP for Single-layer Specimens	51
Table 7 - Field Estimates of RDP	51
Table 8 - RDP values vs dry, saturated and drained ballast	52
Table 9 - Used antenna parameters	54
Table 10 – Total weight of aggregate with percent breakdown	70
Table 11 - Sieve analysis of three samples of fine material from the P6U1 section	71
Table 12 – Average sieve analysis values of fine material from the P6U1 section.....	72
Table 13 - Total weight of aggregate with percent breakdown	74
Table 14 - Sieve analysis of three samples of fine material from the P2U2 section	75
Table 15 - Average sieve analysis values of fine material from the P2U2 section	76
Table 16 – Statistical evaluation of RDP and signal velocity values of stage 3 survey	82
Table 17 - Statistical evaluation of RDP and signal velocity values of stage 5 survey.....	82
Table 18 - Determination of fouling intervals	83
Table 19 - RDP values for each section and survey stage	84
Table 20 - Percentual increase of velocity during the cleaning process	91

SEZNAM ZKRATEK / LIST OF ABBREVIATIONS

1D - One Dimensional	GPR - Ground Penetrating Radar
2D - Two Dimensional	GSSI - Geophysical Survey Systems, Inc.
3D - Three Dimensional	IDS - Ingegneria dei Sistemi S. p. A.
AC - Air-coupled	JTFA - Joint Time-frequency Analysis
AGC - Automatic Gain Control	KDS - Department of Transport Structures
AHM - Excavating unit	KHM - Known Height Method
CMP - Common Mid-point	kph - kilometers per hour
COST - Cooperation in Science and Technology	MIT - Massachusetts Institute of Technology
CRIM - Complex Refractive Index Mode	MTH - Mechanizace traťového hospodářství
ČD - České dráhy a.s.	RADAR - Radio Detection and Ranging
ČSN - Česká státní norma	RDP - Relative Dielectric permittivity
DC - Direct Current	SAW - Recycling unit
DGS - Dynamic track stabilizer	SIM - Control unit with a double three-sided screen
EGU - European Geosciences Union	STFT - Short-time Fourier transform
EM - Electromagnetic	SŽDC - Správa železniční dopravní cesty s.o.
ERDT - Educational and Research Centre in Transport	TEN-T - Trans-European Transport Networks
ERRI - European Railway Research Institute	TÚDC - Technická ústředna dopravní cesty
FTA - Fourier Transform Analysis	twt - Two-way Travel Time
FWD - Falling Weight Deflectometer	US - United States
GC - Ground-coupled	WARR - Wide Angle Reflection and Refraction
GNSS - Global Navigation Satellite System	

ZÁKLADNÍ GPR TERMINOLOGIE / BASIC GPR TERMINOLOGY

- Air-coupled antenna: GPR antenna used with limited offset above the surveyed medium
- Antenna Array: Group of mono- or bi-static antennas working simultaneously
- Antenna: a device which converts electric power into EM waves and vice versa
- A-scan: a curve consisting of amplitudes on the timeline, representing time period between the sending and receiving of the signal
- Attenuation: loss of EM wave energy due to propagation and interaction with media
- Bandwidth: Frequency band defined by the upper and lower frequencies
- Bistatic antenna: the transmitting and the receiving antennas are physically separated
- B-scan: survey line/profile (a series of consecutive A-scans with a certain stationing increment) can be obtained, when the antenna moves at the profile
- Central frequency: the arithmetic mean or the geometric mean of the lower cutoff frequency and the upper cutoff frequency of a band-pass system
- Conductivity: Physical property of a material that describes the ability of its free charges to move in it due to an applied electrical field. It is a frequency dependent property
- Control unit: electronic equipment that controls GPR signal transmission and data collection
- Coupling: the ability of the GPR antenna to transfer electromagnetic energy from transmitter through the surveyed media to the receiver
- C-scan: linking B-scans to a 3D image, recording of such a 3D measurement
- Depth of penetration (range): Maximum depth a radar signal can penetrate and detect a target.
- Dielectric permittivity: physical property of a material that describes the ability to charge or polarize under an electric field. It is a frequency dependent.
- Dipole antenna: a linear polarization antenna consisting of two conductive elements fed at the middle by a balanced source.
- Ground-coupled antenna: GPR antenna designed to maximize the EM coupling with the surveyed medium and to operate in close proximity to it
- Horn antenna: a linear polarization antenna that consists of a flaring metal waveguide.
- Magnetic permeability: physical property of a material that describes the ability of a material to be magnetized.
- Monostatic antenna: the transmitter and the receiver of an antenna are physically the same
- Radargram: 1D, 2D or 3D set of GPR data
- Sample: data point on a trace
- Scattering: phenomenon occurring in a heterogeneous environment, consisting in change of amplitude and direction of electromagnetic waves.
- Survey step: the distance between two adjacent
- Target: heterogeneity in the surveyed media causing scattering or reflection
- Trace: see A-scan
- Two-way travel time: the time required for the radar signal to travel from the transmitting antenna to a target and return to the receiving antenna.

Above-used terminology is based on background literature of COST TU1208 Action - Civil Engineering Applications of Ground Penetrating Radar

0. Introduction

Railways, as one of the most used modes of transport, requires high demands on their maintenance. This maintenance should be performed on the basis of comprehensive and accurate diagnostics. Current diagnostic methods require high financial costs associated with their destructive nature as well as losses caused by traffic constraints and related complications. Requirements of railway infrastructure managers aim to maximize the reduction of diagnostics time and subsequent repairs, in order to maximize the reduction of the related financial costs.

For these reasons, a new, non-destructive form of diagnostics of the railway body, which is the Ground Penetrating Radar (GPR), has recently taken place. This method is still not the most typical way of monitoring the state of the railway body, but it is gradually being applied due to its advantages. These advantages include, in particular, the speed of survey execution and the possibility of continuous measurement of long sections, non-destructive nature, possible depth range, and low transport demands of GPR compared to other types of diagnostics equipment.

GPR use on railways includes the search for watercourses, clogged culverts and other artificial objects, engineering networks, and the actual diagnosis of the condition of railway body construction. The diagnosis of the railway body comprises, above all, railway substructure and the railway superstructure condition assessment. This is the main focus of my bachelor thesis.

Due to cyclic loading and weather effects, railway track ballast gradually deteriorates. When voids in the ballast are filled so-called ballast fouling, i.e. contamination of ballast occurs. This happens when ballast aggregate breakdown and when infiltration of other materials from the ballast surface or infiltration from the base of the ballast layer appears.

To remove fragments and dirt from the ballast, machines called a ballast-cleaners or undercutters are commonly used. These machines perform continuous cleaning of the existing worn material with the possible addition of new fresh ballast. This essential process, followed by tamping, is both costly and time-consuming, therefore it is necessary to accurately determine at what stage of track ballast life cycle, and degree of pollution, is this activity needed and most economically advantageous. To obtain this information, a long-term and repeated monitoring of the track ballast condition is necessary to carry out.

1. Aims of the thesis and methods used

Thanks to my employment at Hrochostroj a.s., the company that is undertaking the reconstruction of the rail superstructure using heavy rail mechanization, I had the opportunity to work directly on the construction sites and get practical experience from this field. In the context of choosing the topic of my bachelor thesis, it was, therefore advantageous to use my employment opportunities and to combine the practice with the research done at the Department of Transport Structures (KDS). Thus, GPR use on the railways was one of the most appropriate options. Then, I have devised and then consulted the specific aim of my thesis resulting from my interest in changing and monitoring the condition of the railway body over the lifetime of the railway track.

Due to the vast majority of professional literature related to the selected topic in the English language and the assumption of publication of thesis results in same language, I chose the English language as the processing language of my thesis.

The bachelor thesis topic was set as:

Determination of fouling level change railway ballast layer during machine cleaning process by measuring changes of relative permittivity using GPR technology

The thesis is focused on the diagnostics of the railway ballast layer condition and the determination of the fouling level change before and after the mechanical cleaning process by measuring the changes in the relative dielectric permittivity (RDP) of the material by the GPR equipment. Before the GPR survey and review the current state of the research, I needed to get acquainted with GPR technology both theoretically and practically (software and practical survey). After these activities, I have set the following partial goals according to the thesis assignment specifications.

Partial goals of the thesis:

1. Implementation of GPR measurements on the ballast layer,
2. Determination of RDP/signal propagation velocity variation before and after the mechanical cleaning process,
3. Description of the relationship between the fouling level and GPR data.

To achieve these goals, I chose the following procedures and methods numbered here in analogy to the partial goals of the thesis:

1. Repeated survey at different stages of the track's life cycle with different antenna configurations and in several sections of a railway line,
2. Time-domain analysis of individual A-scans from each survey phases on each section in ReflexW software using Known Height Method (KHM) for depth/velocity calibration,
3. Comparison of changes in RDP/velocity values before and after the mechanical cleaning process and collation with the literature values and fouling indicators.

2. Machine cleaning process on railways

Cleaning the ballast layer is one of the physically most demanding tasks one can encounter in maintenance and reconstruction process of the railway body. This applies to both manual cleaning and to ballast cleaners (undercutters) operations. The quality of machine cleaning process affects the quality of maintenance and reconstruction itself directly and to a great extent. It is, therefore, necessary to assess the cleaning process of the ballast layer in a complex way, not just in terms of cleaning operation itself. This complex process involves gravel extraction, choked places treatment, ballast cleaning operation itself, controlled reuse and settlement of aggregate under sleepers, cooperation with the spent ballast disposal unit, as well as track grid fixing. This all leads to an increase of a track speed in terms of track geometry for more than 30 km/h. Nowadays, in the framework of reconstruction and maintenance, considerable attention is being given to undercutters' characteristics and performance. The demands in terms of machine performance, their ergonomic and environmental parameters, simple maintenance demands, and above all reliability associated with quality of the cleaning process are raising constantly, and are sought-after parameters in this industry. The same can be stated about the weight and dimensions of the machines and their traction properties.

In history, the Czech Republic, or the Czechoslovak Socialist Republic, was one of the key states producing heavy rail mechanization. MTH (in Czech „Mechanizace traťového hospodářství“, translated like the mechanization of the railway truck economy) Praha company has been producing undercutters since 1966. It is important to mention that the MTH company production had a significant impact on the Czechoslovak economy by the manufacturing the rail mechanization. Nowadays, the market with undercutters in Europe is taken over by the Austrian company Plasser & Theurer, which is also the main developer of other heavy-rail machinery. A new trend is to connect the undercutters together with other machinery to the line assemblies, i.e. one massive machine, and thus significantly speeds up the work.

Machine cleaning process

The ballast layer has to meet certain requirements for track operations, such as uniform load bearing capacity, high resistance to longitudinal and transversal sleepers' displacement, simple track geometry adjustment, track flexibility and water drainage (which affects, for example, sleeper durability or bearing capacity). This is closely related to the ballast/blanket-layer interface, which is also required to have a sufficient load bearing capacity, sufficient frost

resistance, the ability to prevent fine particles from entering the ballast layer and proper drainage of the bottom of the rail body (which is achieved by track bed shape and geometry).

The cause of ballast layer contamination is proportional to the exceedance of fine particles (up to 22.5 mm), dynamic forces and consequent mechanical grinding of the ballast layer aggregate, blow dirt, traffic pollution, tamping and sleepers packing. All these factors result in water throughput limitation, reduction the internal friction, uneven settlements (vertical defects), increase of stress in ballast layer and the formation of choked places due to fine particles penetration into the surface of the track bed.

The purpose of the ballast layer cleaning is to remove fine grain particles and to restore the ballast layer proper characteristics. It is important to note, that the fouling material generated by the capillary action of watery underlying bed cannot be removed by cleaning process in long term, but only by increasing the bearing capacity of the railway substructure.

According to European Railway Research Institute (ERRI) the ballast layer cleaning process should be performed when fouling reaches approximately 30 % of the ballast layer material total weight, in the case of the partial replacement of sleepers, or during the reconstruction of the rail superstructure (before replacing the track grid to prevent its deformation). According to [1], the ballast cleaning process is applied in the interval of 12 to 15 years on a typical intensively operated main line and is undertaken only in connection with other major treatment. In real conditions, it's based on the subjective decision of district inspector. When planning the cleaning process, it is important to set up a work schedule in the following order:

- to determine the fouling level,
- to check the throughput of the excavating equipment (width, thickness, obstacles, bridges),
- to assess the superstructure condition - to ensure the holding of fasteners,
- to determine the direction of work and to restore drainage function,
- to determine the method of removing spent ballast and determine waste deposits,
- to determine the amount of aggregate for profile renewal,
- to develop a technical procedure,
- remove the track earthing,
- to dig the ditch (1 m x 0,3 m) to insert the excavating chain.

Work activities should not start in a transition curve or at the rail joint. Elevation transition as a work starting point, bridges, and work ending point, should be specified. No other parts of the track, such as trails, drainage, traction lines, cables, can be damaged. Spent ballast must not be deposited on the slopes of the track body and near drainage ditches. In case of inappropriate weather conditions, the work efficiency should be checked, in particular, the quality of the cleaning, the depth of excavating, lifting bar inclination and the quality of the new additional aggregate.

The finishing works include the removing the excavating equipment, adding aggregate for profile renewal, assessing the change of the fastening temperature on the continuous welded rail and its repair, attaching the dismantled equipment, disposing of the waste, modifying the track geometric parameters, tamping and other activities. After three months, the geometric parameters of the track have to be re-adjusted due to settlement.

The cleaning process itself consists of inserting an excavating chain beneath the sleepers. This chain extracts the aggregate from the ballast layer to a depth of up to 350 mm below the sleepers (track bed). Extracted material passes through sieves and screens, where the high-quality material is cleaned and returned back to the ballast layer. Spent material is transferred to MFS wagons that transport the material to landfills.

Undercutter types and their division

For the Czech Republic or Czechoslovakia, MTH Praha a.s., which has been developing machines for heavy rail mechanization since 1965, was the major representative for the production of undercutters. Since that year, more than 140 undercutters have been produced and more than 80 units have been produced in the cooperation for Russian railways (until 2015). Other Czech undercutters (namely SČ 600) were also exported to Canada or Croatia. Among the models produced in Czechoslovakia also SČ 100, SČ 200, SČP 200, DELČ 800, SČ 600 S, SČ 800. SČ 1200 and others can be listed.

Nowadays, the undercutters are produced by the Austrian company Plasser und Theurer, the Loram company (US), Matisa Paganelli company (Italy) and others. The undercutters can be divided regarding dry and wet cleaning mode, and according to the number of fingers on the excavating chain. The most frequent are units with the five-fingers excavating chain, which was also employed on the RM 79 unit - the undercutter used on picked railway track section Čáslav-Kutná Hora. The second undercutter used was the new RM 900 unit with three-fingers

excavating chain, which worked in the opposite direction. Above mentioned undercutters can be seen in Figure 1 and Figure 42.



Figure 1 - RM 79 used on railway track section Čáslav – Kutná Hora [2]



Figure 2 – RM 900 VB used on railway track section Kutná Hora – Čáslav [2]

RM 79 is a 100t Plasser und Theurer unit with a length of 28,120 meters, a height of 4,100 mm and a width of 3,150 mm with six axles and a maximum towed speed of 90 km/h. The height of the working shot is from 30 to 40 cm below the sleepers and the actual performance is up to 130 m / hour. When fully excavating, the maximum performance is in between 50 and 70 m / h.

The RM 900 VB Plasser und Theurer unit is now being used as one of the most efficient units. It is equipped with sound-absorbers and other devices, easing the arduous work on these machines. It is used on the railway track at the same time together with a tamping machine and a dynamic stabilizer. The depth of ballast excavation under the sleeper is 35 cm. When integrating all components of the RM 900 VB, the track can be used immediately with the speed up to 30 km/h.

Other undercutters' characteristics:

- **SČ 600** concept: a basic unit for full excavating,
- **RU 800 RU** concept: unit for full excavating, but also for the large stones separation, the base layer building from gravel, crushed stone mixture and sandy gravel
- **SUR 1200 RU** concept: unit for full excavating, large stones separation, and the use of a fine fraction to form a base layer.

Machinery components

In general, the undercutters consist of several components listed here according to the direction of machine work: the network units (SIM), the coarse grinder and the crushing plant (SAW), the AHM excavating unit, in which the aggregate is extracted from ballast layer by the excavating chain (also for undesired fraction removal and for surface of the track bed compaction. In the AHM section, ballast backfilling and compaction behind the sleepers' heads is also performed. In the last section, there is a propulsive car with a sweeping device, a tanker or a measuring car and an integrated DGS device.

When removing fouled aggregate, the MFS wagons are attached in front of the sieve unit (SIM), according to the direction of the work, to capture the excavated aggregate and to transport it to the predetermined landfills, from which the material is removed subsequently.

Schematic view of undercutter unit can be seen in Figure 3,

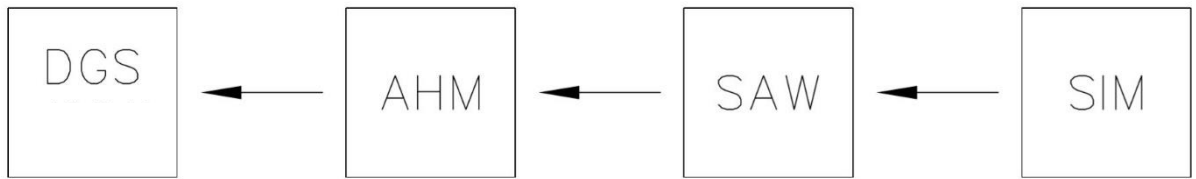


Figure 3 - The schematic view of undercutter unit

where,

SIM means control unit with a double three-sided screen, with the possibility of aligning the machine frame on the overhung tracks,

SAW means recycling unit (rough sorting and grinding machine),

AHM means excavating unit,

DGS means dynamic track stabilizer.

3. Ground Penetrating Radar

The word RADAR is an acronym created in the 1930s for Radio Detection and Ranging. Ground Penetrating Radar, as a special type of radar device, has been in use for about 50 years in order to diagnose and monitor the subsurface and building materials. [3, 4].

The existence of the electromagnetic (EM) waves used by the radar was first described by James Clerk Maxwell (1831-1879) in 1861. The history of exploring the principle of propagation and reflection of these waves dates back to the late 19th century when Heinrich Hertz (1857-1894) carried out first experiments. Hertz verified the EM theory published in the „Treatise on Electricity and Magnetism“, by James Clerk Maxwell, 1873. In 1887, Heinrich Hertz successfully developed an elementary transmitter and receiver. He found out that EM waves could be transmitted through different types of materials and were reflected by others. [5], [6].

The first "modern" GPR was developed in the 1960s at the Massachusetts Institute of Technology (MIT) [7]. In 1972, Geophysical Survey Systems, Inc. (GSSI) company (Rex Morey and Art Drake) began to sell the first commercial GPR system at all, which marked the beginning of rapid development (during 20 years of development, about 300 types of device were patented). In the mid-1990s, there was a massive expansion of GPR technology and the rise of many hardware and software providers [8]. Thanks to improvements in the hardware and software technology, there has been lately a boost in GPR applications all over the world [3].

3.1. The principle of GPR

The basic physics of EM fields, generated by GPR is described by Maxwell's equations, while constitutive equations quantify material properties. Combining the two allows the quantitative description of GPR signals [9]. The spatially and temporally varying coupled electric and magnetic fields and their interdependence are described by equations 1-4. [10]

$$\nabla \times \mathbf{E} = - \frac{\partial \mathbf{B}}{\partial t} \quad (1)$$

Maxwell's modified circuit Law:

$$\nabla \times \mathbf{H} = \frac{\partial \mathbf{D}}{\partial t} + \mathbf{J} \quad (2)$$

Gauss' theorem in electrostatics:

$$\nabla \cdot \mathbf{D} = \rho \quad (3)$$

Gauss' theorem in magnetostatics:

$$\nabla \cdot \mathbf{B} = 0 \quad (4)$$

where

E is electric field strength vector [V/m],

H is magnetic field strength vector [A/m],

D is electric flux density vector [C/m²]

The relevant material property parameters of permittivity, magnetic permeability and conductivity are described by the constitutive relations equations. 5-7,

$$\mathbf{D} = \epsilon \mathbf{E} \quad (5)$$

where ϵ is permittivity of the material [F/m],

$$\mathbf{D} = \sigma \mathbf{E} \quad (6)$$

where σ is conductivity of the material [S/m],

$$\mathbf{B} = \mu \mathbf{H} \quad (7)$$

where μ is permeability of the material [H/m].

GPR itself detects objects and interfaces beneath the earth's surface. By using a GPR, any object that has different EM properties compared to surrounding material can be detected. The size, shape and location, and possibly inherent material of this object can be also determined. A radar record is generally called a radargram.

GPR system uses discrete pulses of EM energy in order to detect variations of electrical properties of the subsurface with a frequency range from 10 MHz to 2,5 GHz for impulse systems and from 1 to 8 GHz for stepped-frequency systems [11]. This way it is possible to reveal the positions and sizes of electrically dissimilar layers and objects [12]. When the impulse reaches the interface of two materials with different EM properties, part of the energy is reflected back, while the remainder continues deeper into the material or construction. Such places, called anomalies, could be for example changes in soil layers, groundwater surfaces, or buried objects [4]. The energy reflected by these anomalies is received, recorded and displayed as a curve consisting of amplitudes on the time line (called A-scan) representing time period between the sending and receiving of the signal. This time period [ns] is called two-way travel time (twt) [8]. On the basis of knowledge of EM wave velocity, travel time can be

transformed into penetration depth [4]. The basic principle of GPR technology on multiple layers medium, as described above, is illustrated in Figure 4.

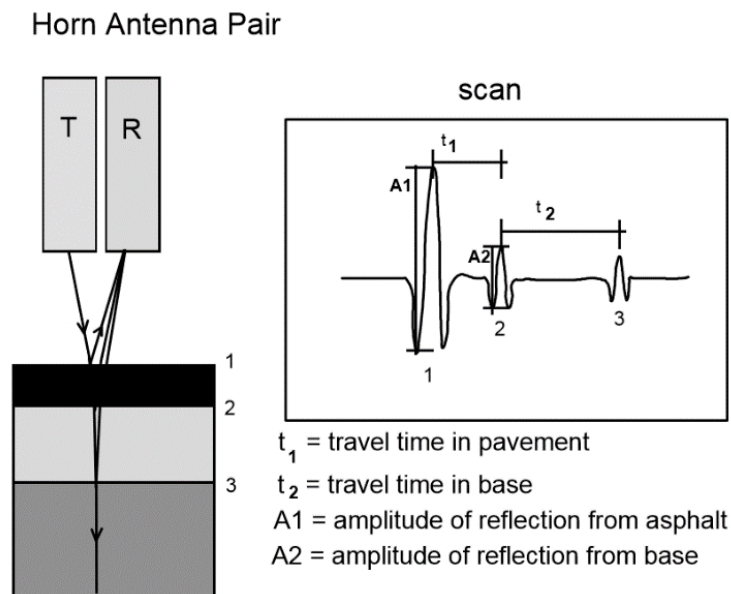


Figure 4 - The basic principle of GPR technology –[12]; T-transmitter, R-receiver, 1 – air/asphalt interface, 2 – asphalt/base course interface, 3 – base course/subgrade interface, A - amplitude, t – time

The reflected signal includes information of the material in the form of twt, amplitude shape, and polarity of the received signal [13]. Changes in the parameters enable to reveal information of the material, the distance of the reflector, signal velocity through the medium and attenuation characteristics. Based on this information, material properties can be estimated [13].

Signals can travel from a transmitter to a receiver along a number of paths. Measured GPR data consist of (as can be seen in Figure 5): direct coupling or ground coupling, surface reflections, stochastic EM interference (from the GPR system or the environment), reflections from subsurface targets, scattered or reflected signals from non-homogeneous signals [14]. To selectively enhance some signals and suppress others, so-called shielding is applied to the antennas. Key shield design objectives are, as follows [15] :

- maximize the energy on the path AA' to and from the subsurface target (i.e. focus or direct signal downward),
- minimize the direct transmitter to receiver energy on path B,
- minimize the energy that escapes into the air as on path CC',
- minimize external EM noise as indicated by signals D.

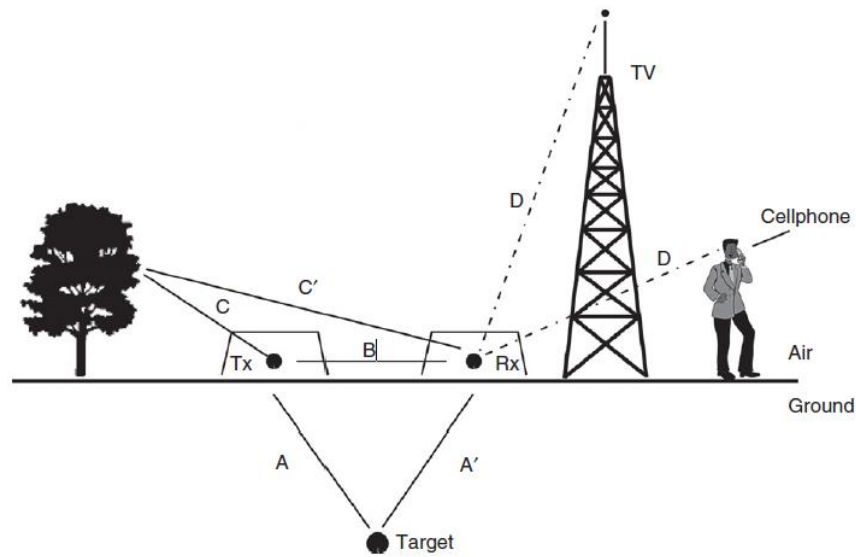


Figure 5 - Emitted and detected radio wave signals by GPR [15]

The advantage of using GPR is the non-invasive and non-destructive character of this technology that allows large areas to be surveyed in a relatively short time with quite low costs. Despite these benefits, GPR also has some limiting factors [14]:

- Use in non-homogeneous soil can increase the number of false detection and limit range,
- Sensitivity to unwanted signals (interference) caused by different natural and artificial factors,
- Sensitivity to other sources of EM fields,
- The need for data interpretation, based on the experience and knowledge of the trained operator.

3.2. EM characteristics of materials

From the physical gist, the possibilities of GPR use are influenced by the EM properties of the material. It is primarily a relative dielectric permittivity (RDP) ϵ_r , magnetic permeability μ , and electrical conductivity σ .

Relative dielectric permittivity (dielectric constant) ϵ [F/m] describes the ability of the material to store and transmit the electric charge induced by the EM field. RDP of material can be defined as the amount of electrostatic energy stored per volume. In fact, it is a number that indicates how fast radar energy passes through the material [14], [16].

The signal velocity depends on the type of material being passed. The permeability values, along with the velocity and conductivity values for the different materials, are shown below in

. In the open space (air), the permeability value is the same as in a vacuum, according to equation 8.

$$\epsilon_0 = \frac{1}{c^2 \mu_0} \sim 8,85 \cdot 10^{-12} \text{ [F/m]} \quad (8)$$

where c is the speed of light [m/s] and μ_0 is the vacuum permeability [H/m]

Relative permittivity RDP (or dielectric constant) can then be expressed according to equation 9 as:

$$\epsilon_r = \frac{\epsilon}{\epsilon_0} \quad (9)$$

where ϵ is the permittivity of the medium [F/m] and ϵ_0 is the vacuum permittivity [F/m].

Table 1 - Conductivity, relative permittivity, and velocity of EM signal – adjusted from [17]

Material	Relative permittivity	Conductivity [S/m]	Velocity [m/ns]
Air	1	0	0,3
Distillated water	80	0,01	0,033
Fresh water	80	0,5	0,033
Salt water	80	0,003	0,01
Dry sand	3-5	0,01	0,15
Wet sand	20-30	0,1-1	0,06
Limestone	4-8	0,5-2	0,12
Slate	5-15	1-100	0,09
Mud	5-30	1-100	0,07
Clay	5-40	2-1000	0,06
Granite	4-6	0,01-1	0,13
Salt	5-6	0,01-1	0,13
Ice	3-4	0,01	0,16
Permafrost	3-6	-	-
Concrete	4-10	-	-
Metal	1-2	-	-

Although the relative permittivity of individual materials can be obtained in the literature, the complex nature of this parameter in the lossy environment is not taken into account in this procedure [18].

All building materials and soils can be described as composite materials whose relative permittivity values depend on the relative permittivity values of individual components, the volume ratio of the components, geometry, and shape of the components, and on electrochemical interactions between these components. In soils and unbounded building materials, these components are air, water (or snow and ice), mineral aggregates and their weathering products, clays, colloidal particles, salts and organic compounds [12].

The amplitude of the reflected signal depends on the difference between the permittivity of the two adjacent layers. The greater difference is, the greater the amount of energy is reflected from the interface [19]. These differences are often associated mainly with water content, also with changes in texture, lithology, porosity, and density of materials in rocks and soils [17]. In the field of transport engineering interface between structural layers, concrete reinforcement, etc are the most common. The ratio of reflected energy to total emitted energy is called the reflection coefficient (R) and is determined by the GPR signal velocity in both environments by equation 10 [19],

$$R = \frac{V_1 - V_2}{V_1 + V_2} \quad (10)$$

where V1 is signal velocity in material 1 [m/s], V2 is signal velocity in material 2 [m/s].

The reflected wave is approximately sinusoidal, and the amplitudes have alternately positive and negative values. When the electromagnetic wave passes through the material with a relatively low relative permittivity and reaches the interface of the material with a higher relative permittivity, the amplitude has a positive value first. If, on the other hand, it passes through a material with a higher relative permittivity and reaches the interface of material with lower relative permittivity, the amplitude is the first negative. [20], [21]

Magnetic permeability μ [H/m] describes the ability of the material to become magnetized in the presence of an electromagnetic field. It is a measure of magnetic polarization of the material. Magnetically more permeable materials more easily interfere with the magnetic portion of the electromagnetic wave, thereby the wave is weakened, which results in the GPR range limitation [14], [16].

Relative permeability can describe according to equation 11.

$$\mu_r = \frac{\mu}{\mu_0} \quad (11)$$

where μ is permeability of material [H/m] and μ_0 is vacuum permeability [H/m], which can be defined by equation 12.

$$\mu_0 = 4\pi \cdot 10^{-7} \approx 1,256 \cdot 10^{-6} \text{ [H/m]} \quad (12)$$

Based on the relative permeability value, the materials are divided into three groups: diamagnetic, paramagnetic and ferromagnetic. Diamagnetic materials have a relative permeability less than 1 (e.g. copper, silver and gold). These materials have very limited interactions with the external magnetic field. Paramagnetic materials have a relative permeability of slightly greater than 1 (e.g. aluminum, magnesium, platinum) and also show little interaction with the external magnetic field. On the contrary, ferromagnetic materials with a relative permeability of much greater than 1 (e.g. cobalt, nickel, iron) strongly react to the outer magnetic field. These materials are considered lossy and their permeability is dependent on the frequency of the exciting EM field [6]. Asphalt, concrete, and most soils and rocks have a relative permeability of approximately 1, so the effect of this factor in the most GPR applications is neglected [14].

The electrical conductivity σ [S/m], described in equation 13 as the reciprocal value of the electrical resistance, indicates the ability of the material to conduct the electrical part of the EM wave. The signal is able to penetrate through a high volume of low conductivity material (e.g. very dry sand, ice or dry concrete), but if the material is conductive (e.g. salt water or wet concrete), EM energy is relatively quickly absorbed, thus reducing the GPR range. [16]

Electrical conductivity is physical quantity, which described the ability to carry electric current [13], where ρ is electrical resistivity [Ω].

$$\sigma = \frac{1}{\rho} \text{ [S/m]} \quad (13)$$

It should also be noted that the conductivity can be dependent on the frequency used. For example for concrete, the conductivity at 1 GHz is 1.5 times higher than conductivity for direct current (DC) [22].

GPR signal velocity v [m/s] depends on the physical properties of the materials, especially on RDP. It is calculated from the signal travel time, which is the only direct measurement obtained in the field. Based on the above mentioned EM characteristics, the signal propagation velocity in the environment can be described as in equation 14,

$$v = \frac{c}{\sqrt{\mu_r \epsilon_r}} \text{ [m/s]} \quad (14)$$

where c is speed of light in vacuum (approximately 3×10^8 m/s), μ_r is relative magnetic permeability [-], ϵ_r is relative dielectric permittivity [-].

If interactions of the GPR signal with the magnetic field are neglected, the relative EM wave velocity can be computed from equation 15,

$$v_r = \frac{c}{\sqrt{\epsilon_r}} \text{ [m/s]} \quad (15)$$

where v_r is relative EM wave velocity, c is the speed of light and ϵ_r is RDP [23].

From the knowledge of the velocity, the depth of object or interface can be calculated based on equation 16,

$$d = v_r \cdot \frac{twt}{2} \text{ [m]} \quad (16)$$

where d is the depth of the object or interface and twt is the two-way radar travel time to and from the target [23].

The signal attenuation α [dB/m] is then determined according to equation 17 [17],

$$\alpha = 1,69 \cdot 10^3 \frac{\sigma}{\sqrt{\epsilon_r}} \text{ [dB/m]} \quad (17)$$

where σ is conductivity [S/m] a ϵ_r ... relative dielectric permittivity [-].

It follows from the above mentioned, that the signal travels faster through a material with low relative permittivity than in the material that has a higher permittivity. The conductivity of the material governs how quickly the signal is attenuated depending on the distance, and thus determines how deep the wave penetrates the material. These two properties are mostly independent. For example, fresh water and salt water have approximately the same permeability (salt water is slightly lower), but salt water has a much higher conductivity than fresh water.

Thus, in both cases, the GPR signal travels at a similar velocity, but in salt water, the signal is very quickly attenuated and does not penetrate so deep [24].

3.3.GPR assembly

The selection of the GPR assembly depends on the particular application. It is governed by the expected depth and the required detection accuracy. The EM characteristics of the environment, the presence of water, etc. affect the results also. There are many complex characteristics which define a ground penetrating radar system [25]. Among the most important characteristics followings can be mentioned:

- Performance factor;
- Centre Frequency;
- Bandwidth;
- Signal Processing;
- Antenna Patterns.

The GPR system usually consists of the following components [14]. The block diagram of the main components is schematically shown in Figure 6.

- Transmitting and receiving antennas or antenna arrays
- Control (central) unit that generates EM pulses and records the received signals
- Imaging units that provide real-time viewing of measured data
- Voltage sources - batteries (usually 12V), to power the central unit
- Measuring platforms - car, rolling stock, measuring trolley, sleigh, etc.

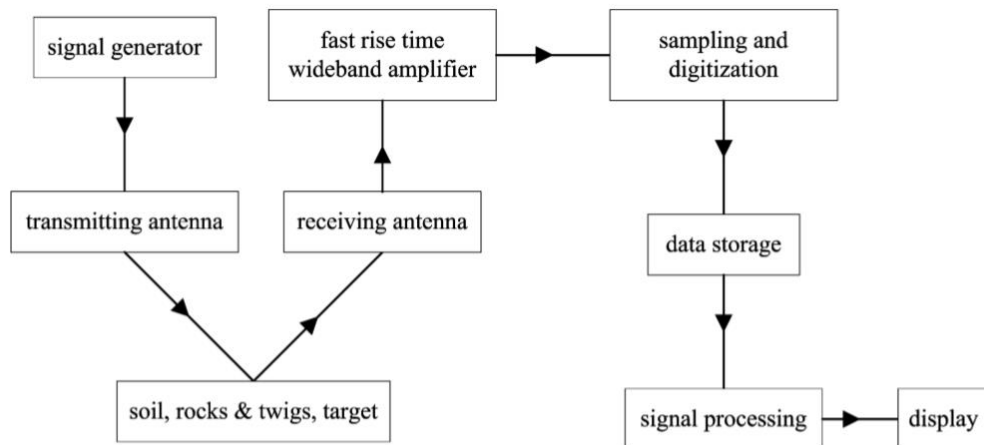


Figure 6 - Block diagram of the main components of a typical GPR [26]

The other components, data and power cables, positioning devices (odometer, Global Navigation Satellite System (GNSS), laser or ultrasonic sensors, camera systems, etc. may be included. Figure 7 shows the GPR assembly used in this bachelor thesis (described in detail in chapter 5).

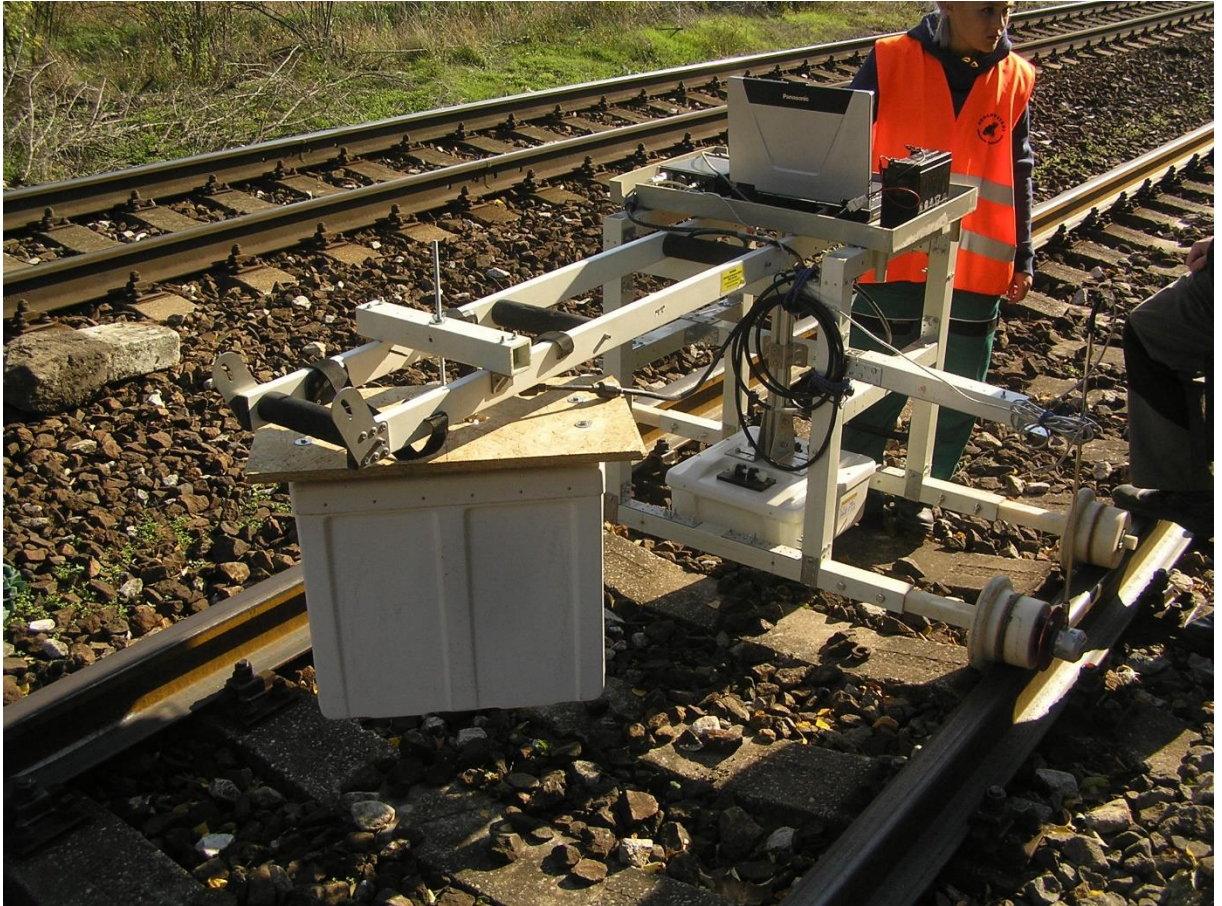


Figure 7 - GPR assembly used in this bachelor thesis

The most important component in the GPR system is the antenna. The size of the antenna increases with the increasing wavelength of the produced EM field. There are monostatic and bistatic systems. Monostatic systems use a common radiating element for transmitting and receiving the signal, while in bistatic antennas, the transmitter and receiver are hosted in the same enclosure [11]. There are also multichannel antennas or antenna arrays where several antennas are used as transmitters and other antennas as receivers [27]. With respect to the generation of waveforms, two types of systems exist, pulse (the most common) and frequency modulated. The most important requirements for antenna construction are high sensitivity and wide dynamic range in order to maximize the usability of GPR so that it can cope with as wide a range of conditions as possible [11].

There are currently many types of antenna constructions (cylindrical monopoles and dipoles, vee dipoles, biconical dipoles, bow-tie, dielectric horn, double-ridged horn, quad-ridged horn, etc.). Some examples of dipole antennas can be seen in Figure 8. The transmitted signal should have a very short duration due to the very short time of the signal path from the transmitter to the receiver (twt). The antenna should be able to transmit a low distortion signal to avoid overlapping the required reflections by noise and interferences.[26]

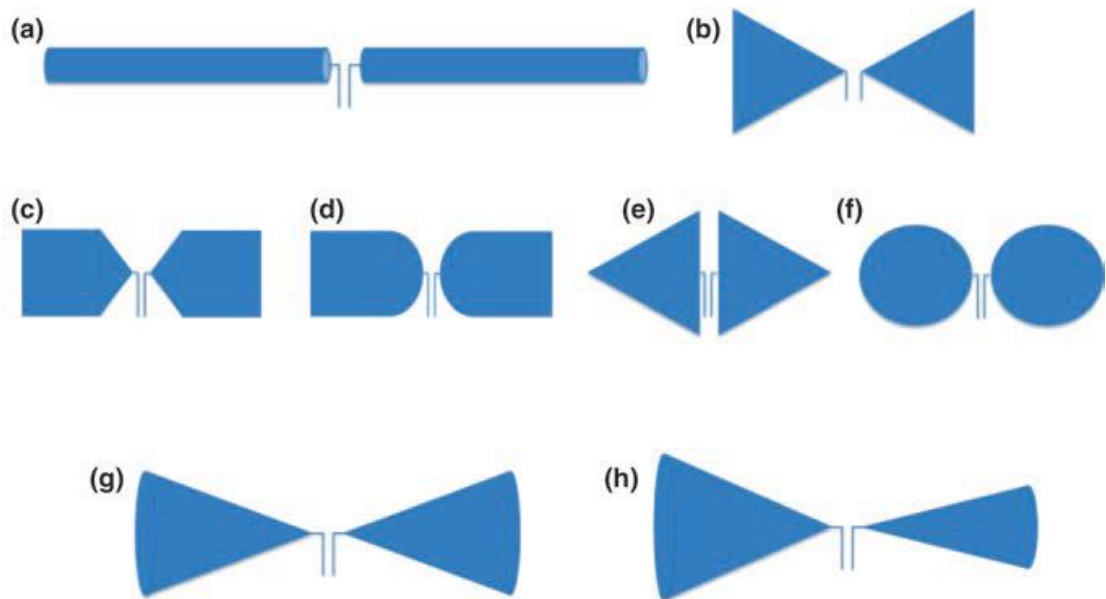


Figure 8 - Examples of dipole antennas: a) fat dipole; b) bow-tie; c) and d) planar rectangular dipoles; e) diamond dipole; f) elliptical dipole; g) and h) biconical antennas with equal and unequal cone angles [11]

One of the most important parameters of the antennas is the so-called central frequency (the most often detected frequency). Frequency selection depends primarily on the required depth range in the particular application. Signal attenuation in the medium is generally more significant at higher frequencies. The greater the required depth is, the lower the center frequency of the antennas should be used. GPR applications necessitate detection range from several centimeters to hundreds of meters. Thus the central frequencies range from several 10 of MHz to about 2.5 GHz.

Another factor affecting antenna selection is the measurement procedure and the position of antenna regarding to the surface. The two basic categories of antennas are air-coupled (AC) and ground-coupled (GC) in this context. Air-coupled antennas (usually horn type) are constructed to be used with an offset from the surface (usually 150 to 500 mm above the surface), i.e. air gap between the antenna and the surface, which is advantageous for collecting data on long sections at high speeds (e.g. on railway lines) [24]. Due to this, there is no limitation of normal traffic during the survey. The disadvantage of these systems is, however,

the low penetration depth of the signal (usually up to 0.5 to 0.9 m) as a portion of the radiated energy is reflected back from the surface. On the other hand, ground-coupled antennas are in full contact with the surface (or at a small constant distance), which allows higher signal penetration depth. These antennas are usually bow-tie type [5]. The disadvantage of this type is the distortion and interference of the signal near the antenna in the area just below the surface (near field zone) [12].

Each antenna has unique parameters and performance. These characteristics vary over time. It is therefore recommended to perform so-called comparative measurement and testing of antenna system parameters [12]. In GPR System Performance Compliance according to COST Action TU1208 Guidelines [28], the following essential tests are described in detail.

- Signal-to-noise ratio
- Signal stability
- Linearity in the time axis
- Long-term stability

An important parameter affecting the survey preparation is also the so-called warm-up period, which is the time elapsed between the turn on the system and moment, when the system signal is relatively stable and survey can be started. Also, this parameter is discussed in [28].

3.4. GPR data acquisition

The GPR can be used to perform measurement either at one exact point, where a single trace of the signal is measured (can be repeated in time) - the record is called A-scan, or survey line/profile (a series of consecutive A-scans with a certain stationing increment) can be obtained, when the antenna moves at the profile - this record is called B-scan [26]. In a 2D B-scan matrix (vertical cut through surveyed material layer or structure), each row represents a single sample on a particular trace and each column then represents one trace (A-scan). The value of every single sample is the voltage amplitude. The matrix can be displayed as the image called radargram [29]. Recently, measurements can be made on large areas, either by repeating measurements on the profiles with a given equidistance (and by linking them to a 3D image) or using antenna arrays. Recording of such a 3D measurement is then called C-scan and allows easier data interpretation and objects identification than previous methods (the ability to create horizontal or vertical slices in any location) [14]. In Figure 11, Figure 10 and Figure 11, A-scan, B-scan and C-scan are displayed [30].

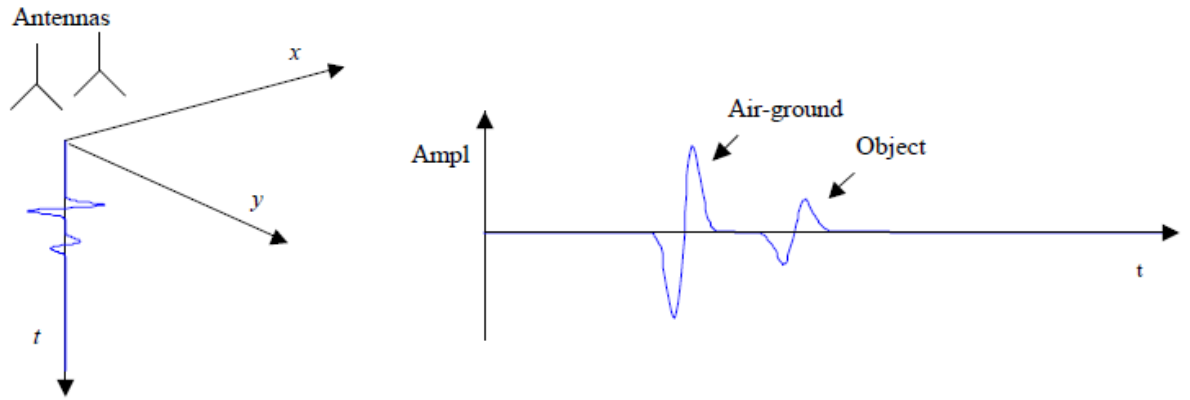


Figure 9 - Configuration and representation of an A-scan [30]

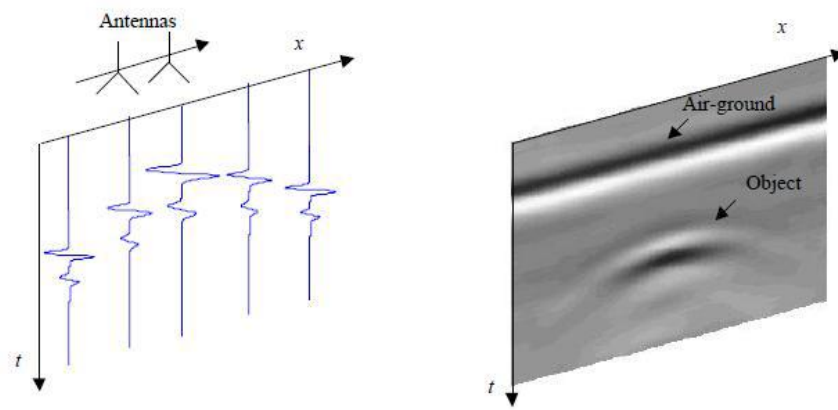


Figure 10 - Multiple A-scans (on left side) forming a B-scan (on right side) [30]

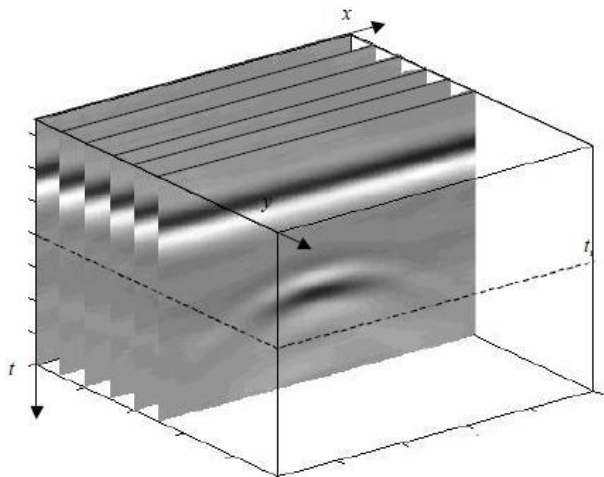


Figure 11 - Multiple parallel B-scans forming a C-scan [30]

The vital question for proper GPR survey is to design a survey in accordance with the objectives and the requirements of that survey in order to conduct an efficient GPR. Several parameters (vertical frequency, sampling interval, maximum depth range, trace increment, etc.) are needed to be tuned.

3.5.GPR applications

GPR has been used in lots of applications. Major fields of applications of GPR is given for example by Daniels [23]. GPR technique provides information about electrical properties of materials and objects under investigation which may subsequently be correlated to mechanical properties which are significant in transport structures [12]. For surveys in transport infrastructure, GPR has been used for several decades.

Roads and Highways

GPR has great potential in road infrastructure diagnostics applications. It is basically the only tool that provides data on the road construction and possibly subsoil, and one that can be used in regular traffic conditions without traffic restriction need. A great advantage of this method is also its non-destructive character. Survey on roads and highways is usually done by a GPR assembly mounted on the vehicle or on a hand cart. When processing GPR data, evaluating and generating outputs, it is also very advantageous to use other methods of road diagnostics. Conversely, GPR data may often be a suitable background or supplement to standard diagnostic methods. As a basis for GPR, it is possible to use for example core boreholes that allow GPR calibration to determine the EM signal velocity in a surveyed construction. GPR data are for example used as input information for Falling Weight Deflectometer (FWD) devices. The result can be an overall assessment of the state of the construction, its residual lifetime, together with a reconstruction and repair plan. A detailed list of applications of GPR use in pavement diagnosis is given in [31]. Main applications on road are the following:

- Determining the thickness of pavement structural layers,
- Determination of the water content in the construction and road base layer,
- Determination of pavement construction material properties,
- Crack detection,
- Detection of rebar and dowels in concrete pavements.

Concrete and masonry structures, Bridges

Concrete condition assessment using GPR involves diagnostics of structures from plain concrete, reinforced concrete, and also pre-stressed or additionally post-tensioned concrete. The typical objective is, among other things, to precisely locate reinforcement bars, prestressing cables, ducts, and cavities, but also to determine the thickness of the concrete elements themselves. The dielectric properties of concrete are influenced by many factors. The primary

and dominant factor for the change in material permittivity is the presence of water. During the hydration process, the amount of water decreases and this water is gradually absorbed and bound by ongoing chemical reactions. An important part of the inspection and rehabilitation of concrete bridges is the assessment of the bridge decks, identification of corrosion and delamination. Potential areas of damage appear in the GPR record as the signal attenuation zones. Delamination almost always occurs around the reinforcement elements in concrete depending on the degree of corrosion of the reinforcement. Corroded areas of reinforcement have lower relative permittivity than uncorded areas and cause discontinuous or weaker reflection of the GPR signal [8]. It is clear, that in the control process of such structures is advantageous to use the mobile system to reduce the scanning time and hence reduce traffic. Knowledge of the current state of construction is also required in the case of tunnels, retaining walls and other similar structures. These data are necessary not only for repairs and maintenance purposes but also for assessing the stability and safety of these structures.

Geology and Geotechnics

Knowledge of subsurface geological layers is very important for many reasons. In the field of transport structures, the contribution of geological and geotechnical applications of GPR lies predominantly in determining the properties of the subsoil, especially its bearing capacity and possible failures, before starting the construction itself. Another benefit is the characterization of geological structures in the vicinity of the building and their possible effects during construction, but also after the finalization of the construction.

Hydrology, moisture and water content

Soil water content is a vital component in the prediction of hydrological conditions in a given location and hydraulic properties of soils. In the area of transport engineering, the knowledge of the bedrock water regime (and its changes in space and time) is important in terms of determining the bearing capacity and consolidation of subsoil, stability of slopes, etc. Water in soils and rocks can be divided into hygroscopic water, viscous or capillary water and free (unbound) water, and their permittivity depends on the degree of coupling between water molecules and the solid particles [12].

The water content can be derived from relative permittivity using empirical correlations. A frequently used relationship is the so-called Topp equation. Another theoretical approach, which describes the relation between relative permittivity and water content in the soil, is based

on so-called dielectric mixing. The resulting permittivity is calculated here by the volume ratio and RDP values of all represented fractions. Other methods are based on estimates of relative permittivity by calculating the reflection delay time. In any case, these are methods requiring gradual calibration, because the signal velocity cannot be accurately determined in advance.

In addition, GPR is also used for example in the following areas: searching for utility networks, archeology, glaciology (ice, snow and permafrost), ecology, forensic sciences, mines detection, mining industry, and volcanology.

3.6. The use of GPR for railway diagnostics

The initial guideline for this thesis regarding problematics described in this chapter was doctoral thesis: *Use of Ground Penetrating Radar in Condition Assessment of Railway Ballast* by Salih Serkan Artagan [32]. The main aim was there to elaborate the implementation of non-destructive GPR methodology in railway track bed surveys (particularly ballast), through both laboratory and field experiments.

Accurate knowledge of the railway body is important for effective evaluation and decision-making process on its maintenance and reconstruction, therefore GPR applications in railway surveys have had very fast growth in recent years. GPR started to become widely accepted regarding railway inspection in the mid-1990's [12]. One of the first successful track inspection tests were performed by Hugenschmidt in Switzerland in 1998 and 2000, and by Galagher et al. (1998) [33]. Since that time, a number of researches have been performed regarding different GPR applications on railways and using many types of equipment and platforms. Examples of GPR assemblies on a two-way vehicle and railcar are shown in Figure 12 and Figure 13.



Figure 12 - GPR equipment on railroad track using two 2GHz antenna and one 500MHz antenna. [34]



Figure 13 - Antenna position in front of the locomotive [35]

At this point, it is important to highlight the major differences in the guidelines for the use of GPR on railways in different countries. For example, in the US in 2009, the US Transport Technology Center launched an extensive project, jointly funded by the American Railways Association and the Federal Railways Administration, aiming at an objective evaluation of the different GPR technologies on railway lines, the development of GPR guidelines in this area

and the identification of further research needs to improve GPR applications [36]. However in many countries, such guidelines are not processed at all, or GPR is not used as a diagnostic tool. GPR survey on railways in the Czech Republic is mainly governed by the following technical regulations:

- *Pokyny pro použití nedestruktivních geofyzikálních metod v diagnostice a průzkumu tělesa železničního spodku* [37]. Here are described, among other things, examples of georadar use, its advantages, drawbacks and limitations, the preparation and method of measuring and processing, and the evaluation of data including the interpretation of results.
- *Podmínky pro měření tratí Českých drah (ČD) georadarem a pro měření překážek prostorové průchodnosti tratí ČD mimodrážními zhotoviteli.*
- *Pokyny pro používání georadaru v měřícím voze pro železniční svršek.*

The presence of rails, sleepers and other objects made railway lines a rather unfavorable environment for GPR survey with high demands on data acquisition and processing [38]. Therefore, for the correct calibration and validation of GPR data with real conditions, it is still necessary to perform transverse ditches or probes at key locations. It is also possible to determine the signal velocity using methods like Wide Angle Reflection and Refraction (WARR) or Common Mid-point (CMP). The basic difficulties and drawbacks are mentioned for example in [12, 39–41], and could be listed as: [32]

- interference from rails and sleepers (especially concrete sleepers)
- electrical wires in case of unshielded air-coupled antennas
- various subsurface and near-track railway assets which require ground and side clearances for the moving antennas
- wavelength-sized ballast (in case of using higher frequencies over large sized ballast medium)

A typical cross-section of the rail body can be seen in Figure 14.

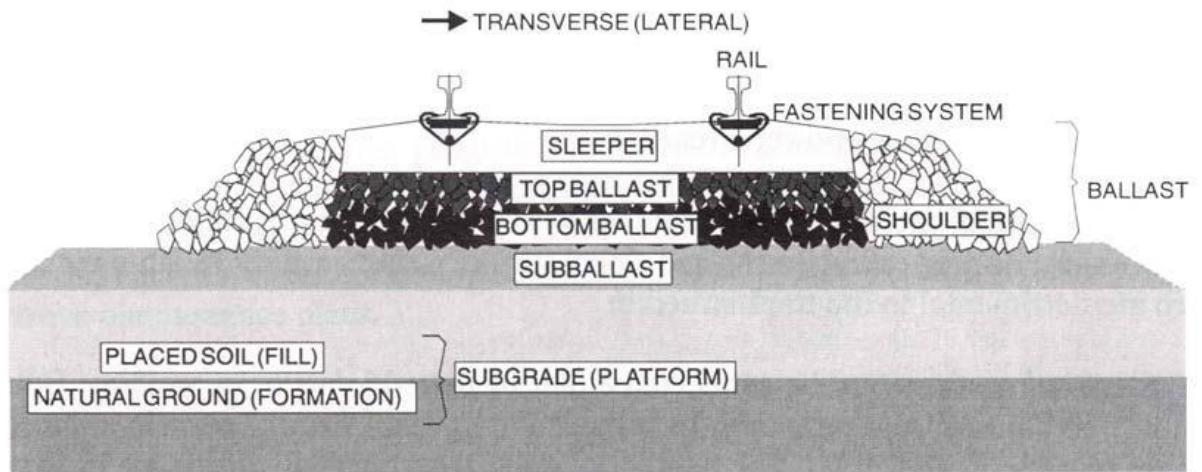


Figure 14 - Conventional permanent way structure [42]

In order to evaluate railway ballast, the minimization or removal of effects of concrete sleepers, ties and rails is the main challenging issue, and it has been addressed by many researchers [43–46]. Surveying between the sleepers (the cribs) was one of the approaches [47], however, the information beneath the sleepers is even more valuable in most cases [48, 49]. In order to enhance the quality of the GPR data in assessing the ballast condition, Al-Qadi et al. [39] developed a time-frequency method, which removed the interference and noise inherent in the railway environment. Hugenschmidt used a set of processing steps in order to reduce the effects caused by sleepers in [40], and to remove the ringing effect of the sleepers in [50]. A time-space filter screen was developed and used to suppress the multiple waves and diffraction occurred due to the sleepers in [51]. In [52], parabolic radon transform was used in order to eliminate the effects of railway sleepers.

Generally, GPR has been used in a wide range of applications on railways. This may involve e.g. the determination of layer thicknesses [53], investigation of embankment stability [50, 54], localization of trapped water areas [43], indirect estimation of track modulus [55], detection of permafrost sections [56–59], etc. Many GPR studies were focused on the ballast and sub-ballast layers assessment, e.g.: [60], [12], [61], [62], [63]. This issue will be described in more detail in chapter four. GPR can be used on the railway to detect anomalies such as voids, water pockets, or subgrade settlement, which allows also for a deeper inspection into the track structure [60], [64]. For example, an overview of an ongoing study to use substructure indices for easier understanding and interpretation of GPR data is listed in [43]. A good example of railway subgrade investigation with GPR, where condition indicators were used is mentioned

in [54]. In Figure 15, there is a schematic view of GPR profile generation over ballasted track substructure.

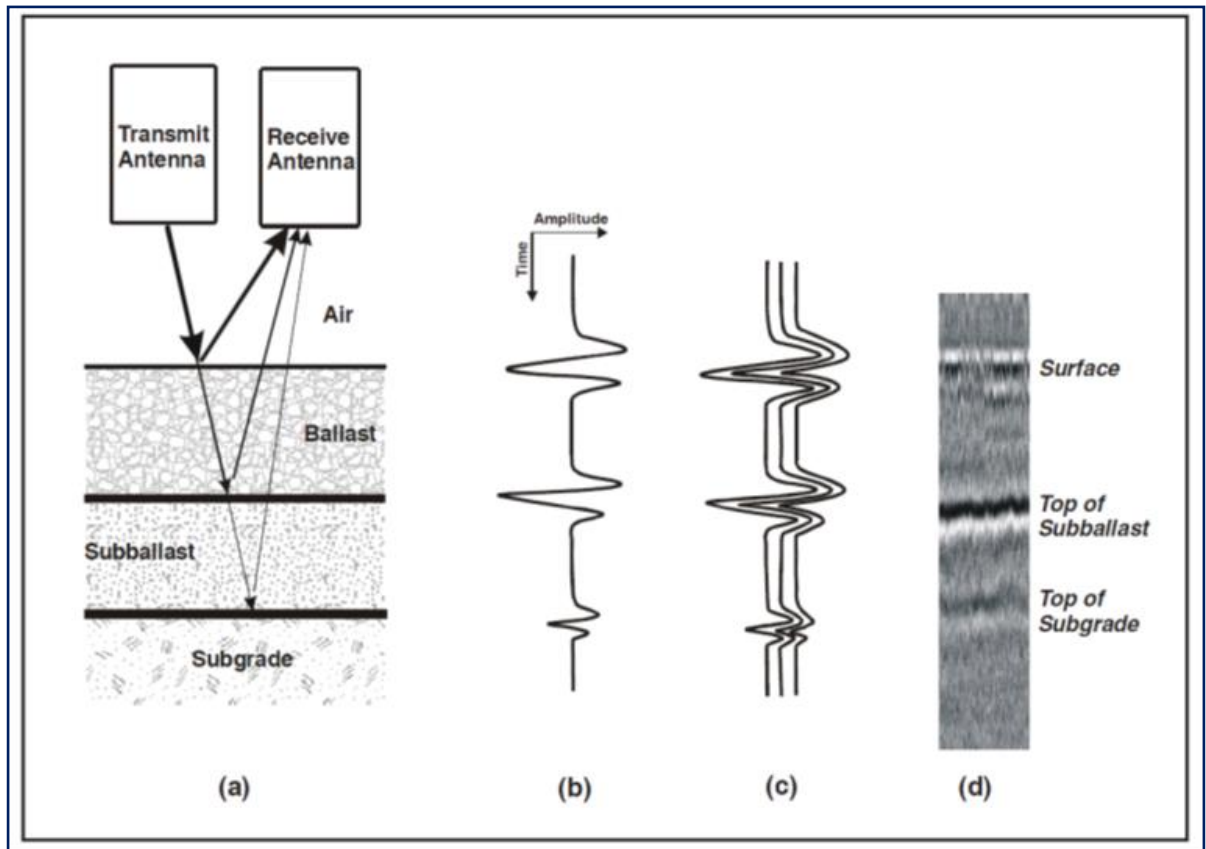


Figure 15 - The generation of a GPR profile with an air-coupled antenna over track bed. a) The transmitted energy is reflected off the boundaries in the substructure, b) A single trace composed of the reflection amplitudes for the reflections in (a), c) Multiples [65]

Finite difference time domain technique was used to simulate GPR signal in the studies [68–70]. Also the combination of GPR with other non-destructive methods is used, e.g. in [71], and the issue of installation of artificial interfaces into the rail body for better diagnostics using GPR is also addressed, e.g. in [72]. Since many commercial hardware and software tools are used nowadays to GPR on railway surveys [73], a mutual comparison of different sets is also an important task. Maturana et al. [74] compared three different proprietary GPR systems in terms of data quality. In [4], six commercial GPR systems with different central frequencies were assessed.

In Figure 16, there is a composite picture of GPR surveyed area on railways.



Figure 16 - Composite picture showing the survey area and the GCB-500 data superimposed [75]

Because of long section survey demands on the railways, the automation of the measured data evaluation is also an important aspect. A novel approach for surveying and analyzing long sections, based mainly on expedite frequency domain analysis is presented in [76]. In [77], Joint Time-Frequency Analysis (JTFA) was applied to GPR data of the rail sub-structure with the aim of selecting relevant data for subsequent use in an automatic detection system. In [78], an automatic system for assessing the condition of the underlying railway material was introduced, based on the selection of amplitudes of reflections of characteristic frequencies and their classification. In [41] an automated system using GPR to assess various maintenance problems along the railway was developed, where automated processing, calibration, and modeling were performed. An automatic classification system has been developed relying on the magnitude spectrum analysis and support vector machines to classify ballast fouling in [79]. In [35] a GPR equipment especially designed for inspecting and verifying railroad tracks in a reliable and effective way, without interruption of regular traffic was presented.

The central frequency selection, as one of the most important parameters of GPR systems, has also been addressed. Higher frequency air-coupled systems, resulting in numerous benefits in terms of ballast condition evaluation are used nowadays instead of low-frequency antennas [48, 80]. The importance of optimizing the central frequencies according to the type of inspection is emphasized in [12]. In [81] a comparison of air-coupled and ground-coupled

antennas to assess the subgrade condition was performed. Tests have been made with 1GHz [41], 400MHz [56, 82] and with 500MHz antennas [13, 83]. More recently, the use of multi-frequency or array GPR systems has demonstrated to be an effective tool for railway super-structure and sub-structure [84]. In [44], the antenna configuration was optimized in the work of in multiple-frequency GPR system. In [85], full-resolution 3D imaging allowed improving the subsoil assessment, and layer discontinuities and damage areas determination.

Basic geotechnical characteristics of subsoil are crucial in terms of railway body condition assessment. One of the most important goals is the moisture content evaluation [74, 86] in this context. In [87], direct estimation of moisture content from amplitude analysis was carried out without the calculation of dielectric permittivity by proposing a variable “integral reflectivity”. Another important parameter of the railway sub-structure is the deformation modulus. Several studies have shown a very high correlation between EM properties and deformation properties in different soil types and aggregates. In research [88] conducted at Transport Technology Center, Inc.(US), authors declare the possibility to predict the elastic modulus by GPR survey with an accuracy of up to 3.4 MPa under certain conditions. In [89] authors used spectral analyses in the frequency domain on the assessment of “critical” geometric features of the ballast aggregates. A procedural GPR-based scheme for performing efficient railway maintenance was proposed in [90]. A view of effective maintenance scheme using GPR is shown in Figure 17.

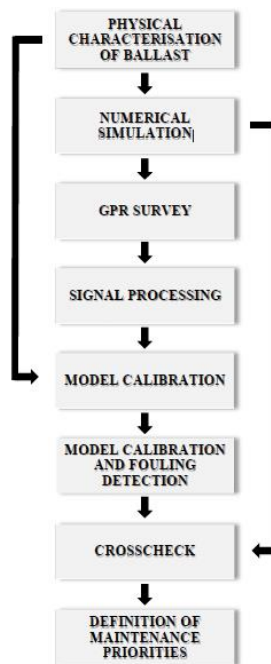


Figure 17 - Scheme of effective maintenance using GPR. [90]

4. State of the art research on railway ballast assessment by GPR

According to [42], ballast structure may be divided into four zones.

- **Crib** – zones between the sleepers
- **Shoulder** – the zone between the end of the sleeper and down to the top of sub-ballast.
- **Top ballast** – the top part of the ballast structure which is usually exposed to tamping.
- **Bottom ballast** – the lower part of the structure which supports the overall structure.

These track structure components can be seen in Figure 18.

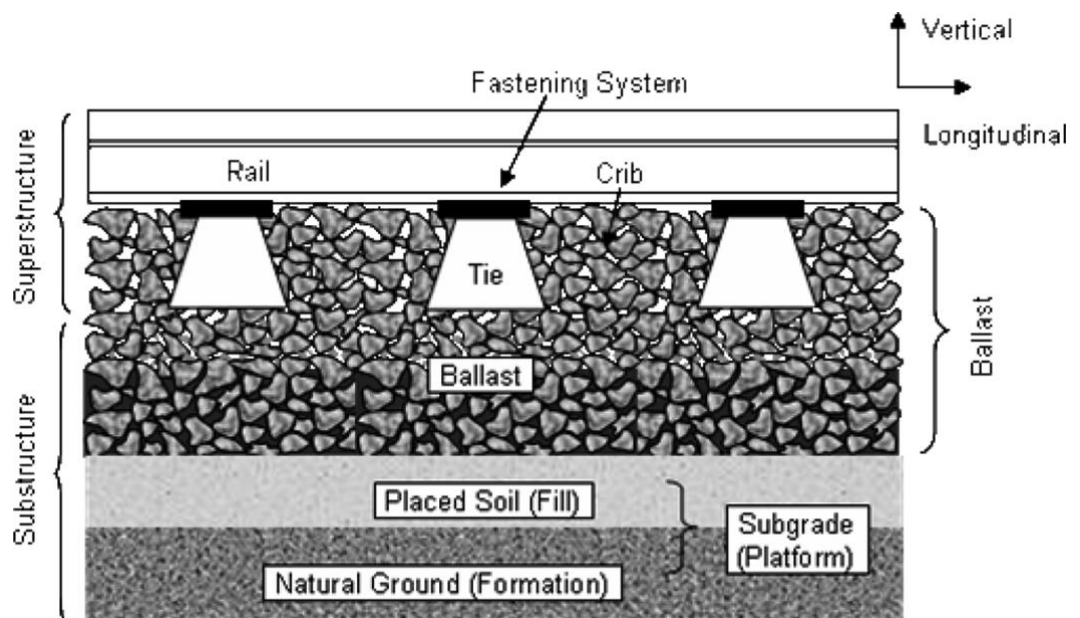


Figure 18 - Track structure components [42]

The crucial function of the ballast layer is to transfer the loads from the superstructure to the subgrade and to provide drainage without structure failure [91]. In detail, the most important functions of ballast structure can be, according to [42], stated as:

- Withstand the actions coming from the sleepers to the substructure (uplift, lateral and longitudinal forces),
- Act as resiliency and energy absorbent for the track structure.
- Provide space for movement and accumulation of crushed aggregates due to fouling (in the voids between the aggregates)

- Provide quick drainage system down to the structure.
- Pressure reducing ballast structure to the allowable stress for the underlying structure just below the slipper.
- Tamping will rearrange ballast particles while adjusting track geometry. This eases and speeds up the maintenance operations.

4.1. Ballast fouling mechanism and quantification

Ballast fouling can differ along the track, resulting in a high variation of both thickness and RDP value. The goal of ballast quality assessment is primarily to distinguish between sections of clean and spent ballast [92]. The texture visible on radargram enables to distinguish coarse-grained layers from finely grained. Clean ballast has a larger volume of air pores, which reduces the average RDP of the layer material.

Over time, the ballast layer is polluted by an increasing amount of fine material capable of binding water, which increases RDP [93]. Since spent ballast contains a higher amount of fine particles in between ballast aggregate, filling the existing voids, the resulting therefrom changes in moisture, contamination, and degradation cause reflections of the signal, that are readily recognizable. RDP is considered to be a reliable indicator of ballast quality [33]. The reasons of ballast fouling can be divided as follows: ballast breakdown (76%), underlying granular layer infiltration (13%), ballast surface infiltration (7%), subgrade infiltration (3%) and sleeper wear (1%) [39, 94]. Repercussions caused by ballast fouling are described in detail in [95]. In case of not sufficient drainage function in ballast layer, water accumulation can appear, which may lead to a reduction in shear strength and stiffness of ballast as well as increasing the rate of deterioration and fouling process. This occurs when ballast finer particles replace air voids. Various degrees of fouling of the ballast material are shown in Figure 19 [96].

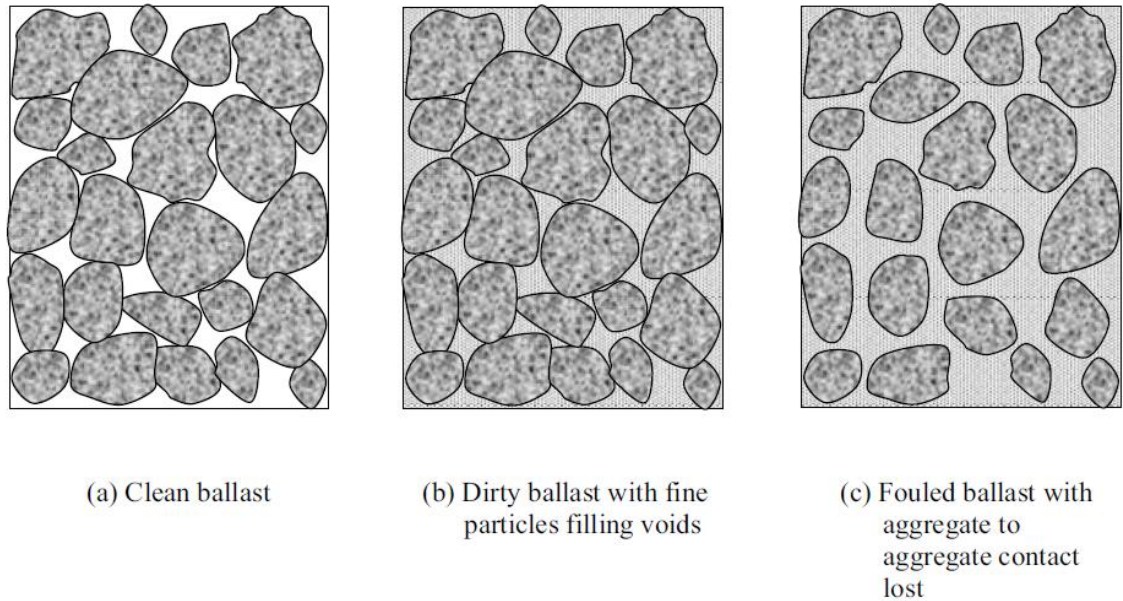


Figure 19 - Ballast with different degree of fouling [96]

Determination of ballast fouling level has come to the forefront of interest recently. Table 2 demonstrates the categories of ballast according to the fouling indexes [94].

Table 2 - Categories of Fouling [94]

Category of Ballast Condition	Abbreviation	Fouling Index
Clean	C	<1
Moderately Clean	MC	1-10
Moderately Fouled	MF	10-20
Fouled	F	20-40
Highly Fouled	HF	>40

There are several fouling indicators, among which the Fouling Index by Selig and Waters [94] is the one most often used. It sums the percentage passing each sieve to determine the fouling index by equation (18).

$$F_{I-SW} = P_{0.075} + P_{4.75} \quad (18)$$

where $P_{0.075}$ is the percentage of material passing the sieve size 0.075 mm and $P_{4.75}$ is the percentage of material passing the sieve size 4.75 mm. Ionescu [97], established suchlike index, given in equation (19) [13].

$$F_{I-I} = P_{0.075} + P_{14} \quad (19)$$

where P_{14} is the percentage of material passing the sieve size 14mm.

In [98], authors also mention the other fouling indexes, such as percentage of fouling, D-bar method, effective degree of fouling, percentage void contamination and relative ballast fouling ratio in a comparative way. De Bold [13] found a high correlation between Ionescu fouling index and the area condition surveyed by GPR.

4.2. Fouling assessment of railway ballast using GPR

The knowledge of RDP values represents a crucial aspect of ballast thickness and condition determination. RDP value is, as stated above, highly dependent on the moisture content and fouling, but an accurate investigation of these phenomena represent still a challenge for GPR railways surveys [99]. According to [74], GPR signal in ballast is affected by the attenuation, the existence of reflectors inside the ballast, loss of reflector at the base of ballast and the decrease of the signal velocity due to several reasons. The repeated GPR survey over time enables to monitor and to predict the condition and deterioration rate of the ballast layer, thus to refine and make the maintenance process more effective. This will facilitate the possibility of effective planning of required maintenance works in short, medium and long-term bases with notable cost and time savings [74]. A possible way to visualize ballast fouling within the monitoring of ballast layer condition during its lifecycle can be seen in Figure 20.

Fouling assessment of railway ballast and thicknesses determination using GPR were addressed partially or wholly in many studies [13, 44, 48, 70, 74, 83, 93, 95, 98, 100–108], some with a particular interest to assess ballast fouling and moisture content [93, 95, 96 and 97]. In [100] four different fouling levels were simulated (from 0% to 76%) and two different air-coupled antennas were used. In [112] GPR tests were conducted on a prototype railway track using antennae with various frequencies under different ballast conditions. Based on the analysis of the processed data, the influence of frequency, moisture content of ballast, the effect of radar detectable geotextile, and the difference in relative dielectric permittivity were discussed and evaluated. As described in [113], Rail Radar™ has developed and implemented a sophisticated system for the non-destructive assessment of ballast and tie condition. Clark et al. [83] presented findings related to the EM properties of ballast in laboratory conditions,

particularly RDP value differences of clean versus fouled ballast and wet versus dry ballast. In [114] authors monitored the condition changes within the ballast layer to categorize the GPR profile into sections based on those condition changes. Gallagher et al. [47] used GPR to assess the level of ballast fouling and detect the interface between ballast and subgrade. In [40], the use of GPR proved very beneficial compared to traditional methods in ballast condition assessment leading to minimization of the number of trenches required and also enabled to determine the sections where subsoil material penetrated into the ballast. The main goal of investigation in [115] was to identify critical factors as well as antennas and central frequencies most suited for the investigation of railway ballast.

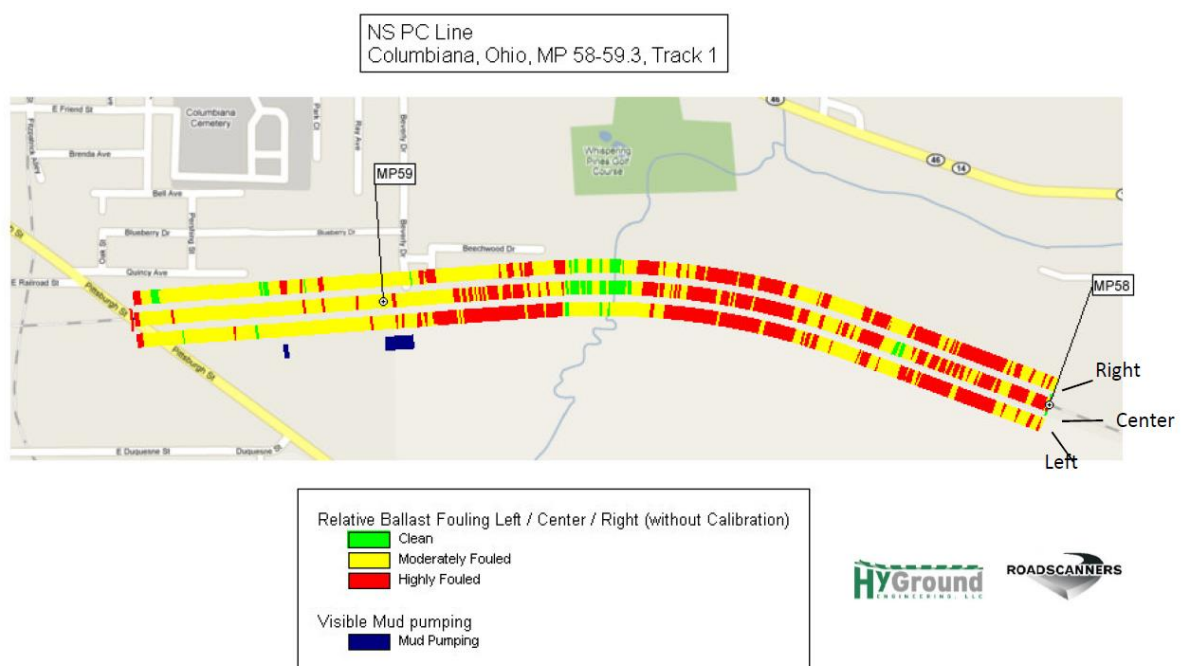


Figure 20 - GPR test results concerning ballast fouling in revenue service [116]

The effective in-situ ballast dielectric was modeled in [113] using the summation of the volumetric ratio of the component material RDP values. This model predicted that there occurs a significant decrease in signal velocity (10-30%) in ballast material during its fouling process. Detailed results can be seen in Table 3.

Table 3 - Modeled Ballast Pulse propagation Velocity at Radar Frequencies [113]

Air ($\epsilon = 1.0$) (% volume)	Ballast ($\epsilon = 5.4$) (% volume)	Water ($\epsilon = 81$) (% volume)	Effective Dielectric	Velocity (mm/ns)
25	75	0	4.30	145
15	85	0	4.74	137
10	90	0	4.96	135
5	95	0	5.18	132
5	90	5	8.96	100
5	85	10	12.7	84

In numerous studies [40, 74, 83, 114, 117] the EM wave velocity value was utilized to undertake time to depth GPR data conversion for the ballast layer. After comparing the radar data with the thicknesses measured directly in trenches, Hugenschmidt [40] recommends using an average signal velocity of 14 cm/ns for ballast medium. Göbel et al. [117] use the ranges of signal velocities from 12 to 21 cm/ns for clean ballast and from 0.8 to 1.2 cm/ns for spent ballast. Jack and Jackson [114] calculate an average signal velocity of 13 cm/ns for ballast in their research. Maturana et al. [74] determined the signal velocity for clean ballast as 17 cm/ns and for highly fouled ballast 10 cm/ns.

In a recent study, Benedetto et al. [100] used GPR to characterize clean and fouled ballast through extensive laboratory experiments, signal processing, and numerical modeling. In a study [74] regarding preventive maintenance of railway track, the authors report the EM signal velocity between 12 cm/ns and 21 cm/ns in the case of clean ballast, and in the case of ballast contaminated with fine material, the velocity ranging from 8 cm/ns to 12 cm/ns.

Series of laboratory tests were also performed in [119] using KHM for velocity calculation and Complex Refractive Index Mode (CRIM) for theoretical confirmation. Ballast material (fraction 31.5 – 63) was surveyed with different levels of fouling and with different fouling materials. For contamination with sand, signal velocity values varied based on the level of fouling between 15.2 and 13.1 cm/ns. For contamination with fine gravel (fraction 5-10) varied between 14.8 and 13.6 cm/ns. In the case of these fouling agent mixture, the velocity was in the interval from 15.2 to 12.9 cm/ns. Signal velocity was determined within laboratory experiments or in-situ surveys in many other studies, e.g. [40], [114] or [117].

RDP values from several studies for clean and fouled ballast are presented in Table 4.

Table 4 - Published RDP values of ballast adapted from Lalagüe [120]

Published RDP values of ballast			
Ballast Material	Clark et al. [83]	Sussmann [121]	Leng & Al-Qadi [122]
Type	Granite	Granite	Granite & Limestone
Dry Clean	3.0	3.6	3.25 (granite) 3.96 (limestone)
Moist Clean (5%)	3.5	4.0	
Saturated Clean	26.9		
Dry spent	4.3*	3.7	3.77 ** (granite) 4.84 ** (limestone)
Moist Spent (5%)	7.8*	5.1	
Saturated Spent	38.5*		
*The spent ballast in these tests was at the end of its economic life, where the fines have reached 10% of the total mass of the ballast			
** 50 % level of fouling corresponding to the 50% of air voids volume filled with dry clay			

In order to evaluate the level of ballast fouling used in Portuguese railways and the influence of antenna frequency on its measurement, laboratory tests were performed on different materials using several antennas in [99] and [111]. Combined influence of several fouling levels and different water content was investigated. Table 5 shows observed RDP values and its coefficient of variation for six antennas with different central frequencies.

Table 5 - RDP values variation with the fouling index for water content between 6 % and 12 %. (AV - average value, CV – coefficient of variation value [111])

FI	6		15		35		55	
	AV	CV	AV	CV	AV	CV	AV	CV
400 MHz IDS S	5.09	0.02	6.00	0.06	7.93	0.07	8.49	0.10
400 MHz IDS G	5.42	0.06	6.60	0.05	7.66	0.09	8.41	0.10
500 MHz GSSI	2.63	0.02	3.23	0.04	3.99	0.09	4.74	0.13
900 MHz GSSI	3.02	0.04	3.68	0.07	4.78	0.12	5.57	0.13
1.0 GHz GSSI	3.58	0.02	4.40	0.05	5.61	0.09	6.55	0.11
1.8 GHz GSSI	3.57	0.03	4.41	0.05	5.67	0.09	6.57	0.11

In [123] both laboratory and field tests were performed with the results given in Table 6 and Table 7.

Table 6 - Laboratory Estimates of RDP for Single-layer Specimens [123]

Material	Depth (mm)	Dielectric Permittivity					
		Dry		Saturated		Drained	
		Time (ns)	ϵ	Time (ns)	ϵ	Time (ns)	ϵ
Granite ballast	230	2.7	3.2	7.7	26.4	6.0	16.0
Dolomite ballast	230	2.9	3.7	7.6	25.5	6.1	16.5
Trap rock ballast (basalt)	230	3.1	4.3	8.4	31.4	3.3	4.8
Trap rock ballast 10% fouled	230	3.4	5.0	7.1	22	6.2	17.0
Trap rock ballast 30% fouled	230	3.5	5.4	7.9	28	6.8	20.6

Table 7 - Field Estimates of RDP [123]

Sample	Average	Number of Samples	Standard Deviation
Clean Ballast	2.6	9	0.5
Fouled Ballast	4.2	8	0.7
Wet Ballast	5.9	1	N/A

The influence of moisture content in the clean and fouled coarse granite ballast on the GPR signal characteristics are assessed in [124]. RDP values of ballast under wet clean and wet fouled conditions by means of KHM were computed. RDP of saturated clean coarse granite ballast was found to be 25.5, whereas the average value of drained ballast 3.1 was observed to have similar values with the dry one. RDP values tend to increase with increasing fouling levels as well. Table 8 indicates a change in RDP measured in 23 days interval during saturation and drainage process of railway ballast sample.

Table 8 - RDP values vs dry, saturated and drained ballast [124]

Day #	1	2	2	3	5	8	9	16	23
Condition	Dry Clean	Saturated Clean	Just after removal of water (same day)	After 1 day of Removal	After 3 days of Removal	After 6 days of Removal	After 7 days of Removal	After 2 weeks of removal	After 3 weeks of removal
RDP	3.090	25.500	3.876	3.203	3.146	3.146	3.125	3.139	3.150

In [125], data from 238 km of track obtained and the ballast fouling condition was automatically interpreted. The comparison showed good agreement between these GPR data and ballast condition assessed via KHM.

Ballast under various fouling conditions generates various EM scattering patterns. According to Roberts et al. [126], the clean ballast near the surface generates a significant scattering pattern, while the scattering pattern generated by the fouled ballast at the bottom is insignificant because the air voids in fouled ballast are much smaller than the signal wavelength. In [127] Al-Qadi et al. conclude that the time-frequency approach may be effective in detecting ballast fouling condition. In addition, a combination of direct method, scattering amplitude envelope approach, and Short-time Fourier transform (STFT), can provide an effective method to quantify the ballast condition. Methods based on scattering has been exploited to distinguish between the clean and fouled ballast also in [61, 117, 118, 121, 122, 98], spectral analysis in [92] and [89], and wavelet and Fourier Transform Analysis (FTA) in [129] [77]. STFT has been used in order to assess the changes in ballast in both time and frequency domains simultaneously also in [39, 122, 44, 130]. Khakiev et al. [86] made a research which quantitatively processed GPR data in order to assess these problematics.

It follows from above-mentioned studies, that GPR is a useful tool to assess railway ballast condition and its fouling level using calculated RDP values. For this purpose so-called ground truth data are needed. Currently often used calibration by KHM (ditches and trenches) is however not accurate due to ballast particle size and due to the instability of the ballast layer during test pits performing. The major problem is also the presence of water in surveyed layer. Compared to ballast fouling due to fine particles, the presence of water has a significantly higher impact on calculated signal velocity and RDP values, although these two phenomena are closely related. Thus, the GPR survey should be performed in dry condition. Three days period after rain could be recommended in case of clean ballast, while in case of fouled ballast, this period could be much longer due to the complexity of water regime, influenced by fine particles presence, and its investigation in-situ on different railway bodies.

5. Equipment used

For all GPR in-situ surveys described in this work, the GPR assembly of the Department of Transport Engineering (KDS) has been used. A manual measuring trolley was used as a platform. K2 FastWave and ReflexW software were used to record and process data.

5.1. Hardware

The used GPR assembly by Ingegneria dei Sistemi S. p. A. (IDS) labeled as RIS Hi-Pave was used. It consists of a MCh Fast Wave DAD Multichannel Controller, a 12V 12 V battery, a pair of antennas, a WHE PAVE (Odometer), Aluminum and Fiber Frame (Thule Carrier, Glass Fiber Console and TRDual F Mechanical Mount), coaxial , power and data cables and the Panasonic CF-53 Toughbook for data recording and processing. Antennas used were a horn air-coupled HN-2000 antenna with a central frequency of 2 GHz and two-frequency ground-coupled antenna TR DUAL-F 400/900 with central frequencies 400 and 900 MHz. Parameters of these antennas can be seen in Table 9. Both antennas are pictured in Figure 21.

Table 9 - Used antenna parameters

	Air-coupled antenna	Ground-coupled antenna
Antenna designation	HN-2000	TR DUAL-F 400/900
Antenna type	shielded dipole horn	bow-tie
Central frequency	2000MHz	400/900MHz
Dimensions	60cm x 22cm x 40cm	43cm x 37cm x 20cm
Weight	7 kg	6 kg
Operating humidity	<90%	<90%
Operating temperature	-40 ° C to 50 ° C	-40 ° C to 50 ° C

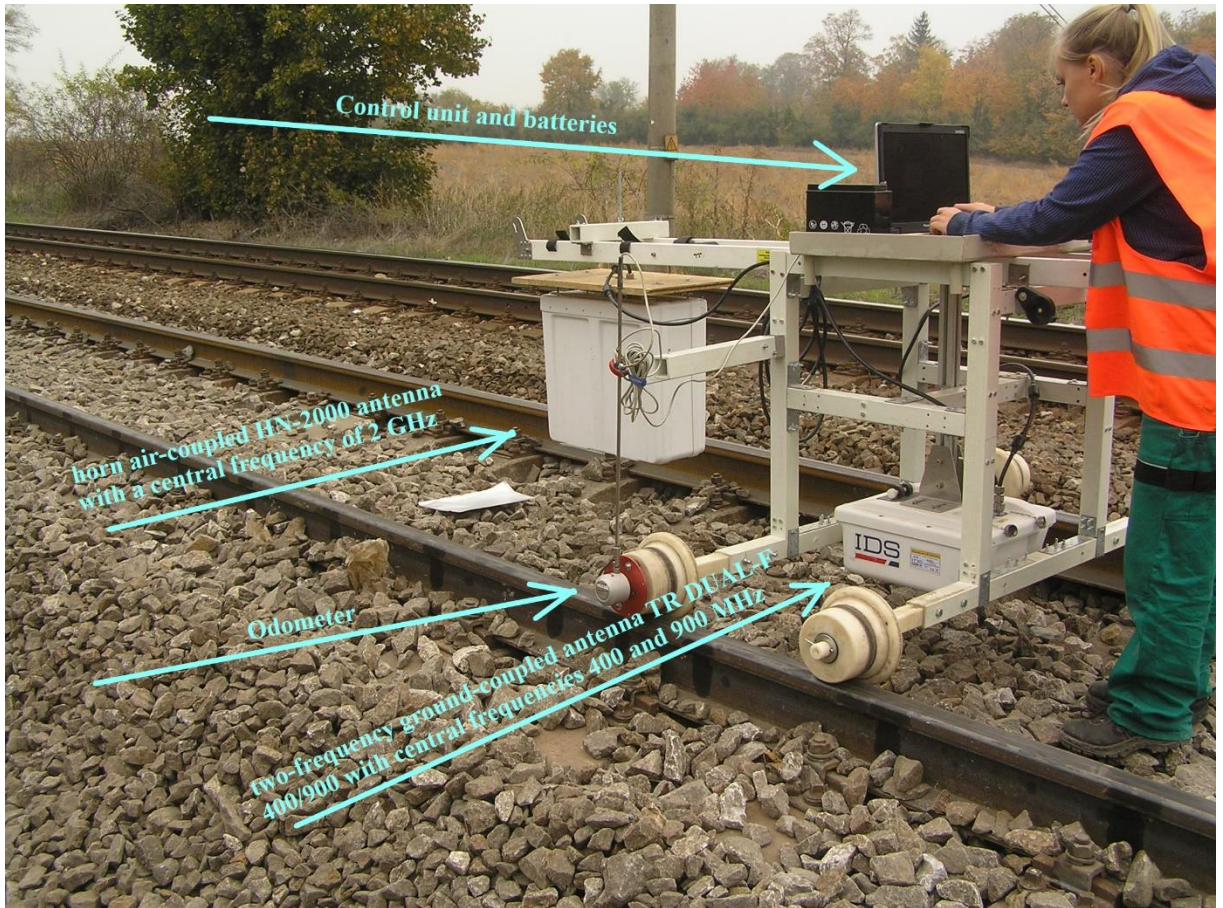


Figure 21 – Description of GPR assembly components

The DAD Fast Wave Control Unit, shown in Figure 22, is the controller responsible for antennas management and digitization of acquired GPR data. Technical specifications (by provider) of control unit DAD Fast Wave:

- Pulse frequency: 400 kHz;
- Scanning speed: up to 4760 scans per second (@ 128 samples per scan)
- Range: up to 9999 ns;
- Number of A / D converters: 2;
- Data acquisition frequency (A / D clock): 400 kHz;
- Sampling: 16bit;
- Resolution: More than 5 psec;
- Number of samples per scan: 128-8192 (1 channel); 128-4196 (2 channels); 128-2048 (4 channels);
- Ports: Antenna 1, Antenna 2, Odometer, LAN, Battery;
- Maximum number of antennas: 2 standard; up to 8 TR with expansion box; up to 4 TR DUAL F;
- Number of Channels 8;
- Dimensions: 22cm x 17cm x 5.5cm;
- Weight: 1.5 kg;
- Dust and water resistance (IP 64);
- Average consumption: <10 W

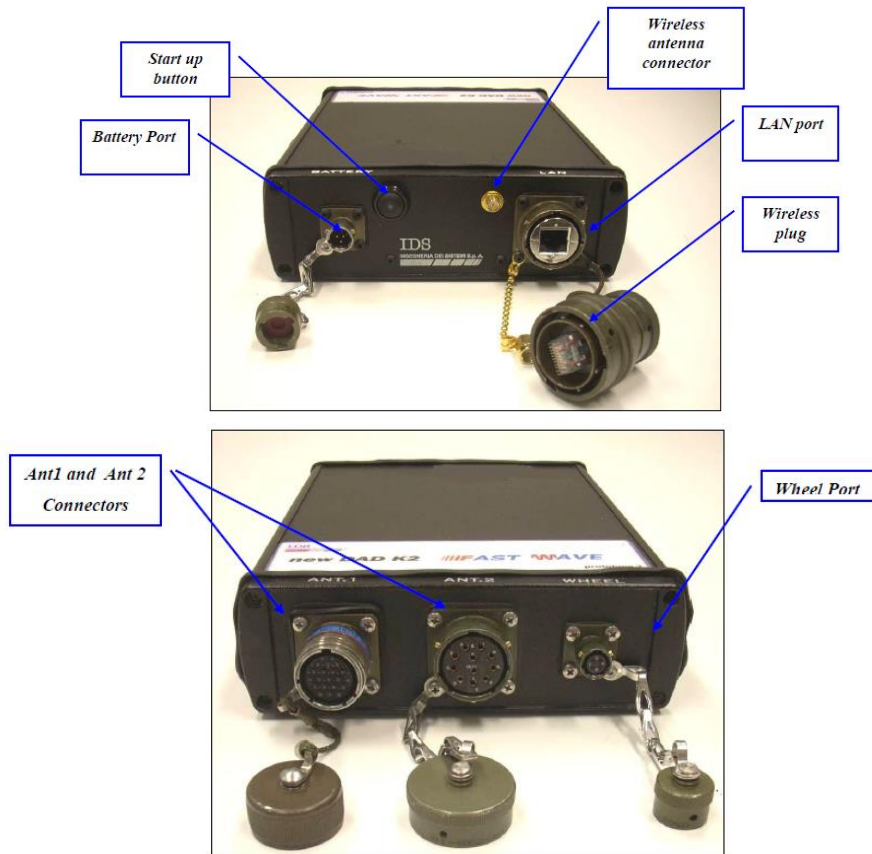


Figure 22 - DAD Fast Wave: a) side with connections to position sensor and antenna b) side with Battery Port, Lan Port and wireless connector [131]

Surveys performed in 2014 and 2017 by SŽDC were performed with 400 MHz ground-coupled GSSI antennas.

5.2. Software

The K2 Fast Wave software from IDS was used to collect data. The ReflexW software was used to process and interpret the data.

The K2 FAST WAVE data collection software (<https://idsgeoradar.com/>) is created to cooperate with IDS DAD FastWave control units and can utilize up to 8 antennas. It enables to display two radar screens simultaneously in real time. It provides tools for customizing parameters for the data record, antenna setup, and calibration of individual channels, and pre-determination of the signal propagation velocity. The software can be linked to GNSS, digital camera, and other external devices. The interface of K2 FAST WAVE software can be seen in Figure 23.

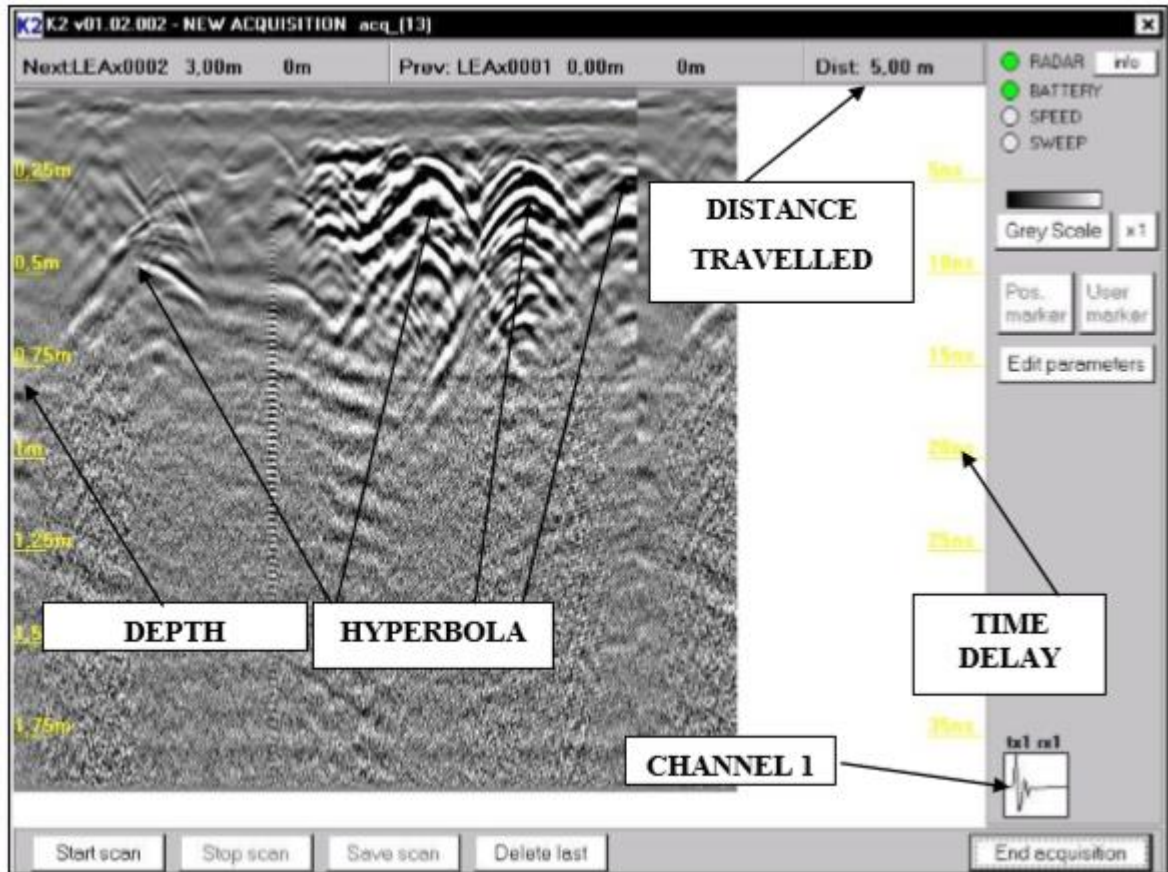


Figure 23 - Interface of K2 FAST WAVE software [131]

The ReflexW program (<https://www.sandmeier-geo.de/reflexw.html>) allows working with all usual data formats. The 2D data analysis module enables the processing of GPR, seismic methods and ultrasonic methods. It contains a large number of data processing algorithms (filtering, profiling, composite and multiple reflexes, static correction, migration, etc.). The 3D Data Interpretation Module allows interpreting by viewing profiles in the x, y or z axis, and from GPR data or seismic methods. It also offers the possibility of composing these cuts into a three-dimensional cube, choosing the reflections in this 3D environment, and also creating video files for a continuous shift display in 3D.

The modeling module (inverse tomography) allows inversion of seismic primal reflection data, tomographic inversion of time domain data and 2D wavelength simulation by finite difference method. The interface of ReflexW software can be seen in Figure 24.

Data collection in 2014 and 2017 by SŽDC was performed with GSSI RADAN software.

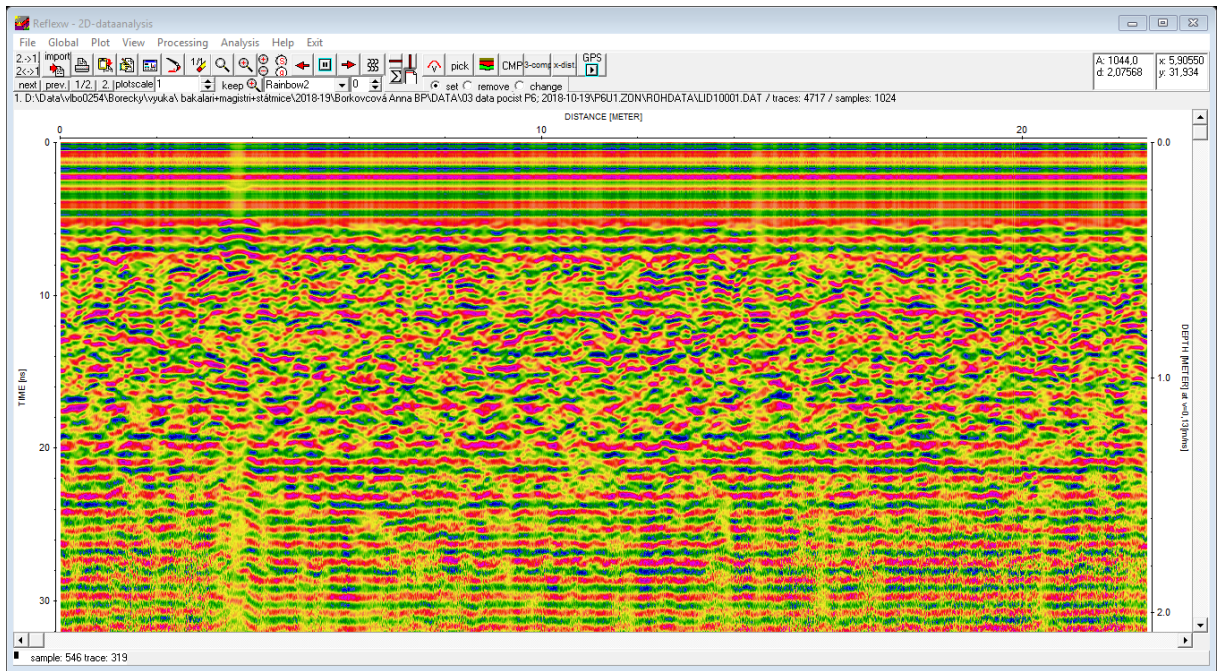


Figure 24 - Interface of ReflexW software [132]

6. Experimental Survey

At the time, when the place of the experiment was to be determined, there were five available construction sites, in where the cleaning process was planned to be performed. Construction site of Čáslav - Kutná Hora railway section was selected, because there was a specific interest in the use of two different undercutters: RM 79 (the property of Hrochostroj a.s.) and RM 900 (the property of the Strabag Inc.), which were to perform the cleaning process in the stationing 278,600 - 286,800. Thus, there was an opportunity to compare the efficiency of the cleaning processes of each unit with an independent and non-destructive measurement. Before any survey initiating works, it was also important to ensure the safety (BOZP) training under SŽDC, which author underwent within service training. Detailed photographic documentation is provided in Annex 1

6.1. Site description

The selected railway track is a two-line track with both passenger and freight train services. Track speed is up to 120 km/h. The affected track section is a part of a nationwide track which belongs to the line of the European TEN-T (Trans-European Transport Networks) railway system within the global passenger and freight network with the character of the non-corridor track of the national railroad. The site is part of the track (Brno -) Havlíčkův Brod - Kolín (- Prague), designated in the passenger timetable as number 230, according to the 324 track tables. The track is electrified in the given section by an alternating traction current system 25 kV / 50 Hz, track-side safety equipment is the 3rd category of AB type. The permitted load class is D4, with a speed of 80 to 120 km/h. The operator is SŽDC s. o., a local administrator is OŘ Praha.

The railway superstructure was composed of the SB8 and SB8P sleepers, which were preserved. In the first phase of the survey, the R 65 and S 45 were used in some sections, which were all changed to 60 E2 during the reconstruction process. Average center to center distance between sleepers was 60 cm. The rail's fastenings were type K. The original ballast layer thickness was reported as 350 mm below the sleepers, but after digging ditches, it was found that 300 mm thickness corresponds to reality in some sections. After the reconstruction, a 350 mm thick ballast layer was set in all sections.

The whole construction project of Čáslav-Kutná Hora was conducted in cooperation with Chládek and Tintěra a.s., Hrochostroj a.s. and GJW Praha spol. s.r.o. Reconstruction of No. 1 rail (where GPR survey took place) was performed by Chládek and Tintěra a.s. and Hrochostroj a.s. The work timetable on this construction site can be seen in Annex 2. Because of many

partial work activities carried out over the whole length of the excluded track by above-mentioned companies, it was not an easy task to carry out the GPR survey to the extent desired. Thus the GPR survey had to be divided into five days. In addition to rail bed cleaning, other rail mechanization such as tampers, ballast plows, two-way excavators, and other devices, were also on site.

Surveyed profiles on this track were chosen near four railway crossing because of the possibility to transport and manipulate the survey cart more easily on the excluded track. Reconnaissance and setting of the survey sections took place on October 3rd, 2018. Eight sections with length of 50 meters were selected near the crossings marked in Čáslav to Kutná Hora direction as number 2 (km 279,223), 3 (km 281,182), 6 (km 283,747) and 8 (km 286,468). All surveyed sections were located in the vicinity and on both sides of these crossings according to the local conditions. Clearly marked position of crossings can be seen in Figure 25. Marking of sections was as follows:

1. P2U1 (km 279,150 – km 279,200) ... Figures 26 and 27
2. P2U2 (km 279,250 – km 297,300) ... Figures 26 and 27
3. P3U1 (km 281,100 – km 281,150) ... Figures 28 and 29
4. P3U2 (km 281,200 – km 281,250) ... Figures 28 and 29
5. P6U1 (km 283,675 – km 283,725) ... Figures 30 and 31
6. P6U2 (km 283,775 – km 283,825) ... Figures 30 and 31
7. P8U1 (km 286,400 – km 286,450) ... Figures 32 and 33
8. P8U2 (km 286,500 – km 286,550) ... Figure 32

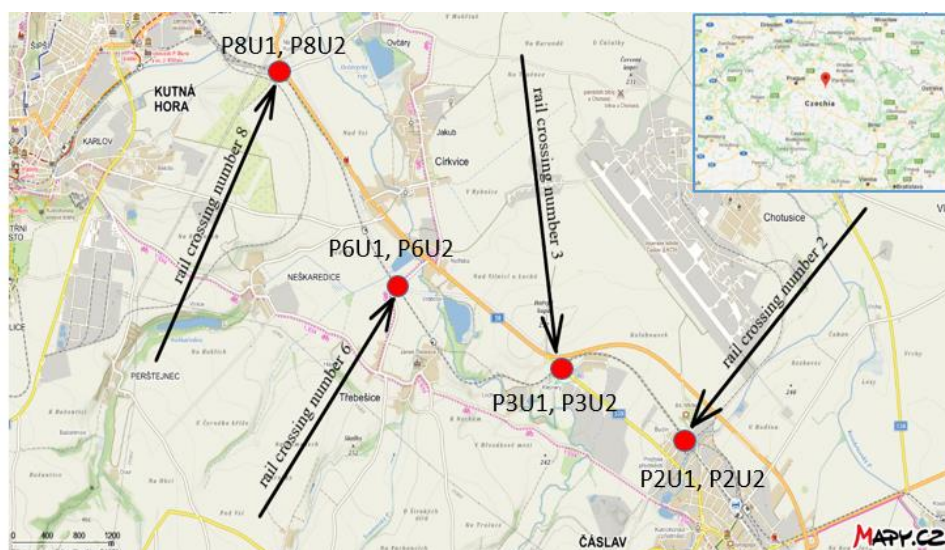


Figure 25 - Marking the measured rail crossings on the map (mapy.cz)



Figure 26 – Marking of survey sections in the area of railway crossing number 2

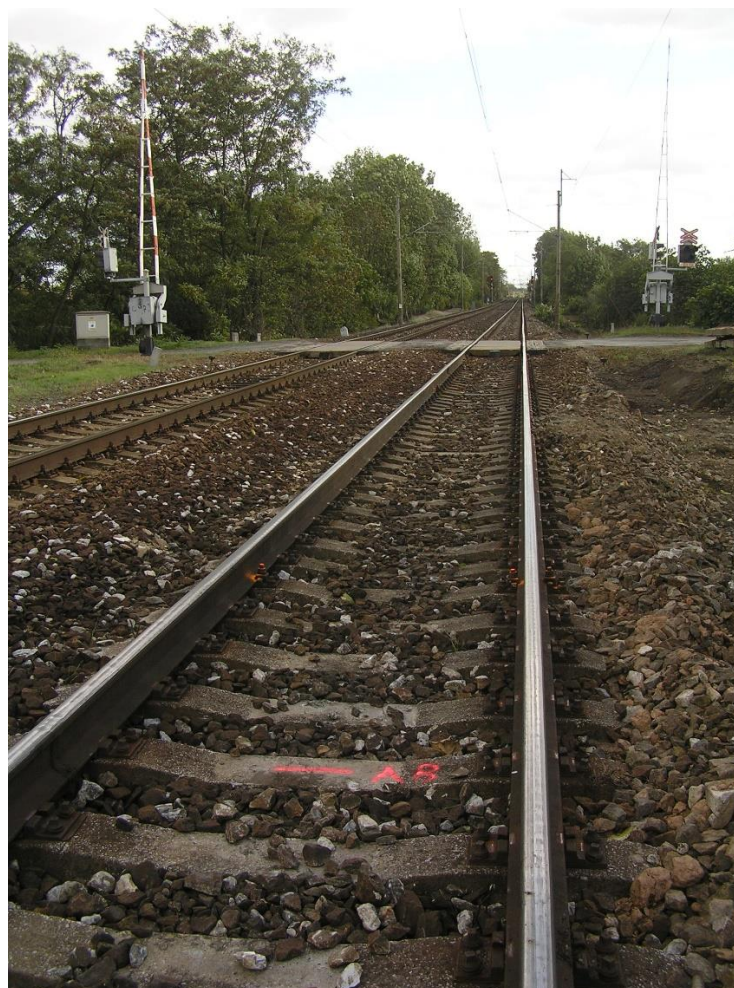


Figure 27 - The railway crossing number 2



Figure 28 - Marking of survey sections in the area of railway crossing number 3



Figure 29 - The railway crossing number 3

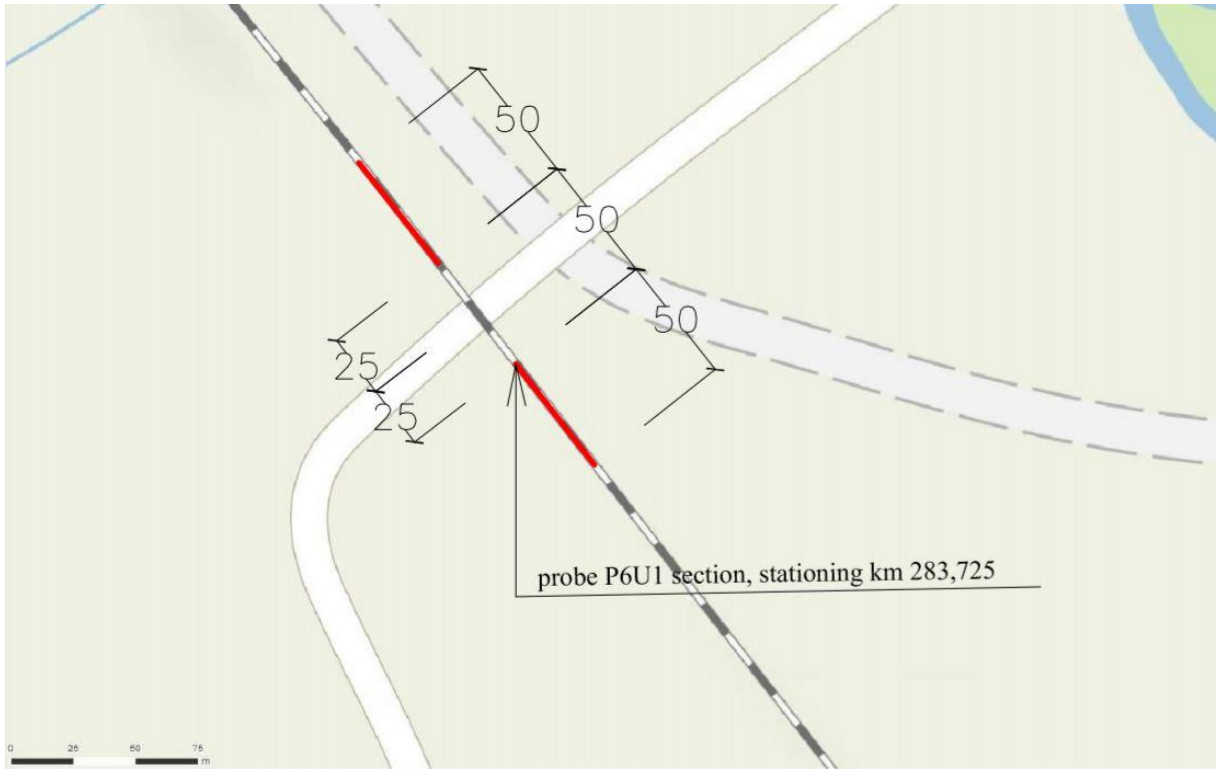


Figure 30 - Marking of survey sections in the area of railway crossing number 6



Figure 31 - The railway crossing number 6



Figure 32 - Marking of survey sections in the area of railway crossing number 8



Figure 33 - The railway crossing number 8

6.2. In-situ survey

Throughout the survey and more than 14 days prior to the survey, there were no precipitations in the site. From the point of view of temperature, the measurements were made in ideal conditions, as the temperature ranged from 20 to 25 ° C during the measurements. The measurements took place in the following phases: in the first, all the sections were measured before the construction work started; in the second phase, the measurements followed immediately after the cleaning of the ballast layer, before the tamping and other treatment of geometric parameters; and in the final phase, the final state was measured after all the work.

Thanks to state railway administrator (SŽDC) it was possible to process also GPR data collected in 2014 and 2017 by Technická ústředna dopravní cesty (TÚDC) of SŽDC. Weather conditions of this survey are not known to the author.

All surveyed GPR data (excluding SŽDC data) are included in Annex 5.

For the data processing purpose, these phases were numbered from 1 to 5 as follows:

1. In 2014 (SŽDC)
2. In 2017 (SŽDC)
3. Before the construction work started (12. 10. 2018)
4. Immediately after the cleaning of the ballast layer (17. 10. 2018)
5. The final state after all the construction activities (19. 10. 2018)

Initial setting of the GPR system

After the system was assembled and mounted on the survey cart, it was set up and calibrated in the above-mentioned K2 Fast Wave software. The calibration file can be seen in Annex 3. It was also necessary to calibrate the odometer to accurately determine the distance traveled, i.e. the stationing values in the profile. The calibration was performed by passing a reference line of a defined length. A reflector (aluminum sheet) was also placed at the beginning and end of each section to accurately identify radar stationing in collected radargrams.

The first step of K2 calibration process was to set the number, type, and position of the transmitters and receivers relative to the selected coordinate system and set the method of the assembly movement regime. After selecting the antennas, the time window (range) [ns] for each individual frequency was selected. The predicted propagation velocity [m/ns] in

the diagnosed medium was then entered. Based on these values, the maximum depth, from which the reflected signal could be recorded, was pre-calculated.

The number of samples per trace was set in the next phase. Each sample is a digital value that defines a portion of the trace. The more samples used, the more accurate the shape of the reflected wave is. Thus for a wider time window, a larger number of samples is required to maintain the accuracy of the trace. This value was set with respect to the velocity of the antennas and the required resolution (512, 1024 samples per trace). At the same time, the odometer factor was set, namely, the multiplication factor for the distance traveled. This factor multiplies the step given by the odometer resolution and results in the distance of each trace of the record (2 cm step for the performed survey). During SŽDC survey, the distance between traces was set in 2014 to 0.25 m and in 2017 to 1 m respectively.

GPR was then calibrated also in terms of so-called initial reflection, which was done after setting the antennas and fixing them to the survey position. Automatic calibration was performed when the antenna (survey cart) moved over the measured profile. The next step used was to set the gain method and values either automatically or manually, according to the operator's requirements.

Following these adjustments, a new measurement folder was created and the identification data was inserted. GPR system was ready to record data from the survey at this phase.

Survey procedure

The overall survey was time-consuming, physically and organizationally challenging as it was necessary to adapt to the regime and the schedule of the works on the site (annex 2). First complications with the survey have begun with traffic constraints on I/38 road and reconstruction of driveways and railway crossings leading to selected sections and crossings. Also to transport GPR system and survey cart between the individual crossings was quite complicated because of the necessity of warming-up the system and the time for preparation of the measuring apparatus, which together lasted more than 40 minutes each time. Therefore the way of transporting the cart with GPR in between the sections had to be considered carefully in relation to the ongoing work on the track. The GPR cart is a quite heavy and poorly transportable device, making it also difficult to quickly remove it from the track when necessary because of mechanization or other equipment passage. Because of the above-mentioned cases and due to GPR and Toughbook battery capacity, it was very

challenging to combine GPR warming-up and assembly, and transport with surveys. To find a place, where the batteries could be recharged was also not an easy task on the construction site.

As a part of the GPR calibration, it was necessary to measure the actual thickness of the gravel bed beneath the sleepers to enable the calculation of the RDP values and thereafter the propagation velocity of GPR signal in the ballast material. Due to the ongoing work, it was not possible to perform intended trenches on each of the measured sections. For this reason, 2 locations were selected where the state of the ballast layer seemed to be the most relevant for the entire track. The first probe (Figure 34), performed in the P6U1 section, stationing km 283,725 was extracted using a two-way excavator, which significantly accelerated and facilitated the work. The second probe (Figure 35), performed in P2U2 section, stationing km 279,251 was excavated manually, which was quite physically demanding. The removed material has been marked and transported to the Educational and Research Centre in Transport (ERDT) laboratories, where the necessary laboratory tests have been carried out.



Figure 34 – Extracting of the probe 1 material (P6U1)



Figure 35 – Excavating of the probe 2 material (P2U2)

Section stationing on the track was determined by stationing marks along the track, and the above-mentioned sections were laid out. To identify the beginning and end of the sections, the spots were marked either on the sleepers or on the rails with a reflective spray. Distances were measured using a digital measuring wheel. The beginning and end of the sections were also marked with aluminum foil, which is easy to distinctly identify on the radargrams.

The survey on each section was always performed in terms of stationing direction for the sake of clarity and consistency of processable information. In each of the sections, two surveys (B-scans) were made with different antenna orientations. In the first case (longitudinal direction of the antenna), it is very easy to identify the sleepers, but these elements partially cover the reflections from the interface on the bottom of the ballast layer. In the second case, the antenna was oriented diagonally. This antenna routing has been chosen to reduce the reflections of the sleepers and to improve the visibility of the reflected signals of the interface described above. Aim was to use transversal orientation also, but there was a limited time, because of ongoing construction works on the site.

The antenna orientation is schematically illustrated in Figure 36.

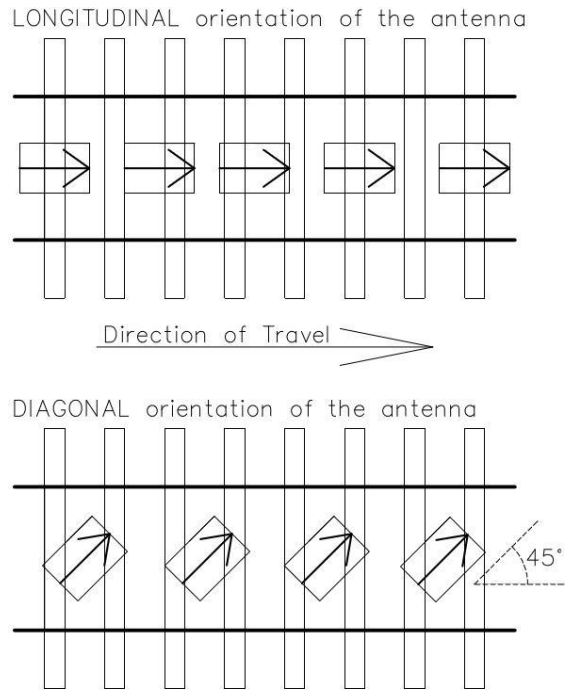


Figure 36 - Antenna orientation

6.3.Laboratory tests

An important part of the bachelor thesis within the complexity of the research was laboratory measurement, the aim of which was to determine the condition of the ballast layer material at selected sections. Due to the demanding schedule of construction work on the site, it was possible to obtain two samples only, which, however, are expected to describe the condition of the superstructure on the entire reconstructed section. Two sets of test were performed on obtained material: volume of air voids and sieve analysis. The weighing was carried out using calibrated KERN DE 60 K 20 (1-144703) scales with a maximum load rating of 60 kg and an accuracy of 20 g and the weighing of the samples obtained from the sieve analysis was performed on MATEST's scales. Sieve analysis was conducted on electro-mechanical sieve shakers AS 200 basic (1-144700) with orbital motion sifting of 80 rpm.

Sample # 1

The first sample was taken in the proximity of railway crossing number 6, more precisely in section P6U1 at stationing km 283,725. It is assumed that this sample condition matches the state of the ballast layer, approximately in the second half of the reconstructed section. By visual inspection and evaluation, it was observed that the railway body was not in ideal shape and condition, but there was not a necessity to perform cleaning by undercutters yet. This process took place anyway in this section due to the complexity of the reconstruction works. It

should be noted that this part of the reconstructed section was cleaned with a new German RM 900 VB unit, a high-performance ballast cleaner manufactured by Strabag Inc., in 2011.

In this dug probe, a total of 92,140 kg of aggregate was obtained, and the weight of ballast aggregate and fine fouling material was determined as can be seen in Table 10.

Table 10 – Total weight of aggregate with percent breakdown of coarse and fine material at sample #1

Aggregate weight of fraction 31,5-63 mm	79,240 kg	86 %
Aggregate weight of fraction less than 31,5 mm	12,900 kg	14 %
Total weight of aggregate	92,140 kg	100,00 %

By comparing the weight of fouling material (less than 31.5 mm) with the weight of aggregate (31.5 - 63 mm), the percentage of fouling according to formula 20 was determined to 14 %. Aggregate sample of fraction 31,5 - 63 from P6U1 can be seen in Figure 37.

$$\text{percentage of fouling} = \frac{\text{total weight of material}}{\text{weight of fine fouling material}} \quad (20)$$



Figure 37 - Aggregate sample of fraction 31,5 - 63 from P6U1.

From the 31,5 - 63 fraction, 56,12 kg of aggregate was taken from which the volume of air voids was roughly determined by filling of free space with water. The total volume of measuring

container was 40 l, which was filled with aggregate and free space was filled up with water (17.05 l). The resulting volume of air voids was found to be 42,6 %.

Sieve analysis according to ČSN EN 933-1 (721183) - Testing of geometric properties of aggregates - Part 1: Determination of grain size - Sieve analysis (with exception of weight of sieved material 1 kg for each test, and other minor discrepancies), was performed for fine material (smaller than 31,5 mm). The test was performed on three samples with 1 kg weight of each. The results are shown in Table 11. Used sieving test devices can be seen in Figure 38.

Table 11 - Sieve analysis of three samples of fine material from the P6U1 section

Fraction - sieve opening size	Weight of sample #1 fractions (g)	Weight of sample #2 fractions (g)	Weight of sample #3 fractions (g)
>6,3 mm	790,3	752,5	796,2
5,6 – 6,3 mm	2,1	2,9	1
4,5 – 5,6 mm	26,3	25,3	28,4
3,55 – 4,5 mm	24,6	26,3	23,1
2,5 – 3,55 mm	27,1	31,8	25,4
2 – 2,5 mm	12,9	16,9	12,8
1,6 – 2 mm	12,3	15,7	11,9
0,5 – 1,6 mm	39,3	53,5	37,5
0,25 – 0,5 mm	21,9	27,3	19,4
0,063 – 0,25 mm	33,4	36,7	30,5
< 0,063 mm	7,9	9,3	6,5
Total	998,1	998,2	992,7



Figure 38 - Electro-mechanical sieve shakers AS 200 basic (I-144700)

Values from Table 11 were averaged (Table 12) and a grain curve was generated from these results (Figure 39 - Figure 39).

Table 12 – Average sieve analysis values of fine material from the P6U1 section

Fraction - sieve opening size (mm)	%
6,3	100,00
5,6	21,74
4,5	19,07
3,55	216,59
2,5	13,77
2	12,36
1,6	11,01
0,5	6,65
0,25	4,36
0,063	0,99
bottom residue	0,20
Average total weight	996,33 g

The final phase of laboratory test was comparing of sieving test result with fouling index by equation (18). Default values were used from the grain curve (Figure 39). Grain curves for individual tests are contained in annex 4. Fraction 4,75 mm had value 20 % and 0,075mm had value 1,05%. Thus the fouling index is 21,05 %, which corresponds to fouled ballast according to Table 2.

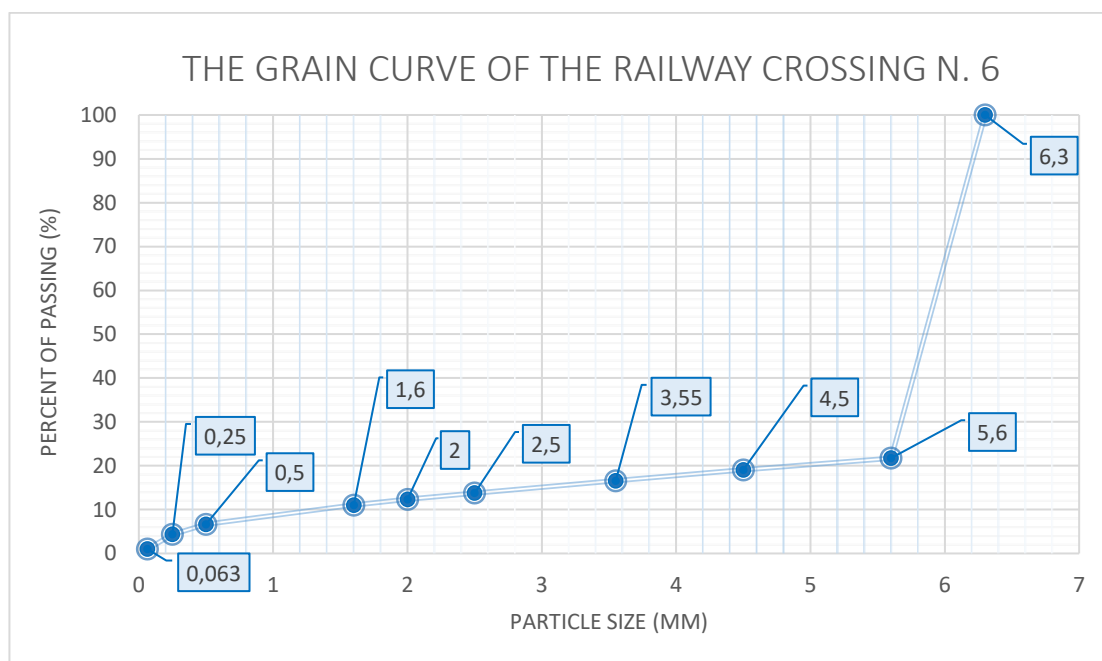


Figure 39 - Grain curve for the sample from P6U1 section

Sample # 2

The second sample was taken in the proximity of railway crossing number 2, more precisely in P2U2 section at stationing km 279,251. Even visually, it was clear that the railway body was not in good shape and condition and there was a necessity to perform cleaning by undercutters. It should be noted that this part of the rail was cleaned by the older type RM 79 unit of Hrochostroj a.s. company. The location, where the second sample was obtained was very atypical in terms of the absence of water drainage ditches. This condition raised the initial question of whether this place would be abnormally polluted by the insufficient drainage of the section.

In this dug probe, a total of 47,331 kg of aggregate was obtained, and the weight of ballast aggregate and fine fouling material was determined as can be seen in Table 13.

Table 13 - Total weight of aggregate with percent breakdown of coarse and fine material at sample #2

Aggregate weight of fraction 31,5-63 mm	31,551 kg	66,66 %
Aggregate weight of fraction less than 31,5 mm	15,780 kg	33,34 %
Total weight of aggregate	47,331 kg	100,00 %

By comparing the weight of fouling material (below 31,5 mm) with the weight of aggregate (31,5 - 63 mm), the percentage of fouling according to formula 20 was determined to 33,34 %.

This confirms the presumption based on a visual inspection that cleaning was necessary in this section due to the absence of drainage facilities.



Figure 40 – Aggregate sample of fraction 31,5 - 63 from P2U2 section.

From the 31,5 - 63 fraction, 29,710 kg of aggregate was taken from which the volume of air voids was roughly determined by filling of free space with water. The total volume of measuring container was 20 l, which was filled with aggregate and free space was filled up with water (8,066 l). The resulting volume of air voids was found to be 40,33 %.

Sieve analysis according to ČSN EN 933-1 (721183) - Testing of geometric properties of aggregates - Part 1: Determination of grain size - Sieve analysis (with exception of weight of sieved material 1 kg for each test, and other minor discrepancies), was performed for fine material (smaller than 31,5 mm). The test was performed on three samples with 1 kg weight of each. The results are shown in Table 14.

Table 14 - Sieve analysis of three samples of fine material from the P2U2 section

Fraction - sieve opening size	Weight of sample #1 fractions (g)	Weight of sample #2 fractions (g)	Weight of sample #3 fractions (g)
>6,3 mm	529	605	598,9
5,6 – 6,3 mm	0,4	0,5	0,5
4,5 – 5,6 mm	13,6	15	14,5
3,55 – 4,5 mm	20,3	17,6	19
2,5 – 3,55 mm	30,9	29,1	30,3
2 – 2,5 mm	22,7	19,5	20,2
1,6 – 2 mm	27,7	23,1	21,6
0,5 – 1,6 mm	146,7	122,7	114,8
0,25 – 0,5 mm	80,1	65,2	63,4
0,063 – 0,25 mm	89,6	68,2	70,2
< 0,063 mm	19,4	19,4	20,8
Total	1003,1	985,3	974,1

Values from Table 14 were averaged (Table 15) and a grain curve was generated from these results (Figure 39 - Figure 41).

The final phase of laboratory test was comparing of sieving test result with fouling index by equation (18). Default values were used from the grain curve (Figure 41). Grain curves for individual tests are contained in annex 4. Fraction 4,75 mm had value 40 % and 0,075mm had value 1,78%. Thus the fouling index is 41,78 %, which corresponds to highly fouled ballast according to Table 2.

Table 15 - Average sieve analysis values of fine material from the P2U2 section

Fraction - sieve opening size (mm)	%
6,3	100
5,6	41,06
4,5	39,59
3,55	37,65
2,5	34,58
2	32,46
1,6	30,00
0,5	16,93
0,25	9,83
0,063	2,08
bottom residue	0,05
Average total weight	979,97 g

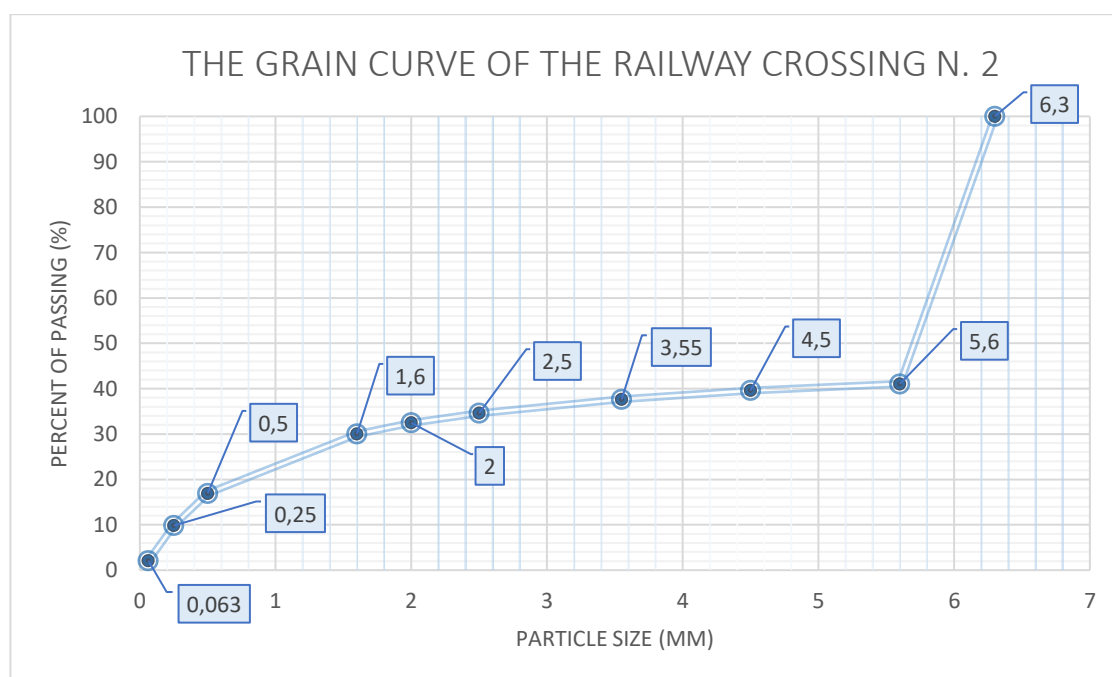


Figure 41 - Grain curve for the sample from P2U2 section

7. Data processing and outputs

In this chapter, the processing steps used to utilize measured data are described. The main goal was to determine the signal velocity and relative permittivity of the ballast layer in each surveyed sections of the picked railway line. It should be noted, that although similar approaches were chosen for each survey stage, there were small differences in processing steps settings due to surrounding conditions and differences in the ballast layer itself. Also, it needs to be pointed out, that there is not the only correct approach to process GPR data, and there is always the subjective opinion of person processing the data involved. Therefore the operator should have always some experience with GPR data evaluation and as much information about surveyed subject and surroundings condition he/she can obtain, to ensure the most accurate and valid data processing.

The interpretation of GPR data is affected by many factors related to the complexity of the subsurface. Accepting the fact, that GPR measurements are dense enough for the delineation of the target and that the optimum frequency is selected, processing should enhance the GPR signal, providing sufficient data for interpretation. The GPR data processing system consists mainly of time-zero corrections, dewow, band-pass filtering, spatial filters and gain [11].

7.1.Data post-processing

Data recorded with GPR always contains less or more noise (also referred to as reverberations, interference, multiples, clutter, spikes, snow). The data is also recorded with an imprecise determination of the signal propagation velocity. Therefore, the record must first be modified before the data interpretation, to amplify the essential phenomena and to minimize the undesirable effects. These activities are called post-processing.

Noise or interference in GPR may be caused not only by the GPR itself and its components but also by interference from cell phones, radio transmitters, wireless internet and other electronic devices that work in frequencies band used by GPRs [133]. The amount of these sources of interference causes a considerable complexity of data processing and, in some cases, makes interpretation impossible. In the literature, interferences are mostly divided into noise and clutter. [5]. Noise is mainly caused by GPR interference with other sources of EM fields that affect the device during data collection. Clutter, on the other hand, presents unwanted reflections and interferences of the GPR signal, either inherent (GPR) or external (independent) caused by reflections and refraction of the signal in the measured media. To minimize clutter

and noise, filters are employed. Filters can be generally divided into time filters (applied over individual tracks in the time domain) and spatial filters (application in a range of tracks in the selected interval of time). These are often combined into advanced two-dimensional filters. Simple mean, simple median, low-pass or high-pass, band-pass filters, and simple average, average subtraction, background removal filters are examples of commonly used filters.

In this thesis, a **horizontal and vertical scale setting** was used as the first step of data processing. Also other adjustments related to the signal velocity and the stationing of significant reflections were made including settings of the desired time range. Viewing, formatting, and saving options were set after. Sorting the measured data, dividing the measuring profiles and selecting sections to be processed was also performed. The **“envelope”** function has often been used to confirm the correct identification of the surface reflection. (Hilbert's transformation). However, this step was not included in the resulting processing, because there occurred an undesirable distortion of amplitude values.

A dedicated processing scheme was used considering the spacing of the sleepers (SB 8 type) and the width of the sleepers (SB 8 type) such that RDP calculations will be based on the extracted traces located exactly in the cribs which allowed us avoiding the effects of the sleepers on the GPR responses. In order to realize this situation, the **“extract traces”** function in edit traces/trace-ranges submenu was used. A text file was created containing calculated trace intervals as the beginning and the end of each crib. Those intervals were determined according to the observed sleepers from the radargrams, spacing of sleepers and the width of the sleepers. Subsequently, this text file was loaded to this processing step settings, and only the crib regions were extracted that way.

The **“move start time”** (zero timing) function in static correction/muting submenu was used to adjust surface reflection to shift the first reflection from the surface to the start (zero value) of the time axis of the GPR data record (the reflection from the surface is shifted to zero depth).

Additionally, for air-coupled antenna, **“correct max phase”** function in static correction submenu was used to compensate antenna bumping and make the surface reflection horizontal.

The next step was to remove the inherent nonlinear noise (wow noise) which is related to the characteristics of the used antenna by using a 1D so-called **“dewow filter”**. With this filtering, the low-frequency components of the signal of each trace, that are caused by EM induction in the apparatus (internal noise of the system), were removed using the running average. The value

used for settings this filter is limited by the frequency. For the used 2 GHz frequency, a maximum of 0.5 ns, for 900 MHz a maximum of 1.1 ns and a maximum of 2.5 ns for 400 MHz was set.

Another step used was to remove the background signal (using a so-called “**background removal filter**”) in the form of horizontal bars in the record of measured profiles, which is one of the most common data processing methods. This phenomenon is caused by the "ringing" of some antennas, which may be caused by either system noise or external EM interference, but also reflections from surface objects that have the same distance from the antenna as the evaluated reflections from the diagnosed material. This type of filter increases the so-called noise to signal ratio and eliminates the waves (reflections) that appear in the record in the long term.

Due to the fact the signal diffuses in the form of a cone and is damped during the passage through the material, the increasing depth reduces the amplitude of the reflection. Anomalies at a greater depth will, therefore, produce a smaller amplitude than the same anomaly located closer to the surface. There are several **signal amplification options**. These include a constant increment, exponential increment, or so-called Automatic Gain Control (AGC). All amplification functions use a certain multiplication factor applied to the selected radargram interval. It should be emphasized that when the gain function is applied to areas with very low or near zero reflections, there is a significant increase in noise.

In addition, “**bandpassbutterworth**” (Vertical Filtering in Time Domain) was used mainly to eliminate high-frequency noise. The range of this filter is set with two boundary frequencies (low-cut and high cut frequency). The frequency limits are determined according to the spectrum of the received antenna signal, and the GPR record then uses only the signals in between this frequency interval after use.

Also “**running average**” for 5 traces in 2D filter submenu to better display horizontal interfaces (to highlight horizontal consistent energy and avoid trace dependent clutter) was used.

After removing the noise, in some cases, the removal of multiple reflections (multiples) may be applied. Multiples were caused by the repeated reflection of the signal between the detected anomaly and the surface or between layers of the material, and cause the overlapping or suppression of important reflections that are recorded at the same time. Such record may lead to erroneous interpretations, however, these multiple reflections can be distinguished by their

regular spacing. In some cases, interference of antennas may also lead to multiple reflections in an area known as near field zone. The process used to remove multiples is called deconvolution (predictive deconvolution) [134], which can be interpreted as solving/decomposing the multiple reflections into basic elements. It is a process of restoring the original shape of the reflected waves. In Reflex W, this algorithm is called Suppress multiples.

7.2. Data interpretation and outputs

The output of the data processing phase was the radargram (B-scan) of the ballast layer and its base layer with the display of the interfaces and the local inhomogeneity for each track section and each measurement phase. In the Point Mode view, where the individual sleepers could be distinguished, the traces located between the sleepers were selected (as described above) and therefore their footprint was not affected by the reinforcement in the sleepers. The signal thus penetrated only through the ballast layer. The position of ballast layer/base layer interface was obtained from the construction drawings, according to the cleaning machines settings and verified by performing the trenches with a subsequent sampling of the ballast layer material for laboratory testing purposes. Point mode record can be seen in Figure 42.

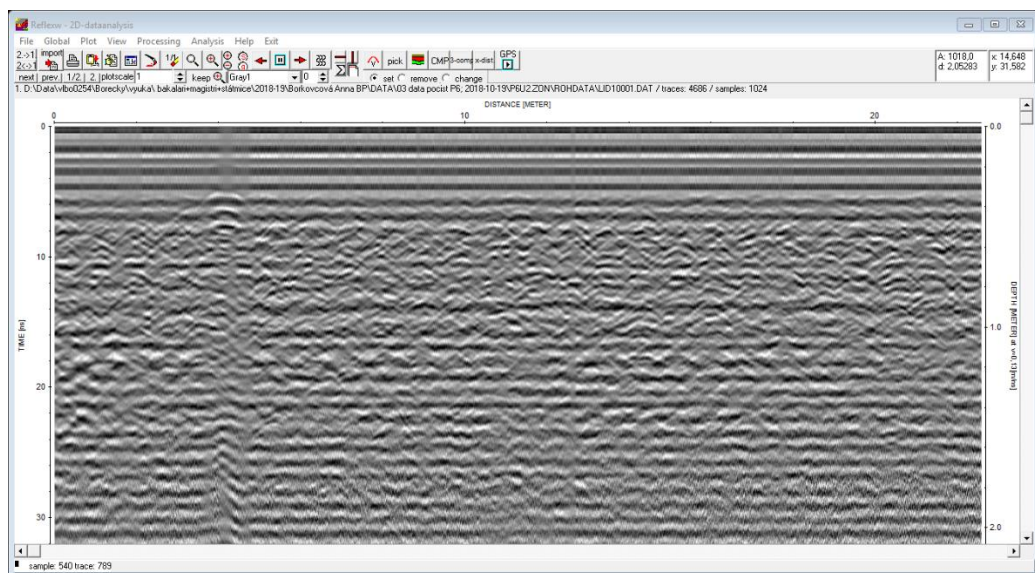


Figure 42 - Point Mode display in ReflexW

After identifying desired traces, amplitude values for reflection from the surface and ballast layer/base layer interface were subtracted together with their twt values for each trace. This was done in the Wiggle Mode display. From the difference of the twt values and from the knowledge of the depth of the interface, the propagation velocity of the signal in the ballast layer was

computed. Subsequently, the RDP value was calculated. Considering the possibility of local inhomogeneity and interferences, RDP values for individual sections and phases were determined as the arithmetic mean. Wiggle mode record can be seen in Figure 43. The values obtained here are presented in the form of tables for individual sections and survey phases. The number of tracks and the length of the section for each phase is also shown. The original data sets are listed in Annex 5.

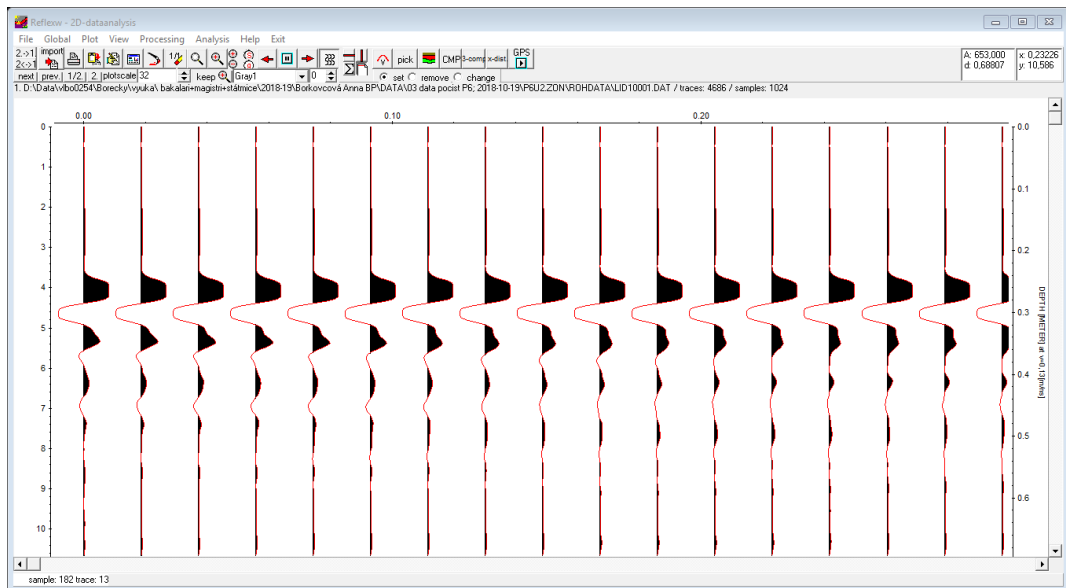


Figure 43 - Wiggle Mode display in ReflexW

The following tables (Table 16 and Table 17) contain a basic statistical evaluation of RDP values and EM signal velocity values for the two most important phases of all survey, i.e. phase 3 – before cleaning stage, and phase 5 - after finishing all construction activities. Data is listed for all measured sections and all frequencies used. The tables contain maximum (RDPmax), minimum (RDPmin) and average (RDPave) RDP values including standard deviation (STD_RDP) values, and also maximum (EMWVmax), minimum (EMWVmin) and average (EMWVave) EM wave velocity values including standard deviation (STD_EMWV) values of this variable too. The number of evaluated samples for all sections and all frequencies is indicated in the most right column. In total, 228 traces were evaluated in each stage. In case of stage 3, an average STD_RDP equals to 2,1 % of average RDPave, and STD_EMWV equals to 1,0 % of average EMWVave. In case of stage 5, these values are 3,9 % for RDP and 2,2 % for EMWV. Average standard deviation value for EMWV than represents at maximum (the most unfavourable case) 3,46 % of the range of fouling interval suggested in Table 18 contained in chapter 8.

Table 16 – Statistical evaluation of RDP and signal velocity values of stage 3 survey

	Stage 3 - Before Cleaning									
	Freq. (GHz)	RDPave	RDPMax	RDPMin	STD_RDP	EMWVave	EMWVmax	EMWVmin	STD_EMWV	# of samples
P2U1	0,4	3,65	3,75	3,46	0,080	15,70	16,13	15,48	0,180	10
	0,9	3,65	3,92	3,40	0,165	15,70	16,28	15,15	0,355	10
	2,0	4,31	4,36	4,26	0,030	14,45	14,53	14,37	0,051	7
P2U2	0,4	4,92	5,15	4,70	0,156	13,52	13,84	13,22	0,215	8
	0,9	4,34	4,41	4,19	0,074	14,41	14,65	14,29	0,125	10
	2,0	4,26	4,31	4,21	0,021	14,53	14,61	14,45	0,035	10
P3U1	0,4	4,70	4,92	4,48	0,148	13,84	14,18	13,52	0,215	9
	0,9	4,34	4,48	4,19	0,081	14,41	14,65	14,18	0,134	10
	2,0	4,29	4,31	4,24	0,025	14,49	14,57	14,45	0,042	10
P3U2	0,4	3,85	4,48	3,65	0,318	15,29	15,70	14,18	0,581	8
	0,9	4,26	4,34	4,12	0,084	14,53	14,77	14,41	0,145	10
	2,0	4,29	4,34	4,26	0,020	14,49	14,53	14,41	0,033	10
P6U1	0,4	4,85	5,02	4,68	0,094	13,62	13,87	13,39	0,131	10
	0,9	4,68	4,85	4,35	0,154	13,87	14,38	13,62	0,237	10
	2,0	4,35	4,41	4,27	0,042	14,38	14,51	14,29	0,069	10
P6U2	0,4	3,31	3,44	3,18	0,073	16,48	16,83	16,18	0,185	10
	0,9	4,43	4,51	4,19	0,097	14,25	14,65	14,12	0,160	10
	2,0	4,43	4,46	4,33	0,055	14,25	14,42	14,20	0,090	9
P8U1	0,4	3,35	3,63	3,29	0,108	16,38	16,55	15,75	0,253	7
	0,9	3,84	4,06	3,77	0,088	15,31	15,46	14,89	0,171	10
	2,0	3,89	3,91	3,86	0,015	15,22	15,26	15,17	0,030	10
P8U2	0,4	3,73	3,85	3,66	0,044	15,53	15,68	15,28	0,091	10
	0,9	3,98	4,06	3,84	0,071	15,03	15,31	14,89	0,137	10
	2,0	3,91	3,93	3,86	0,020	15,17	15,26	15,12	0,038	10

Table 17 - Statistical evaluation of RDP and signal velocity values of stage 5 survey

	Stage 5 - Final									
	Freq. (GHz)	RDPave	RDPMax	RDPMin	STD_RDP	EMWVave	EMWVmax	EMWVmin	STD_EMWV	# of samples
P2U1	0,4	2,20	2,36	2,15	0,070	20,21	20,44	19,53	0,312	7
	0,9	2,68	2,74	2,63	0,037	18,31	18,50	18,12	0,128	9
	2,0	3,44	3,50	3,40	0,033	16,18	16,28	16,03	0,078	8
P2U2	0,4	1,80	1,87	1,69	0,058	22,36	23,08	21,97	0,370	8
	0,9	2,88	2,98	2,77	0,070	17,69	18,01	17,37	0,217	10
	2,0	3,10	3,24	3,07	0,047	17,03	17,12	16,68	0,125	10
P3U1	0,4	2,75	2,85	2,57	0,100	18,09	18,70	17,76	0,334	10
	0,9	2,52	2,63	2,31	0,097	18,90	19,75	18,50	0,372	10
	2,0	3,50	3,57	3,42	0,043	16,03	16,23	15,88	0,098	10
P3U2	0,4	2,72	2,97	2,47	0,142	18,18	19,11	17,40	0,477	10
	0,9	2,57	2,63	2,15	0,181	18,70	20,44	18,50	0,734	9
	2,0	3,11	3,23	3,09	0,043	17,00	17,07	16,69	0,114	10
P6U1	0,4	2,33	2,45	2,04	0,138	19,66	20,99	19,17	0,611	10
	0,9	2,57	2,89	2,21	0,209	18,71	20,17	17,65	0,791	10
	2,0	2,80	2,89	2,76	0,043	17,92	18,06	17,65	0,137	8
P6U2	0,4	2,27	2,57	2,04	0,146	19,91	20,99	18,71	0,631	10
	0,9	3,37	3,58	3,23	0,109	16,35	16,70	15,85	0,262	10
	2,0	2,82	2,91	2,74	0,052	17,85	18,13	17,58	0,164	10
P8U1	0,4	3,63	3,70	3,49	0,070	15,75	16,06	15,60	0,152	10
	0,9	2,66	3,03	2,54	0,146	18,41	18,83	17,25	0,479	10
	2,0	2,72	2,90	2,56	0,118	18,19	18,76	17,62	0,392	10
P8U2	0,4	1,99	2,20	1,89	0,115	21,28	21,85	20,23	0,592	10
	0,9	2,04	2,31	1,55	0,256	21,01	24,09	19,74	1,444	9
	2,0	1,94	2,33	1,79	0,169	21,56	22,44	19,66	0,887	10

8. Results and Discussion

Based on the literature review values, the intervals for the level of ballast fouling were defined. These intervals shown in Table 18 are as follows:

Table 18 - Determination of fouling intervals

Fouling Category	Lower limit of velocity (cm/ns)	Upper limit of velocity (cm/ns)	Lower limit RDP	Upper limit RDP
Clean	16	-	-	3,52
Slightly fouled	13	16	3,52	5,33
Highly fouled	9	13	5,33	11,11
Unfit for traffic	-	9	11,11	-

There were no significant changes or trends in the resultant RDP/signal velocity values for the diagonal and longitudinal orientation of the antennas during radar evaluation. However, the measurement data from both methods were used to verify each other and compare the positions of the determined interfaces and sleepers, which was the initial reason for the measurement in more ways.

The comparison and assessment of changes in the assessed indicators were first performed in each section separately for all measurement phases and subsequently, the sections were compared with each other. The final phase was to compare the work of the undercutters on pre-determined sections. The measurement phase marking used in this chapter has been described in chapter 6.2.

Frequencies of 2 GHz, 900 MHz, and 400 MHz were used to the mutual comparison of acquired data and because of the limited reach of the 2GHz antenna and more attenuated higher frequencies. All calculated RDP values for each section and measurement phase are listed in Table 19. Here it is clearly seen the difference in results with respect to frequencies and antennas used. Although the results obtained with antennas of different frequencies were dissimilar, the explicit dependency of signal velocity/RDP on central frequency was not found (from measured data, or from the literature). For this reason, the other following tables and graphs give averaged values for the frequencies used.

Table 19 - RDP values for each section and survey stage (colors correspond to Table 18)

SECTIONS	#1		#2		#3				#4				#5 OR #6			
	SZDC		SZDC		THE RDP BEFORE CLEANING PROCESS				THE RDP AFTER CLEANING PROCESS				THE RDP AFTER HANDING OVER THE CONSTRUCTION			
	23.09.2014	400 MHz GSSI	29.08.2017	401 MHz GSSI	12.10.2018	400 MHz IDS	900 MHz IDS	2 GHz IDS	17.10.2018	400 MHz IDS	900 MHz IDS	2 GHz IDS	19.10.2018 + 22.10.2018	400 MHz IDS	900 MHz IDS	2 GHz IDS
P2	U1	4,311	4,391	4,391	3,653	3,653	4,311	4,133	3,090	3,418	4,133	2,204	2,684	2,204	2,684	3,439
	U2	4,311	4,391	4,391	4,922	4,335	4,264	4,420	3,090	3,787	4,420	1,800	2,877	1,800	2,877	3,102
P3	U1	4,430	4,718	4,718	4,698	4,335	4,288	3,454	2,877	2,722	3,454	2,749	2,519	2,749	2,519	3,503
	U2	4,430	4,718	4,718	3,852	4,264	4,288	2,964	2,935	3,357	2,964	2,722	2,574	2,722	2,574	3,114
P6	U1	5,676	6,188	6,188	4,849	4,681	4,352	3,415	3,727	4,292	3,415	2,329	2,571	2,329	2,571	2,803
	U2	6,676	5,626	5,626	3,315	4,433	4,433	2,235	2,560	2,820	2,235	2,270	3,368	2,270	3,368	2,824
P8	U1	5,100	5,239	5,239	3,353	3,839	3,887	-	-	-	-	3,626	2,656	3,626	2,656	2,720
	U2	5,239	5,560	5,560	3,731	3,983	3,911	-	-	-	-	1,988	2,040	1,988	2,040	1,936

Assessment in each section separately for all measurement phases

In Figure 44, Figure 45, Figure 46, Figure 47, the velocities for each individual measured section (P2 - P8) are recorded at each measurement stage (as described in chapter 6.2).

Within the evaluation of the section P2 signal velocity, the value better than expected were observed. On the basis of the initial visual observation of this non-typical section, very poor results were assumed due to the absence of ditches or any other drainage facility in P2U2, thus also very poor ballast layer condition was expected. The calculated values are surprising as the velocity values are relatively high, even in the pre-cleaning state. Here, it can be assumed that, despite the substantial proportion of fine particles (33.34 %) detected by laboratory tests (sample #2), there is no water present in the track bed. It is clear that during the construction process the track bed condition improved, which is underlined in Figure 44. Between phases 3 and 5, the signal velocity increased by 19.3% in the P2U1 section and by 34.4% in the P2U2 section.

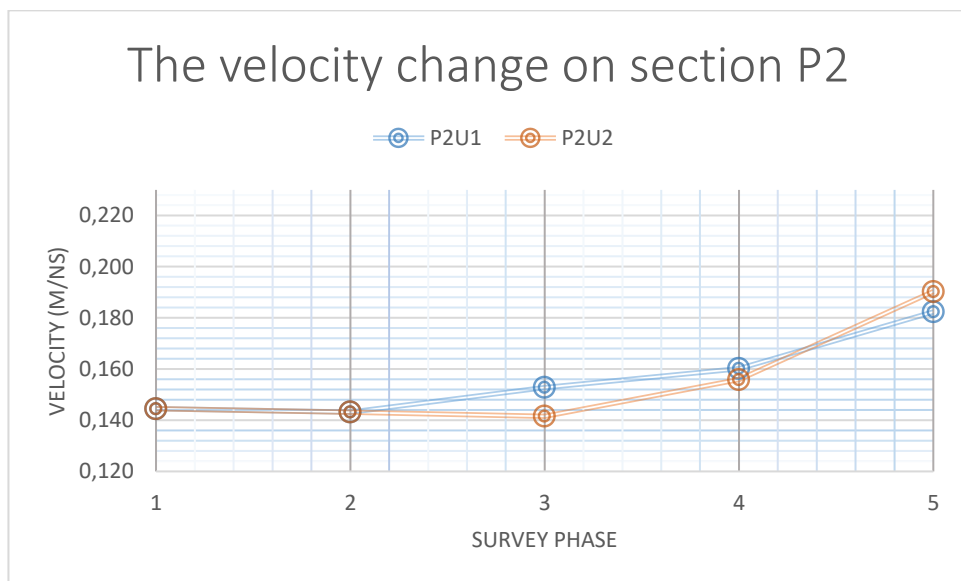


Figure 44 - The change of velocity during lifecycle of the railway track on section P2

A relatively good condition of the ballast layer was assumed in the P3 section, which was confirmed both by the SŽDC measurement and own measurement. Drainage facilities was fully functional. It is clear that during the construction process the track bed condition improved, which is underlined in Figure 45. Between phases 3 and 5, the signal velocity increased by 24.1 % in the P3U1section and by 21.6 % in the P3U2 section.

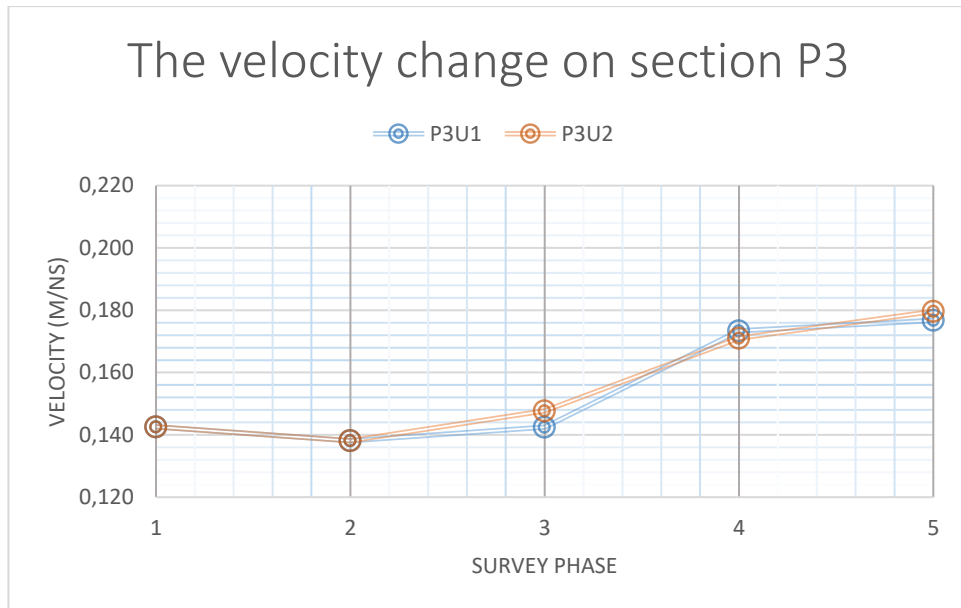


Figure 45 - The change of velocity during lifecycle of the railway track on section P3

The P6 section was characterized by the presence of undesirable vegetation (especially in P6U1), which indicates increased humidity in the railway body. This can be caused by poor drainage of the superstructure (poor function of a drainage facility) or by the presence of muddy places or presence of water below the railway body. Although the proportion of fine particles detected by laboratory tests (14%) is not higher in this section than in the section P2, water was probably present in the track bed, as confirmed by the velocity/RDP values measured before cleaning stage. This would be confirmed by the observation of strong reflections at greater depths at P6U1, which may be caused just by the presence of aquifer places. It is clear that during the reconstruction process the ballast layer condition improved, which is underlined in Figure 46. Between phases 3 and 5 the signal velocity increased by 34.4% in the P6U1 section and by 20.3% in the P6U2 section. It is necessary to point out the non-standard trend between phases 3 to 5. More specifically, a higher signal velocity value is observed in phase 4 than in phase 5. It is possible that by combining the use of the RM 900 VB undercutter and Unimat 08-275/3S tamping machine, the ballast layer was hoed (hence the bulk density was reduced). It is important to take into account the exact moment of GPR measurement (if the measurement was taking place in the phase immediately after cleaning or during tamping cycles), which could not be precisely influenced by the schedule.

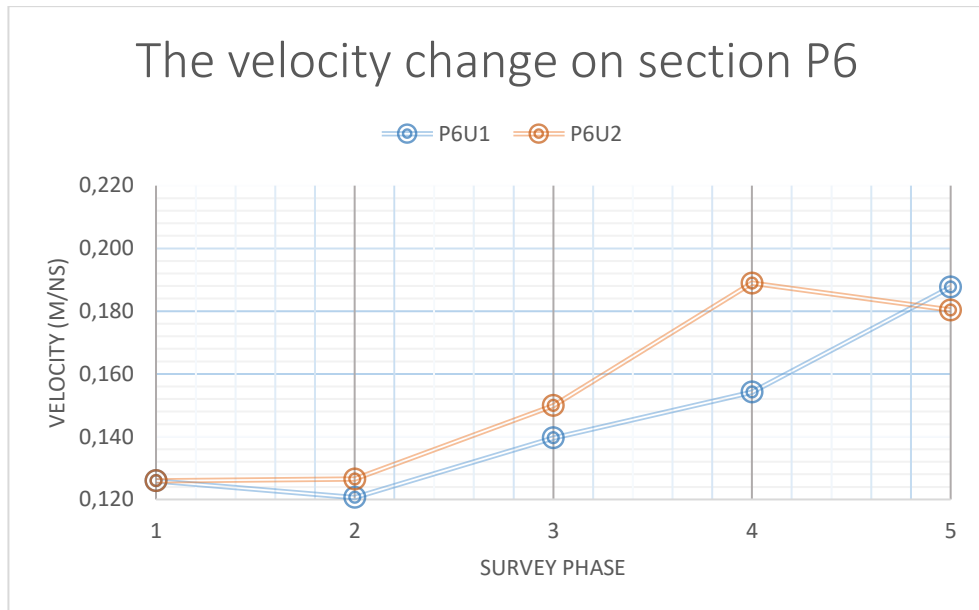


Figure 46 - The change of velocity during lifecycle of the railway track on section P6

In section P8, as well as in section P6 (although to a lesser extent), there was also vegetation observed. It is clear that during the construction process the track bed condition improved, as shown in Figure 47. Between phases 3 and 5 the signal velocity increased by 11.6% in the P8U1 section and 39.6% in the P8U2 section, which is the highest observed difference. This can be explained by draining the water due to ballast layer cleaning.

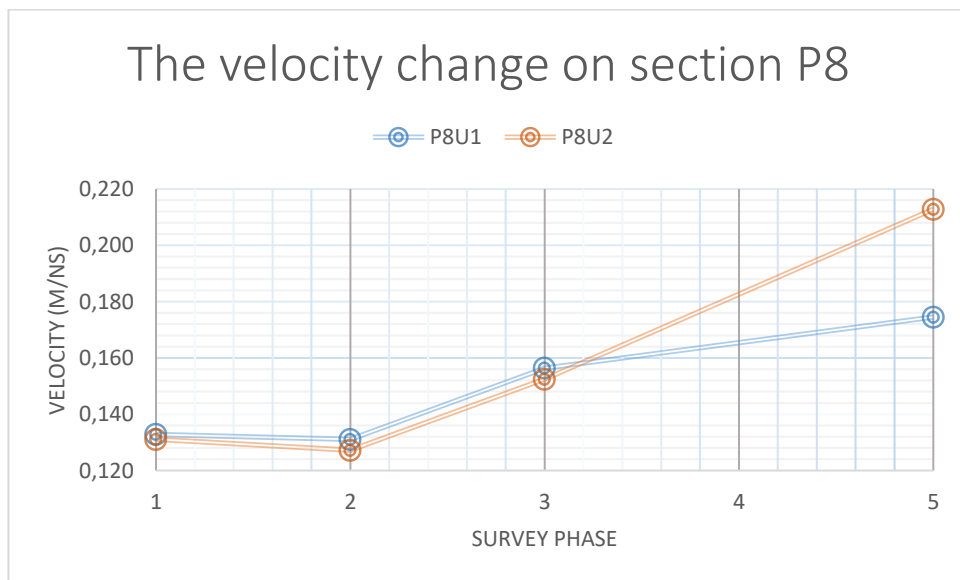


Figure 47 - The change of velocity during lifecycle of the railway track on section P8

No significant changes were observed between phases 1, 2 and 3, at P2 and P3, but were more obvious at P6 and P8 – this may be due to generally water content in case of P6 and P8. This

may be due to assumed higher water content in case of crossings 6 and 8 - here the different signal attenuation depending on the frequency used should be taken into account. Changes observed between survey stages 3 (before cleaning) and 5 (final state) corresponds and even exceeds literature values, which may be caused by performing a survey in final phase directly after the end of the cleaning process. Stage 4 data serve as complementary values to describe the ballast cleaning process but are not examined in detail, since all work at this stage involves a large number of non-quantifiable processes in the track bed itself (repeated vertical alignment change and re-addition of new material during each phase tamping).

Mutual comparison of all sections

In Figure 48, Figure 49, Figure 50, Figure 51, Figure 52, the signal velocity values are displayed for each individual measurement phase (1-5) on each section (as marked in chapter 6.2).

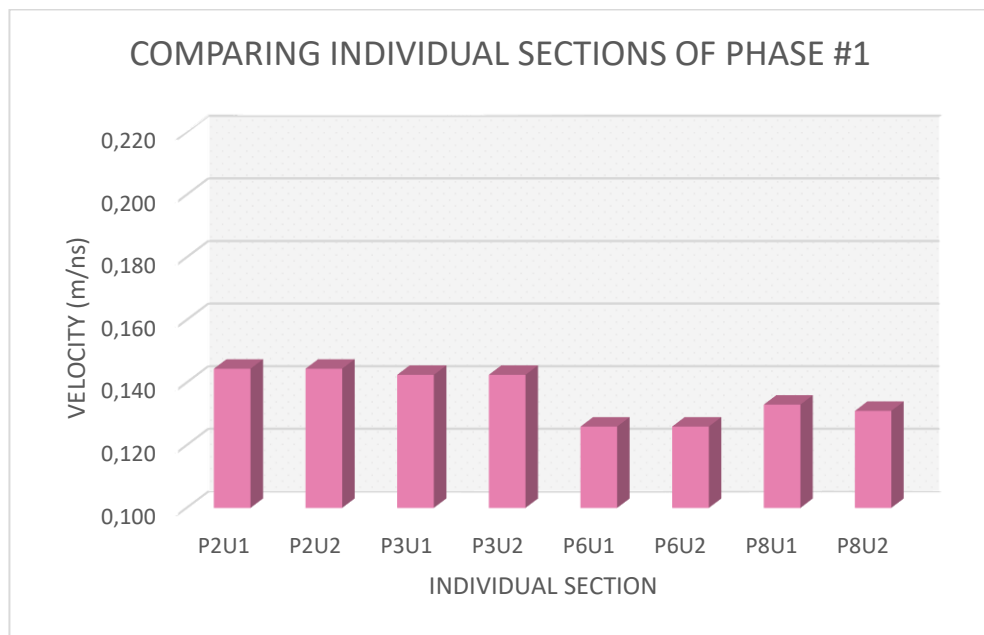


Figure 48 - Comparison of signal velocity in each section of the first phase

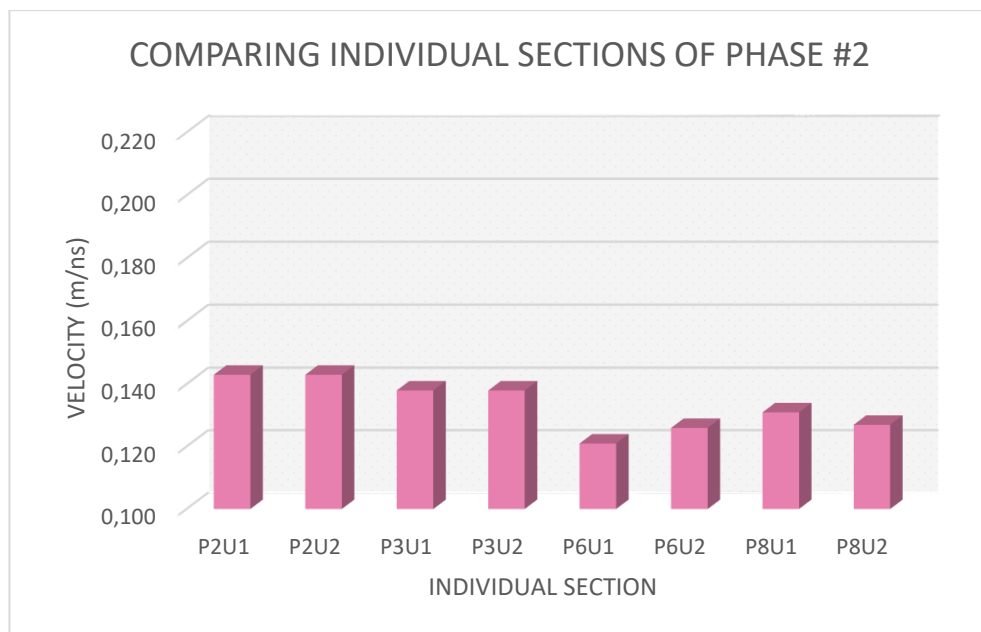


Figure 49 - Comparison of signal velocity in each section of the second phase

Differences between the values measured by SŽDC (# 1, # 2) and my own survey (# 3 to # 5) were caused, in my opinion, by different antenna parameters from different GPR providers.

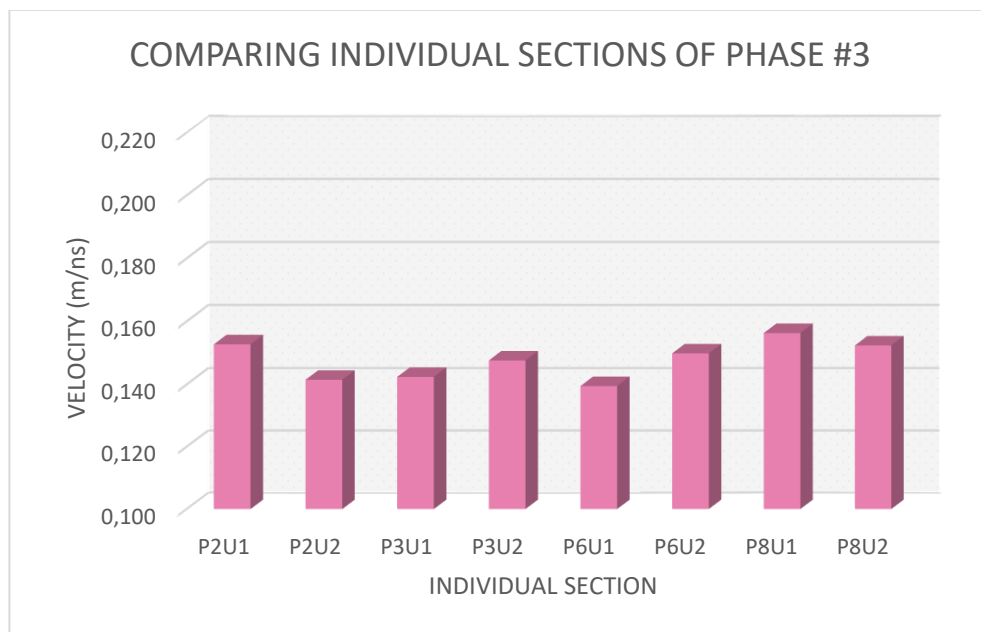


Figure 50 - Comparison of signal velocity in each section of the third phase

As indicated in Figure 50 there is a clear difference in the ballast layer properties in the sections before cleaning. The reasons for that difference are described above.

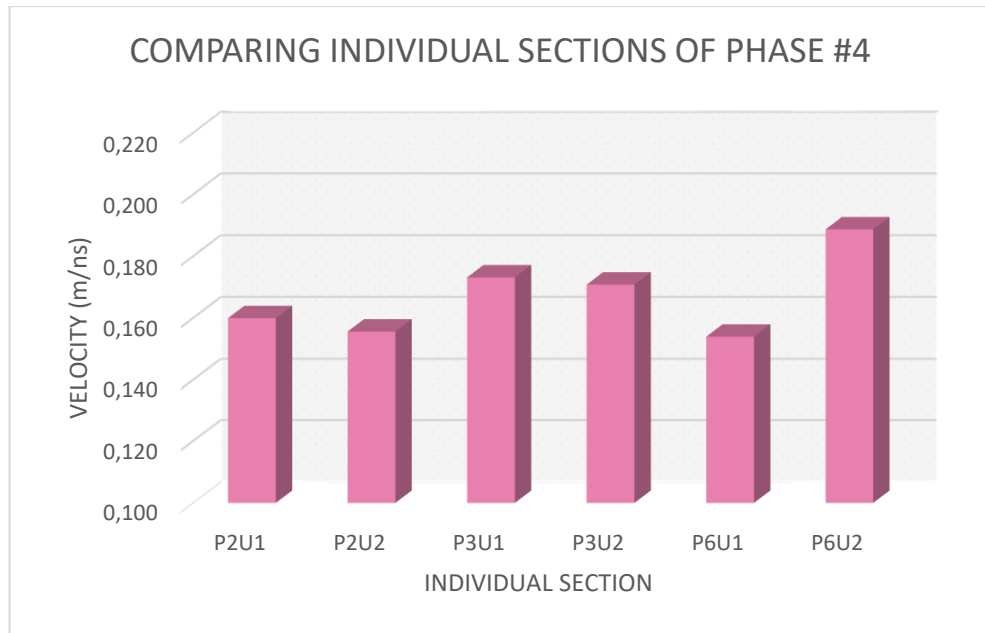


Figure 51 - Comparison of signal velocity in each section of the fourth phase

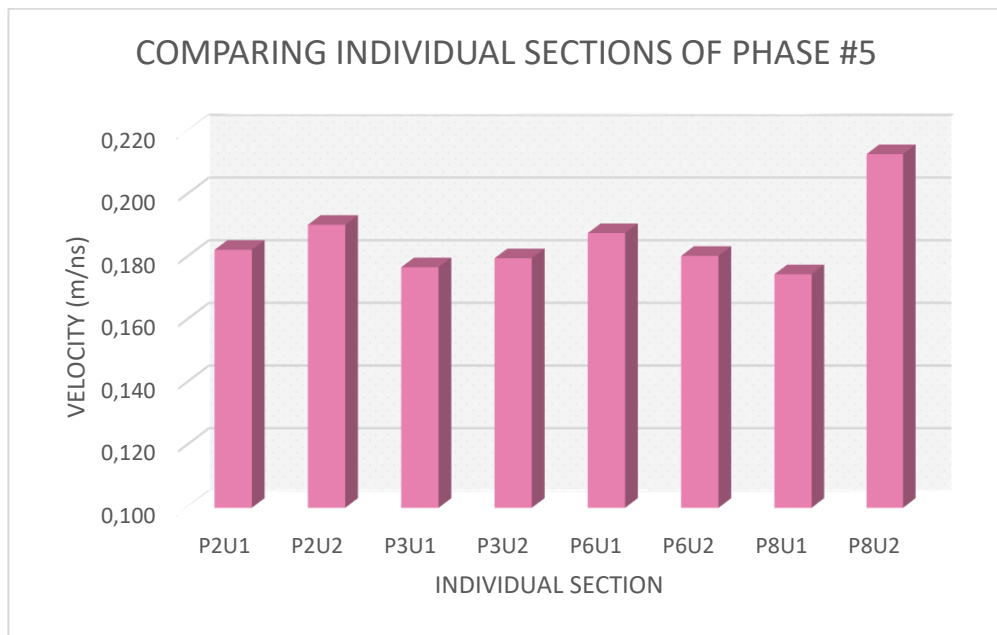


Figure 52 - Comparison of signal velocity in each section of the fifth phase

Obviously, in phases # 4 and # 5, according to Figure 51 a Figure 52, the velocities are diametrically different from phase # 3. This confirms the eligibility of ballast layer cleaning using machine cleaners. All in all, the aggregate properties of the ballast layer have been homogenized and improved throughout the reconstructed section and overall improved.

The percent change in speed during the track bed cleaning process between phases 3 and 5 is shown in Table 20.

Table 20 - Percentual increase of velocity during the cleaning process

SECTION	THE VELOCITY BEFORE CLEANING, STAGE #3 (m/ns)	THE VELOCITY IN THE FINAL STATE, STAGE #5 (m/ns)	PERCENTUAL IMPROVEMENT
P2U1	0,153	0,182	19,3
P2U2	0,142	0,19	34,4
P3U1	0,142	0,177	24,1
P3U2	0,148	0,18	21,6
P6U1	0,14	0,188	34,4
P6U2	0,15	0,18	20,3
P8U1	0,156	0,175	11,6
P8U2	0,152	0,213	39,6

Improvement has occurred in all sections and the highest improvement was in the P8U2 section while the lowest improvement was in the P8U1 section. This phenomenon can be elucidated due to the presence of water before cleaning in both sections of P8 and due to the filling of gravel grains by emptying the wagon with new material after cleaning in section P8U1. It was in the P8U1 section where the wagon with newly-added ballast was finally emptied, which causes an uncontrollable fraction fill and a higher portion of dust particles. This was also observed visually on the track.

Significant increases are seen in the P2U2 section, where higher initial pollution was observed, compare to P2U1. A similar difference can be observed between the P6U1 and P6U2 sections, where the presence of water in both sections was assumed, although higher in P6U1 than in P6U32.

It can be stated that, due to the relative permittivity and signal velocity changes, higher efficiency of the RM 900 VB was observed by 6.5%. However, it is important to note that the initial conditions for cleaning the ballast layer were different due to the dissimilar water content and fine particles distribution.

9. Conclusion

The submitted thesis was focused on the diagnostics of the railway ballast layer condition and the determination of the fouling level change before and after the mechanical cleaning process by measuring the changes in the RDP of the material by the GPR equipment. There were three partial goals of the thesis set in the beginning, consisting of the implementation of GPR measurements on ballast layer and subsequent determination of RDP variation in different periods of the track's life cycle with aim to describe the relationship between the fouling level and RDP values of the railway ballast (described in chapter one).

The first partial goal was achieved by performing a survey on the Čáslav-Kutná Hora railway track section, where eight sections with a total length of 400 m (each 50 m) was set and surveyed by three different central frequencies, using two antenna orientations. The survey was repeated three times at different stages of the track's life cycle, in particular before and after the machine cleaning process.

The second partial goal was achieved by the time-domain analysis of recorded data (phase 3, 4, 5) and data obtained from SŽDC (phase 1, 2). A dedicated processing scheme was used in ReflexW software taking into account the spacing of the sleepers (SB 8 type) and the width of the sleepers. For the calibration, KHM was used based on ground truth data. Two probes were performed with this aim and with the goal to sample material, necessary for the laboratory test.

In laboratory, the sieve analysis was performed, air voids and fine material distribution was determined and the fouling index was calculated. Changes in RDP were seen between survey stages 3 (before cleaning) and 5 (final state), which are the same or even higher than literature values (10 % to 30 %). This may be caused by performing a survey in final phase directly after cleaning process finished. Change in EM wave velocity values in individual sections for stages 1, 3, 5 can be seen in Figure 53.

COMPARING INDIVIDUAL SECTIONS OF PHASE #1, #3, #5

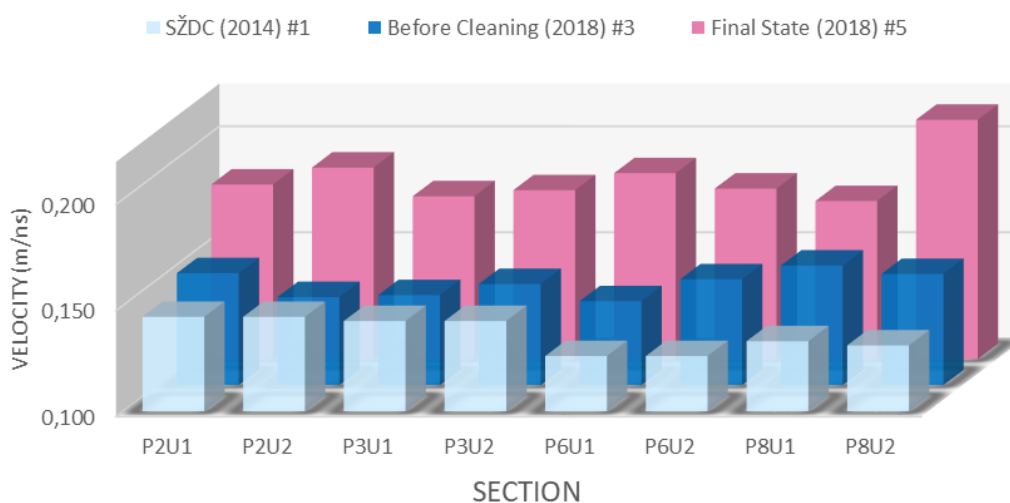


Figure 53 – Comparing individual section of phase 1, 3, 5.

The third partial goal was partly achieved by literature review part and partly in Results and Discussion chapter by presented graphs and tables with relevant comments. The ballast condition was determined as fouled for sample #1 (P6U1) and highly fouled for sample #2 (P2U2). This was also confirmed by the evaluation of RDP/velocity in these sections, where, on the basis of the determined intervals, the gravel bed material in the P2U2 section was classified as slightly fouled and in the P6U2 section it was classified as highly fouled. By comparing laboratory tests and in-situ measurements, it can also be confirmed that the presence of water has a significantly higher influence on the RDP/signal velocity than only the proportion of fine particles. However, these phenomena are closely related. Improving in the ballast condition has occurred in all sections. Higher efficiency of the RM 900 VB undercutter was reported by 6.5%. However, it is important to note that the initial conditions for cleaning the ballast layer were different due to the dissimilar water content and fine particles distribution. Based on track measurements, laboratory tests and subsequent comparisons with literature, the cleaning process should, in my opinion, start at approximately when RDP rises to 9 and the speed drops to 10 cm/ns. However, it should be considered whether the presence of water or fine material is the cause of the higher RDP value. If it is the presence of water, then it should be examined whether it is a temporary condition (e.g. after rain) or a steady state given by non-functional drainage, etc. In any case, GPR measurements should not take place in wet conditions.

According to the author’s opinion, all partial goals were achieved based on the chosen thesis topic and regarding available GPR equipment.

From the perspective of chosen methods, the following summary can be formulated regarding the thesis topic, i.e. what needs to be done, while assessing the condition of the railway ballast using GPR with time-domain evaluation:

1. To define measurement conditions, GPR equipment parameters, and settings,
2. To define a data processing algorithm based on #1, (time-domain)
3. To obtain RDP/velocity values based on #1 and #2, (time-domain)
4. To define/choose standard fouling indicator(s) or similar parameter(s) for ballast material(s), and its value for cleaning process launching.
5. To compare (set relationship) RDP from #3 and standard fouling indicator from #4
6. To decide when/whether the cleaning process should start.

The time-domain method, used in this study, has although its limitations. As stated before, there is a high dependency of RDP/velocity absolute values on the precision of depth determination by direct measurement. This phenomenon is demonstrated in Figure 54 (a), and (b).

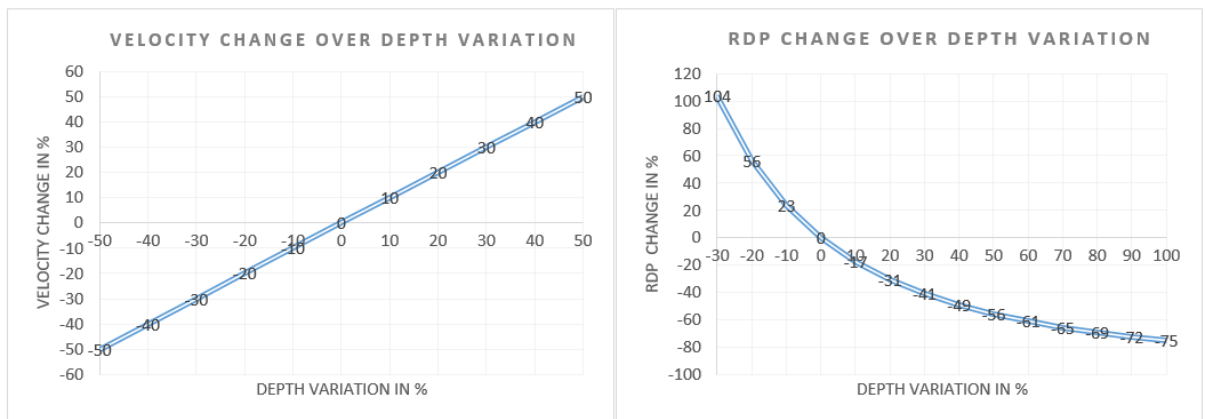


Figure 54 – Velocity (a) and RDP (b) change over depth variation

Future work

Since only traditional approach in time-domain was used in this study, with its limitations, also the time–frequency technique, based on short-time Fourier transform (STFT), can be used and also scattering pattern/response (especially in case of the 2GHz antenna). Wavelet Technique can be used too. Determining ballast velocity from a radar detectable geosynthetic could be also another tool to approach to the problematics, solved in this thesis.

During my bachelor thesis elaboration, I get acquainted with GPR technology through the study of relevant professional literature, through practical survey on a real track and in the laboratory, and through the data evaluation process. I acquired not only theoretical knowledge of this technology, but practical experience as well. During that time my English also improved by widening my vocabulary in the relevant field. I found GPR technology very interesting and useful in terms of transport structures diagnostics. I presented my work at the European Geosciences Union (EGU) 2019 international conference, where I met experts from the GPR technology field. I plan to continue studying this problematics also in the framework of my diploma thesis.

Bibliography

- [1] TZANAKAKIS, Konstantinos. *The railway track and its long term behaviour: A handbook for a railway track of high quality*. Heidelberg ; New York: Springer, 2013. Springer tracts on transportation and traffic, 2. ISBN 978-3-642-36050-3.
- [2] <http://strabag-rail.com>. *Strabag-rail* [online]. 2019 [vid. 2019-03-24]. Dostupné z: http://strabag-rail.com/databases/internet/_public/files.nsf/
- [3] ANNAN, A. P. a J. L. DAVIS. *Ground penetrating radar—coming of age at last*. In: proceedings of Exploration [online]. 1997, s. 515–522 [vid. 2015-08-11]. Dostupné z: http://dmecc.ca/ex07-dvd/Decennial%20Proceedings/Expl97/06_05____.pdf
- [4] U.S. DEPARTMENT OF TRANSPORTATION, FEDERAL RAILROAD ADMINISTRATION; *GPR Evaluation and Implementation*; July 2014, FRA Office for Railroad Policy and Development, Washington, DC, USA
- [5] LAHOUAR, Samer. *Development of data analysis algorithms for interpretation of ground penetrating radar data* [online]. B.m., 2003 [vid. 2014-04-05]. Virginia Polytechnic Institute and State University. Dostupné z: <http://scholar.lib.vt.edu/theses/available/etd-10242003-162114/>
- [6] LOULIZI, Amara. *Development of ground penetrating radar signal modeling and implementation for transportation infrastructure assessment* [online]. B.m., 2001 [vid. 2014-04-04]. Virginia Polytechnic Institute and State University. Dostupné z: <http://scholar.lib.vt.edu/theses/available/etd-02062001-220414/>
- [7] MATULA, RADEK. *Nedestruktivní diagnostika konstrukcí vozovek pozemních komunikací georadarem* [online]. Brno, 2013. Doctoral Thesis. University of Pardubice. Dostupné z: <http://hdl.handle.net/10195/54072>
- [8] WANG, Zhe Wendy. *Automatic Detection of Bridge Deck Condition from Ground Penetrating Radar Images*. IEEE transactions on automation science and engineering [online]. 2011, 8(3), 633–640. ISSN 1545-5955. Dostupné z: doi:10.1109/TASE.2010.2092428
- [9] JOL, Harry M., *Ground penetrating radar: theory and applications*. 1. ed. Amsterdam: Elsevier Science, 2009. ISBN 978-0-444-53348-7.
- [10] CASSIDY, Nigel J., *Electrical and Magnetic Properties of Rocks, Soils and Fluids*. In: *Ground Penetrating Radar Theory and Applications* [online]. B.m.: Elsevier, 2009 [vid. 2018-12-05], s. 41–72. ISBN 978-0-444-53348-7. Dostupné z: doi:10.1016/B978-0-444-53348-7.00002-8
- [11] BENEDETTO, Andrea and Lara PAJEWSKI, ed. *Civil Engineering Applications of Ground Penetrating Radar* [online]. Cham: Springer International Publishing, 2015 [vid. 2018-12-11]. Springer Transactions in Civil and Environmental Engineering. ISBN 978-3-319-04812-3. Dostupné z: doi: 10.1007/978-3-319-04813-0

- [12] SAARENKETO, Timo. *Electrical properties of road materials and subgrade soils and the use of Ground Penetrating Radar in traffic infrastructure surveys*. Oulu, 2006. University of Oulu.
- [13] DE BOLD, Robert Paul. *Non-destructive evaluation of railway tracked ballast* [online]. 2011 [vid. 2015-09-16]. Dostupné z: <http://www.era.lib.ed.ac.uk/handle/1842/5027>
- [14] NURUL Jihan Farhah Bostanudin. *Computational Methods for Processing Ground Penetrating Radar Data*. Portsmouth, 2013. University of Portsmouth.
- [15] ANNAN, A.P. *Electromagnetic Principles of Ground Penetrating Radar*. In: *Ground Penetrating Radar Theory and Applications* [online]. B.m.: Elsevier, 2009 [vid. 2018-12-05], s. 1–40. ISBN 978-0-444-53348-7. Dostupné z: doi:10.1016/B978-0-444-53348-7.00001-6
- [16] KIMBERLY, MARIE BELLI. *Ground penetrating radar bridge deck investigations using computational modeling*. Boston, Massachusetts, 2008. Northeastern University.
- [17] DI PRINZIO, Monica. *Application of GPR to the monitoring of river embankments*. *Journal of applied geophysics* [online]. 2010, 71(2–3), 53–61. ISSN 0926-9851. Dostupné z: doi:10.1016/j.jappgeo.2010.04.002
- [18] GROTE, K. *Evaluation of infiltration in layered pavements using surface GPR reflection techniques*. *Journal of applied geophysics* [online]. 2003, 57(2). ISSN 0926-9851. Dostupné z: <http://www.sciencedirect.com/science/journal/09269851/57/2>
- [19] NI, Sheng-Huoo. *Buried pipe detection by ground penetrating radar using the discrete wavelet transform*. *Computers and Geotechnics* [online]. 2010, 37(4), 440–448. ISSN 0266-352X. Dostupné z: doi:10.1016/j.compgeo.2010.01.003
- [20] PLATI, Christina and Andreas LOIZOS. *Estimation of in-situ density and moisture content in HMA pavements based on GPR trace reflection amplitude using different frequencies*. *Journal of Applied Geophysics* [online]. 2013, 97, 3–10. ISSN 09269851. Dostupné z: doi:10.1016/j.jappgeo.2013.04.007
- [21] GEHRIG, Michael D., Derek V. MORRIS a John T. BRYANT. *Ground Penetrating Radar for Concrete Evaluation Studies*. Technical Presentation Paper for Performance Foundation Association. 2004, 197–200.
- [22] DE BOLD, Robert Paul. *Non-destructive evaluation of railway tracked ballast* [online]. Edinburgh, 2011 [vid. 2014-04-05]. School of Engineering University of Edinburgh. Dostupné z: <http://www.era.lib.ed.ac.uk/handle/1842/5027>
- [23] DANIELS, David J. *Ground penetrating radar* [online]. B.m.: Iet, 2004 [vid. 2015-08-11]. Dostupné z: <http://books.google.com/books>
- [24] HYSLIP, James P., Stanley S. SMITH, Gary R. OLHOEFT and Ernest T. SELIG. *Assessment of railway track substructure condition using ground penetrating radar*. In: *2003 Annual Conference of AREMA* [online]. 2003 [vid. 2014-04-27]. Dostupné z: http://205.252.224.180/files/library/2003_Conference_Proceedings/0010.pdf

- [25] ANNAN, A P. *Ground Penetrating Radar Workshop Notes*. 2013, 197. Sensors & Software Inc.
- [26] UDUWAWALA, Disala. *A comprehensive study of resistor-loaded planar dipole antennas for ground penetrating radar applications*. Stockholm, 2006. Division of Electromagnetic Engineering, School of Electric Engineering, Royal Institute of Technology.
- [27] CONYERS, Lawrence B. *Ground-penetrating radar for archaeology*. Walnut Creek, CA: AltaMira Press, 2004. ISBN 0-7591-0772-6.
- [28] PAJEWSKI, Lara, Milan VRTUNSKI, Eljko BUGARINOVI, Aleksandar RISTI, Miro GOVEDARICA, Colette GRÉGOIRE, Carl Van GEEM, Xavier DEROBERT, Vladislav BORECKY, Salih Serkan ARTAGAN, Simona FONTUL, Vânia MARECOS a Sébastien LAMBOT. *GPR System Performance Compliance According To Cost Action TU 1208 Guidelines*. *Ground Penetrating Radar*. 2018, 1(2), 35.
- [29] ARTAGAN, SALIH SERKAN a BORECKÝ, VLADISLAV. *Estimation Methods for Obtaining GPR Signal Velocity*. *International Journal of Civil and Structural Engineering*. 2016, 3(1), 59–63. ISSN 2372-3971.
- [30] SHEERS, Bart. *Ultra-Wideband Ground Penetrating Radar, with Application to the Detection of Anti-Personnel Landmines*, Doctoral Thesis, Université Catholique De Louvain, March 2001
- [31] BENEDETTO, Andrea and Lara PAJEWSKI, ed. *Civil Engineering Applications of Ground Penetrating Radar* [online]. Cham: Springer International Publishing, 2015 [vid. 2016-07-23]. Springer Transactions in Civil and Environmental Engineering. ISBN 978-3-319-04812-3. Dostupné z: <http://link.springer.com/10.1007/978-3-319-04813-0>
- [32] ARTAGAN, S. S., *Use of Ground Penetrating Radar in Condition Assessment of Railway Ballast*, Doctoral Thesis, University of Pardubice, 2018
- [33] SAARENKETO, Timo. *Electrical properties of road materials and subgrade soils and the use of Ground Penetrating Radar in traffic infrastructure surveys*. Doctoral Thesis, Oulu, 2006. University of Oulu.
- [34] AL-QADI, Imad, Wei XIE a Roger ROBERTS. *Optimization of antenna configuration in multiple-frequency ground penetrating radar system for railroad substructure assessment*. *NDT & E International* [online]. 2010, 43(1), 20–28. ISSN 09638695. Dostupné z: doi:10.1016/j.ndteint.2009.08.006
- [35] MANACORDA, Guido, Davide MORANDI and Antonio SARRI. *Railroad tracks verification*. nedatováno, 5.
- [36] LI, Dingqing, David READ, Hugh THOMPSON, Ted SUSSMANN, Russell MCDANIEL, Norfolk Southern RAILWAY a V. A. ROANOKE. *Evaluation of Ground Penetrating Radar Technologies for Assessing Track Substructure Conditions* [online]. nedatováno [vid. 2014-04-27]. Dostupné z: http://www.arena.org/files/library/2010_Conference_Proceedings/Evaluation_of_G

round_Penetrating_Radar_Technologies_for_Assessing_Track_Substructure_Conditions.pdf

- [37] POKYNY PRO POUŽITÍ NEDESTRUKTIVNÍCH GEOFYZIKÁLNÍCH METOD V DIAGNOSTICE A PRŮZKUMU TĚLESA ŽELEZNIČNÍHO SPODKU. B.m.: Správa železniční dopravní cesty s. o., České dráhy a. s., 2006
- [38] HUGENSCHMIDT, J. *Non-destructive-testing of traffic-infrastructure using GPR*, 2003. EMPA, Swiss Federal Laboratories for Materials Testing and Research
- [39] AL-QADI, Imad L., Wei XIE, Roger ROBERTS a Zhen LENG. *Data analysis techniques for GPR used for assessing railroad ballast in high radio-frequency environment*. *Journal of Transportation Engineering*. 2010, 136(4), 392–399.
- [40] HUGENSCHMIDT, J. *Railway track inspection using GPR*. *Journal of Applied Geophysics*. 2000, 43(2), 147–155.
- [41] OLHOEFT, Gary R., Samuel SMITH, J. P. HYSLIP a E. T. SELIG. *GPR in railroad investigations*. In: *Ground Penetrating Radar, 2004. GPR 2004. Proceedings of the Tenth International Conference on* [online]. B.m.: IEEE, 2004, s. 635–638 [vid. 2015-08-04]. Dostupné z: http://ieeexplore.ieee.org/xpls/abs_all.jsp?arnumber=1343547
- [42] Ernest T. Selig and John M. Waters. (1994). *Track Geotechnology and Substructure Management*. London: Thomas Telford Publications
- [43] HYSLIP, James P., Stanley S. SMITH, Gary R. OLHOEFT and Ernest T. SELIG. *Assessment of railway track substructure condition using ground penetrating radar*. In: *2003 Annual Conference of AREMA* [online]. 2003 [vid. 2015-08-04]. Dostupné z: https://www.arema.org/files/library/2003_Conference_Proceedings/0010.pdf
- [44] AL-QADI, Imad, Wei XIE a Roger ROBERTS. *Optimization of antenna configuration in multiple-frequency ground penetrating radar system for railroad substructure assessment*. *NDT & E International* [online]. 2010, 43(1), 20–28. ISSN 09638695. Dostupné z: [doi:10.1016/j.ndteint.2009.08.006](https://doi.org/10.1016/j.ndteint.2009.08.006)
- [45] GARY R. OLHOEFT and ERNEST T. SELIG. *Ground-penetrating radar evaluation of railway track substructure conditions*. In: [online]. 2002, s. 4758–6. Dostupné z: <https://doi.org/10.1117/12.462264>
- [46] MANACORDA, Guido, Davide MORANDI, Antonio SARRI a Giuseppe STACCONE. *Customized GPR system for railroad track verification*. In: *Ninth International Conference on Ground Penetrating Radar (GPR2002)* [online]. B.m.: International Society for Optics and Photonics, 2002, s. 719–723 [vid. 2016-04-19]. Dostupné z: http://proceedings.spiedigitallibrary.org/data/Conferences/SPIEP/32070/719_1.pdf
- [47] GALLAGHER, G. P., Q. LEIPER, R. WILLIAMSON, M. R. CLARK a M. C. FORDE. *The application of time domain ground penetrating radar to evaluate railway track ballast*. *NDT & E International*. 1999, 32(8), 463–468.
- [48] ROBERTS, Roger, John RUDY a Salem GSSI. *Railroad ballast fouling detection using ground penetrating radar*. A new approach based on scattering from voids.

- ECNDT 2006–Th. 4.5 [online]. 2006, 1 [vid. 2015-10-26]. Dostupné z: <http://citeseerx.ist.psu.edu/viewdoc/download?doi=10.1.1.159.4471&rep=rep1&type=pdf>
- [49] ERIKSEN, Asger, Ben VENABLES, Jon GASCOYNE a Shubho BANDYOPADHYAY. *Benefits of high speed GPR to manage trackbed assets and renewal strategies*. In: PWI Conference, June [online]. 2006 [vid. 2015-09-21]. Dostupné z: http://www.researchgate.net/profile/Asger_Eriksen/publication/239586033_Benefits_of_high_speed_GPR_to_manage_trackbed_assets_and_renewal_strategies/links/54c664b80cf256ed5a9e5f54.pdf
- [50] DONOHUE, S., K. GAVIN and A. TOLOOIYAN. *Geophysical and geotechnical assessment of a railway embankment failure*. Near Surface Geophysics [online]. 2011, 9(1767) [vid. 2015-10-20]. ISSN 18730604. Dostupné z: doi:10.3997/1873-0604.2010040
- [51] D.-B. ZHU, J.-N. GENG a M. HUANG. *Algorithm for suppressing sleeper interferences in railway subgrade GPR signals*. Journal of the China Railway Society [online]. 2013, 5(35), 75–79. Dostupné z: doi:10.3969/j.issn.1001-8360.2013.05.012
- [52] LIAO LIJIAN, YANG XINAN a DU PANFENG. *Processing GPR Detection Data of Railway Subgrade*. China Railway Science. 2008, 03. ISSN 1001-4632.
- [53] CALDEIRA, L, A GOMES CORREIA, M PEREIRA, F FERNANDES a P LOURENÇO. *Assessment of layer thickness and uniformity in railway embankments with ground penetrating radar*. Advances in Transportation Geotechnics [online]. B.m.: CRC Press, 2008 [vid. 2015-10-20], s. 571–575. ISBN 978-0-415-47590-7. Dostupné z: <http://www.crcnetbase.com/doi/abs/10.1201/9780203885949.pt8>
- [54] SUSSMANN, Theodore R., Ernest T. SELIG a James P. HYSLIP. *Railway track condition indicators from ground penetrating radar*. NDT & E International. 2003, 36(3), 157–167.
- [55] NARAYANAN, Ram M., Justin W. JAKUB, Dingqing LI a Samy E.G. ELIAS. *Railroad track modulus estimation using ground penetrating radar measurements*. NDT & E International [online]. 2004, 37(2), 141–151. ISSN 09638695. Dostupné z: doi:10.1016/j.ndteint.2003.05.003
- [56] SAARENKETO, T., M. SILVAST a J. NOUKKA. *Using GPR on Railways to Identify Frost Susceptible Areas*. Proceedings of the international conference and exhibition railway engineering 2003, held london, uk, 30 april - 1 may 2003 - cdrom [online]. 2003 [vid. 2015-09-20]. Dostupné z: <http://trid.trb.org/view.aspx?id=749415>
- [57] GUO, Zhenwei, Hefeng DONG a Jianping XIAO. *Detection of Permafrost Subgrade Using GPR: A Case Examination on Qinghai-Tibet Plateau*. Journal of Geoscience and Environment Protection [online]. 2015, 03(05), 35–47. ISSN 2327-4336, 2327-4344. Dostupné z: doi:10.4236/gep.2015.35005
- [58] NURMIKOLU, Antti. *Key aspects on the behaviour of the ballast and substructure of a modern railway track: research-based practical observations in Finland*. Journal of

- Zhejiang University SCIENCE A [online]. 2012, 13(11), 825–835. ISSN 1673-565X, 1862-1775. Dostupné z: doi:10.1631/jzus.A12ISGT1
- [59] DU, Li Zhi, Xiao Pei ZHANG, Jian Hui QIU a Wen Bo LIU. *Study on Ground Penetrating Radar in Detecting of Zero-Temperature Boundary under the Railway Bed*. *Advanced Materials Research* [online]. 2011, 255–260, 3975–3978. ISSN 1662-8985. Dostupné z: doi:10.4028/www.scientific.net/AMR.255-260.3975
- [60] CHIARA, De. *Non-destructive tests for railway infrastructure stiffness evaluation* (2011) *Proceedings of the 13th International Conference on Civil, Structural and Environmental*. nedatováno, 1.
- [61] CLARK, M.R, R GILLESPIE, T KEMP, D.M MCCANN a M.C FORDE. *Electromagnetic properties of railway ballast*. *NDT & E International* [online]. 2001, 34(5), 305–311. ISSN 09638695. Dostupné z: doi:10.1016/S0963-8695(00)00006-2
- [62] HUGENSCHMIDT, J. *Railway track inspection using GPR*. *Journal of Applied Geophysics* [online]. 2000, 43(2–4), 147–155. ISSN 09269851. Dostupné z: doi:10.1016/S0926-9851(99)00054-3
- [63] JACK, R. a P. JACKSON. *Imaging attributes of railway track formation and ballast using ground probing radar*. *NDT & E International*. 1999, 32(8), 457–462.
- [64] FONTUL, Simona, Eduardo FORTUNATO, Francesca DE CHIARA, Rui BURRINHA a Marco BALDEIRAS. *Railways Track Characterization Using Ground Penetrating Radar*. *Procedia Engineering* [online]. 2016, 143, 1193–1200. ISSN 18777058. Dostupné z: doi:10.1016/j.proeng.2016.06.120
- [65] HYSLIP, James P., *Substructure Maintenance Management*, 2007, HyGround Engineering, Williamsburg, Massachusetts, USA
- [68] BRANCADORO, M. G., L. Bianchini CIAMPOLI, C. FERRANTE, A. BENEDETTO, F. TOSTI and A. M. ALANI. *An Investigation into the railway ballast grading using GPR and image analysis*. In: *Advanced Ground Penetrating Radar (IWAGPR)*, 2017 9th International Workshop on. B.m.: IEEE, 2017, s. 1–4.
- [69] BIANCHINI CIAMPOLI, Luca, Fabio TOSTI, Maria Giulia BRANCADORO, Fabrizio D'AMICO, Amir M. ALANI and Andrea BENEDETTO. *A spectral analysis of ground-penetrating radar data for the assessment of the railway ballast geometric properties*. *NDT & E International* [online]. 2017, 90, 39–47. ISSN 09638695. Dostupné z: doi:10.1016/j.ndteint.2017.05.005
- [70] ZHANG, Q., J. GASCOYNE a A. ERIKSEN. *Characterisation of ballast materials in trackbed using ground penetrating radar: Part 1*. In: *Railway Condition Monitoring and Non-Destructive Testing (RCM 2011)*, 5th IET Conference on [online]. B.m.: IET, 2011, s. 1–8 [vid. 2017-01-09]. Dostupné z: http://ieeexplore.ieee.org/xpls/abs_all.jsp?arnumber=6191861
- [71] CLARK, Max, Michael GORDON a Mike C. FORDE. *Issues over high-speed non-invasive monitoring of railway trackbed*. *NDT & E International* [online]. 2004, 37(2), 131–139. ISSN 09638695. Dostupné z: doi:10.1016/j.ndteint.2003.05.002

- [72] CARPENTER, D, P.J JACKSON and A JAY. *Enhancement of the GPR method of railway trackbed investigation by the installation of radar detectable geosynthetics*. *NDT & E International* [online]. 2004, 37(2), 95–103. ISSN 09638695. Dostupné z: doi:10.1016/j.ndteint.2003.06.003
- [73] LI, Dingqing, David READ, Hugh THOMPSON, Ted SUSSMANN, Russell MCDANIEL, Norfolk Southern RAILWAY a V. A. ROANOKE. *Evaluation of Ground Penetrating Radar Technologies for Assessing Track Substructure Conditions* [online]. nedatováno [vid. 2015-08-04]. Dostupné z: https://www.arena.org/files/library/2010_conference_proceedings/evaluation_of_ground_penetrating_radar_technologies_for_assessing_track_substructure_conditions.pdf
- [74] MATURANA, Raúl Mínguez, Begoña Duclos BAUTISTA, Álvaro Andrés AGUACIL, Miguel Rodríguez PLAZA a Senén Sandoval CASTAÑO. *Preventive Maintenance of Railway Infrastructures using GPR–Ground Penetrating Radar* [online]. nedatováno [vid. 2015-08-04]. Dostupné z: http://www.railway-research.org/IMG/pdf/g7_minguez_maturana_raul.pdf
- [75] CABRERA, Reinaldo Alvarez. *GPR antenna selection*. 2011, GeoScanners AB
- [76] FONTUL, Simona, André PAIXÃO, Mercedes SOLLA a Lara PAJEWSKI. *Railway Track Condition Assessment at Network Level by Frequency Domain Analysis of GPR Data*. *Remote Sensing* [online]. 2018, 10(4), 559. ISSN 2072-4292. Dostupné z: doi:10.3390/rs10040559
- [77] SHIHAB, S., O. ZAHARAN a W. AL-NUAIMY. *Time-frequency characteristics of ground penetrating radar reflections from railway ballast and plant*. In: [online]. B.m.: IEEE, 2002, s. 8 [vid. 2016-06-10]. ISBN 978-0-7803-7618-2. Dostupné z: doi:10.1109/HFPSC.2002.1088424
- [78] SHAO, Wenbin, Abdesselam BOUZERDOUM, Son Lam PHUNG, Lijun SU, Buddhima INDRARATNA a Cholachat RUJIKIATKAMJORN. *Automatic Classification of Ground-Penetrating-Radar Signals for Railway-Ballast Assessment*. *IEEE Transactions on Geoscience and Remote Sensing* [online]. 2011, 49(10), 3961–3972. ISSN 0196-2892. Dostupné z: doi:10.1109/TGRS.2011.2128328
- [79] SHAO, Wenbin, Abdesselam BOUZERDOUM, Son Lam PHUNG, Lijun SU, Buddhima INDRARATNA a Cholachat RUJIKIATKAMJORN. *Automatic Classification of Ground-Penetrating-Radar Signals for Railway-Ballast Assessment*. *IEEE Transactions on Geoscience and Remote Sensing* [online]. 2011, 49(10), 3961–3972. ISSN 0196-2892. Dostupné z: doi:10.1109/TGRS.2011.2128328
- [80] BIANCHINI CIAMPOLI, L. et al., *Efficient practices in railway ballast maintenance and quality assessment using GPR*, 2017, DOI:10.1201/9781315281896-56
- [81] MARECOS, Vânia, Mercedes SOLLA, Simona FONTUL a Vitor ANTUNES. *Assessing the pavement subgrade by combining different non-destructive methods*. *Construction and Building Materials* [online]. 2017, 135, 76–85. ISSN 09500618. Dostupné z: doi:10.1016/j.conbuildmat.2017.01.003

- [82] SILVAST, M., *NDT Techniques in Railway Structure Analysis*, 2006, Proceedings of the 7th World Congress on Railway Research, Montreal, Canada
- [83] CLARK, M. R., R. GILLESPIE, T. KEMP, D. M. MCCANN a M. C. FORDE. *Electromagnetic properties of railway ballast*. *NDT & E International*. 2001, 34(5), 305–311.
- [84] SIMI, Alessandro, Guido MANACORDA, Mario MINIATI, Stefania BRACCIALI and Andrea BUONACCORSI. *Underground asset mapping with dual-frequency dual-polarized GPR massive array*. In: 2010 13th International Conference on Ground Penetrating Radar (GPR 2010): Proceedings of the XIII International Conference on Ground Penetrating Radar [online]. Lecce: IEEE, 2010, s. 1–5 [vid. 2019-02-22]. ISBN 978-1-4244-4604-9. Dostupné z: doi:10.1109/ICGPR.2010.5550236
- [85] SANTOS-ASSUNÇÃO, S.; PEDRET RODÉS, J.; PÉREZ-GRACIA, V. *Ground Penetrating Radar Railways Inspection*. In Proceedings of the 75th EAGE Conference & Exhibition Incorporating SPE EUROPEC 2013, London, UK, 10–13 June 2013.
- [86] KHAKIEV, Zelimkhan, Vladimir SHAPOVALOV, Alexander KRUGLIKOV and Victor YAVNA. *GPR determination of physical parameters of railway structural layers*. *Journal of Applied Geophysics* [online]. 2014, 106, 139–145. ISSN 09269851. Dostupné z: doi:10.1016/j.jappgeo.2014.04.017
- [87] KHAKIEV, Zelimkhan, Vladimir SHAPOVALOV, Alexander KRUGLIKOV, Andrey MOROZOV a Victor YAVNA. *Investigation of long term moisture changes in trackbeds using GPR*. *Journal of Applied Geophysics* [online]. 2014, 110, 1–4. ISSN 09269851. Dostupné z: doi:10.1016/j.jappgeo.2014.08.014
- [88] NARAYANAN, Ram M. *Railroad track modulus estimation using ground penetrating radar measurements*. *NDT & E international : independent nondestructive testing and evaluation* [online]. 2004, 37(2), 141–151. ISSN 0963-8695. Dostupné z: doi:10.1016/j.ndteint.2003.05.003
- [89] BIANCHINI CIAMPOLI, Luca, Fabio TOSTI, Maria Giulia BRANCADORO, Fabrizio D'AMICO, Amir M. ALANI a Andrea BENEDETTO. *A spectral analysis of ground-penetrating radar data for the assessment of the railway ballast geometric properties*. *NDT & E International* [online]. 2017, 90, 39–47. ISSN 09638695. Dostupné z: doi:10.1016/j.ndteint.2017.05.005
- [90] DELL'ACQUA, Gianluca a Fred WEGMAN, ed. *Transport Infrastructure and Systems*; proceedings of the AiiT International Congress on Transport Infrastructure and Systems (Tis 2017), Rome, Italy, 10-12 April 2017 [online]. CRC Press/Balkema P.O. Box 11320, 2301 EH Leiden, The Netherlands: CRC Press/Balkema, 2017 [vid. 2018-12-20]. ISBN 978-1-138-03009-1. Dostupné z: doi:10.1201/97811315281896
- [91] ALEMU, Abateneh Yitayew. *Survey of Railway Ballast Selection and Aspects of Modelling Techniques*. nedatováno, 61.

- [92] DE CHIARA, Francesca. *Improvement Of Railway Track Diagnosis Using Ground Penetrating Radar*, Doctoral Thesis, Laboratório Nacional de Engenharia Civil (LNEC), submitted to the University of Rome “Sapienza”, 2014
- [93] ANBAZHAGAN, P., P.S. Naresh DIXIT a T.P. BHARATHA. *Identification of type and degree of railway ballast fouling using ground coupled GPR antennas*. Journal of Applied Geophysics [online]. 2016, 126, 183–190. ISSN 09269851. Dostupné z: doi:10.1016/j.jappgeo.2016.01.018
- [94] SELIG, Ernest Theodore a John M. WATERS. *Track Geotechnology and Substructure Management*. B.m.: Thomas Telford, 1994. ISBN 978-0-7277-2013-9.
- [95] ANBAZHAGAN, P., Su LIJUN, Indraratna BUDDHIMA a Rujikiatkamjorn CHOLACHAT. *Model track studies on fouled ballast using ground penetrating radar and multichannel analysis of surface wave*. Journal of Applied Geophysics [online]. 2011, 74(4), 175–184. ISSN 09269851. Dostupné z: doi:10.1016/j.jappgeo.2011.05.002
- [96] ANBAZHAGAN, Dr P. *Characterization of Rail Track Ballast Fouling Using Ground Penetration Radar and Field Sampling*. nedatováno, 54.
- [97] IONESCU, D. *Ballast degradation and measurement of ballast fouling*. In: *7th International Railway Engineering Conference: Proceedings of 7th International Railway Engineering Conference*. London: Engineering Technics Press, 2004.
- [98] ANBAZHAGAN, P. *Characterization of Rail Track Ballast Fouling Using Ground Penetration Radar and Field Sampling* [online]. 2013 [vid. 2015-10-20]. Dostupné z: <http://cistup.iisc.ernet.in/Demo/cistup/presentations/Research%20project/CIST024.pdf>
- [99] FONTUL, S, E FORTUNATO and F De CHIARA. *Evaluation of ballast fouling using GPR*. 2014, 5.
- [100] BENEDETTO, Andrea, Fabio TOSTI, Luca BIANCHINI CIAMPOLI, Alessandro CALVI, Maria Giulia BRANCADORO and Amir M. ALANI. *Railway ballast condition assessment using ground-penetrating radar – An experimental, numerical simulation and modelling development*. Construction and Building Materials [online]. 2017, 140, 508–520. ISSN 09500618. Dostupné z: doi:10.1016/j.conbuildmat.2017.02.110
- [101] DE CHIARA, Francesca, Simona FONTUL and Eduardo FORTUNATO. *GPR Laboratory Tests For Railways Materials Dielectric Properties Assessment*. Remote Sensing [online]. 2014, 6(10), 9712–9728. ISSN 2072-4292. Dostupné z: doi:10.3390/rs6109712
- [102] AL-QADI, Imad L., Wei XIE a Roger ROBERTS. *Scattering analysis of ground-penetrating radar data to quantify railroad ballast contamination*. NDT & E International [online]. 2008, 41(6), 441–447. ISSN 09638695. Dostupné z: doi:10.1016/j.ndteint.2008.03.004
- [103] ROBERTS, Roger, I. L. AL-QADI, Erol TUTUMLUER a Andreas KATHAGE. *Ballast fouling assessment using 2 GHz horn antennas-GPR and ground truth*

- comparison from 238 km of track. In: 9th International Railway Engineering Conference [online]. 2007 [vid. 2015-10-26]. Dostupné z: http://alphageofisica.com.br/gssi/gpr_2008/RailEng%202007_br.pdf*
- [104] FAGHIHI KASHANI, Hamed. *Evaluating the Influence of Breakdown Fouling and Moisture Content on Mechanical and Electromagnetic Properties of Ballasted Railroad Track*. 2017.
- [105] SUITS, L. D., T. C. SHEAHAN, Li-Jun SU, Cholachat RUJIKIATKAMJORN a Buddhima INDRARATNA. *An Evaluation of Fouled Ballast in a Laboratory Model Track Using Ground Penetrating Radar*. *Geotechnical Testing Journal* [online]. 2010, 33(5), 103045. ISSN 01496115. Dostupné z: doi:10.1520/GTJ103045
- [106] AL-QADI, Imad L., Wei XIE a Roger ROBERTS. *Time-Frequency Approach for Ground Penetrating Radar Data Analysis to Assess Railroad Ballast Condition*. *Research in Nondestructive Evaluation* [online]. 2008, 19(4), 219–237. ISSN 0934-9847, 1432-2110. Dostupné z: doi:10.1080/09349840802015107
- [107] ROBERTS, Roger, Imad AL-QADI and Erol TUTUMLUER. *Track Substructure Characterization Using 500 MHz and 2 GHz Ground Penetrating Radar: Results from over 250 Miles of Track in Wyoming and Alaska*. *Urbana*. nedatováno, 51, 61801.
- [108] KASHANI, Hamed Faghihi, Carlton L. HO, Charles P. ODEN a Stanley S. SMITH. *Model Track Studies by Ground Penetrating Radar (GPR) on Ballast with Different Fouling and Geotechnical Properties*. In: [online]. B.m.: ASME, 2015, s. V001T01A006 [vid. 2017-12-15]. ISBN 978-0-7918-5645-1. Dostupné z: doi:10.1115/JRC2015-5643
- [109] DE BOLD, R., G. O'CONNOR, J.P. MORRISSEY a M.C. FORDE. *Benchmarking large scale GPR experiments on railway ballast*. *Construction and Building Materials* [online]. 2015, 92, 31–42. ISSN 09500618. Dostupné z: doi:10.1016/j.conbuildmat.2014.09.036
- [110] SUSSMANN, Theodore R., Kenneth R. MASER, Doria KUTRUBES, Francois HEYNS and Ernest T. SELIG. *Development of Ground Penetrating Radar for Railway Infrastructure Condition Detection*. In: [online]. B.m.: Environment and Engineering Geophysical Society, 2001, s. RBA4–RBA4 [vid. 2016-06-10]. Dostupné z: doi:10.4133/1.2922936
- [111] DE CHIARA, Francesca, Simona FONTUL and Eduardo FORTUNATO. *GPR Laboratory Tests For Railways Materials Dielectric Properties Assessment*. *Remote Sensing* [online]. 2014, 6(10), 9712–9728. ISSN 2072-4292. Dostupné z: doi:10.3390/rs6109712
- [112] SUITS, L. D., T. C. SHEAHAN, Li-Jun SU, Cholachat RUJIKIATKAMJORN a Buddhima INDRARATNA. *An Evaluation of Fouled Ballast in a Laboratory Model Track Using Ground Penetrating Radar*. *Geotechnical Testing Journal* [online]. 2010, 33(5), 103045. ISSN 01496115. Dostupné z: doi:10.1520/GTJ103045
- [113] KEOGH, T, D E MESHER a T R KEEGAN. *An Integrated System for Accurate Tie and Ballast Condition Assessment*. nedatováno, 31.

- [114] JACK, R. a P. JACKSON. *Imaging attributes of railway track formation and ballast using ground probing radar*. NDT & E International. 1999, 32(8), 457–462.
- [115] TOSTI, Fabio, Luca BIANCHINI CIAMPOLI, Alessandro CALVI, Amir M. ALANI and Andrea BENEDETTO. *An investigation into the railway ballast dielectric properties using different GPR antennas and frequency systems*. NDT & E International [online]. 2018, 93, 131–140. ISSN 09638695. Dostupné z: doi:10.1016/j.ndteint.2017.10.003
- [116] LI, Dingqing, David READ, Hugh THOMPSON, Ted SUSSMANN a Russell MCDANIEL. *Evaluation of Ground Penetrating Radar Technologies for Assessing Track Substructure Conditions*. nedatováno, 17.
- [117] GÖBEL, C., R. HELLMANN a H. PETZOLD. *Georadar-model and in-situ investigations for inspection of railway tracks*. In: Fifth International Conference on Ground Penetrating Radar [online]. 1994 [vid. 2015-09-21]. Dostupné z: <http://www.earthdoc.org/publication/publicationdetails/?publication=61000>
- [118] JACK, R. a P. JACKSON. *Imaging attributes of railway track formation and ballast using ground probing radar*. NDT & E International. 1999, 32(8), 457–462.
- [119] KUREL, Robin, *Analýza metod pro určení rychlosti signálu GPR*, Bachelor Thesis, University of Pardubice, 2018
- [120] LALAGÜE, Anne. *Use of Ground Penetrating Radar for Transportation Infrastructure Maintenance*, Doctoral Thesis, Norwegian University of Science and Technology, Trondheim, June 2015
- [121] Sussman, T.R. *Application of ground penetrating radar to railway track substructure maintenance management*, Doctoral Thesis, University of Massachusetts, Amherst, 1999
- [122] LENG, Zhen and Imad AL-QADI. *Railroad Ballast Evaluation Using Ground-Penetrating Radar: Laboratory Investigation and Field Validation*. Transportation Research Record: Journal of the Transportation Research Board [online]. 2010, 2159, 110–117. ISSN 0361-1981. Dostupné z: doi:10.3141/2159-14
- [123] SUSSMANN, Theodore R., Katherine R. O’HARA and Ernest T. SELIG. *Development of material properties for railway application of ground-penetrating radar*. In: Steven KOPPENJAN a Hua LEE, ed. Ninth International Conference on Ground Penetrating Radar (GPR2002) [online]. 2002, s. 42–47 [vid. 2018-12-12]. Dostupné z: doi:10.1117/12.462259
- [124] ARTAGAN, Salih Serkan, BORECKÝ Vladislav, BARTOŠ Jaromír and KUREL Robin. *Moisture influence on the gpr-measured rdp values of granite ballast under clean and fouled conditions*. 2018, 9.
- [125] ROBERTS, Roger, Imad AL-QADI, Erol TUTUMLUER and Andreas KATHAGE. *Ballast Fouling Assessment Using 2 Ghz Horn Antennas – GPR and Ground Truth Comparison from 238 km of Track*. nedatováno, 17.

- [126] ROBERTS, Roger, John RUDY, Imad AL-QADI, Erol TUTUMLUER a Jeff BOYLE. *Railroad Ballast Fouling Detection Using Ground Penetrating Radar – A New Approach Based on Scattering from Voids*. nedatováno, 9.
- [127] AL-QADI, Imad L., Wei XIE a Roger ROBERTS. *Time-Frequency Approach for Ground Penetrating Radar Data Analysis to Assess Railroad Ballast Condition*. *Research in Nondestructive Evaluation* [online]. 2008, 19(4), 219–237. ISSN 0934-9847, 1432-2110. Dostupné z: doi:10.1080/09349840802015107
- [128] ROBERTS, Roger, John RUDY, I. AL-QADI, E. TUTUMLUER a J. BOYLE. *Railroad ballast fouling detection using ground penetrating radar—a new approach based on scattering from voids*. In: *Ninth European Conference on NDT* [online]. B.m.: Citeseer, 2006 [vid. 2016-07-06]. Dostupné z: <http://citeseerx.ist.psu.edu/viewdoc/download?doi=10.1.1.159.4471&rep=rep1&type=pdf>
- [129] SHANGGUAN, Pengcheng, Imad L. AL-QADI a Zhen LENG. *Ground-Penetrating Radar Data to Develop Wavelet Technique for Quantifying Railroad Ballast–Fouling Conditions*. *Transportation Research Record: Journal of the Transportation Research Board* [online]. 2012, 2289(1), 95–102. ISSN 0361-1981, 2169-4052. Dostupné z: doi:10.3141/2289-13
- [130] SHIHAB, S., O. ZAHRAN a W. AL-NUAIMY. *Time-frequency characteristics of ground penetrating radar reflections from railway ballast and plant*. In: [online]. B.m.: IEEE, 2002, s. 8 [vid. 2015-10-20]. ISBN 978-0-7803-7618-2. Dostupné z: doi:10.1109/HFPSC.2002.1088424
- [131] INGEGNERIA DEI SISTEMI S.p.A. manual K2, Rev. 1.2, N°doc: MN/2008/031, March 2011
- [132] SANDMEIER, K J a Zipser STRAßE. REFLEXW -program for the processing of seismic, acoustic or electromagnetic reflection, refraction and transmission data. nedatováno, 574.
- [133] NEAL, Adrian. *Ground-penetrating radar and its use in sedimentology: principles, problems and progress*. *Earth-science reviews* [online]. 2004, 66(3–4), 261–330. ISSN 0012-8252. Dostupné z: doi:10.1016/j.earscirev.2004.01.004
- [134] LEUCCI, Giovanni. *Ground Penetrating Radar: A Useful Tool for Shallow Subsurface Stratigraphy Characterization* [online]. nedatováno [vid. 2014-04-14]. Dostupné z: <http://cdn.intechopen.com/pdfs/36318.pdf>

Annex

1. Photodocumentation (DVD)
 - a. Railway Track
 - b. GPR Survey
 - c. Laboratory experiments
2. Work schedule reconstruction Čáslav – Kutná Hora rail number 1 (DVD)
3. K2 Calibration File printout

```
[CONFIGURATION]
DESCRIZIONE=___Caslav_Kutna_Hora
ARRAY_INFO=___Caslav_Kutna_Hora
N_CHANNEL=4
ARRAY_N_TX=3
ARRAY_N_RX=3
TX_SEQUENCE=1 2 3 0
RX_SEQUENCE=1 2 3 0
ARRAY_TX_FREQ=900 400 2000
ARRAY_RX_FREQ=900 400 2000
ARRAY_RX_X0=0 0 0
ARRAY_RX_Y0=-1.415 -1.545 -0.205
ARRAY_RX_ALPHA=0 0 0
ARRAY_TX_X0=0 0 0
ARRAY_TX_Y0=-1.485 -1.355 -0.435
ARRAY_TX_ALPHA=0 0 0
SweepTime= 0.00000006 0.00000006 0.00000002 0.00000002
Sample= 1024 1024 1024 1024
Wheel_Compress= 25 25 25 25
Wheel_dx=0.000744
Wheel=2
Max_sampling_RF_MAX=400
Max_sampling_AD=400000.00
SOS_high=100
Fase_DDS_TX=0
Fase_DDS_RX=0
Model=4
RemoteType=5
Interleaving=1
UD=2
UD_Channel=1
RemoteEnabled=0
```

Annex I- K2 Calibration File

4. Grading curves

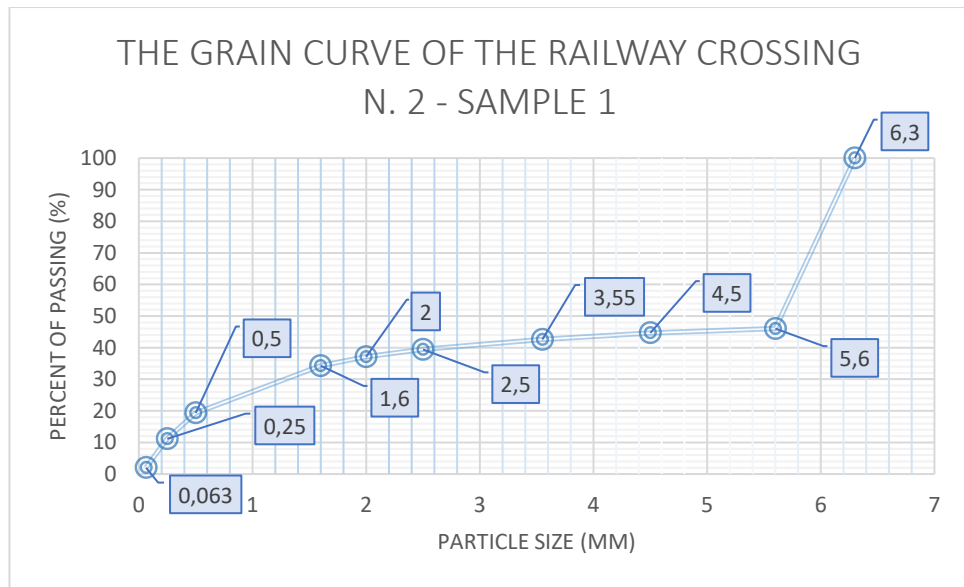


Figure 55 - The grain curve of the railway crossing n. 2 - sample 1

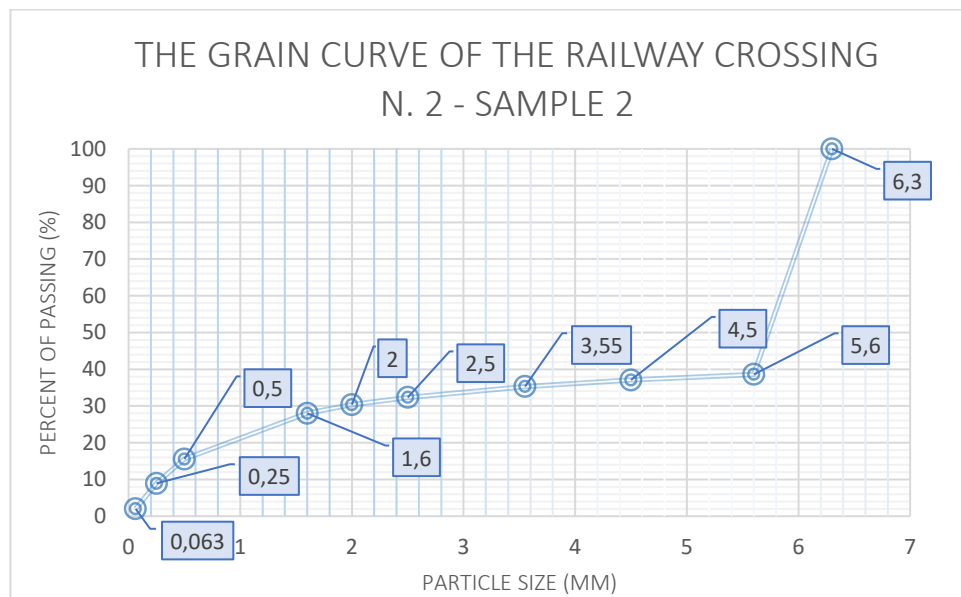


Figure 56 - The grain curve of the railway crossing n. 2 - sample 2

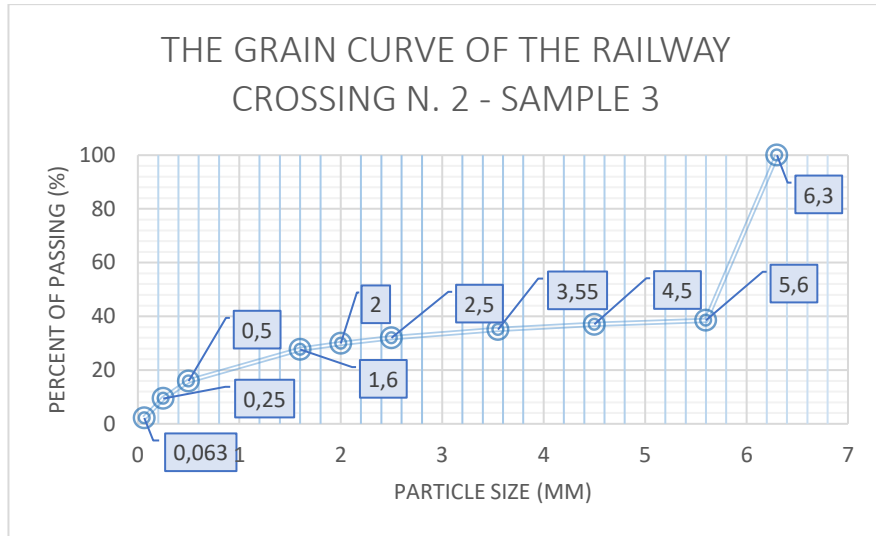


Figure 57 - The grain curve of the railway crossing n. 2 - sample 3

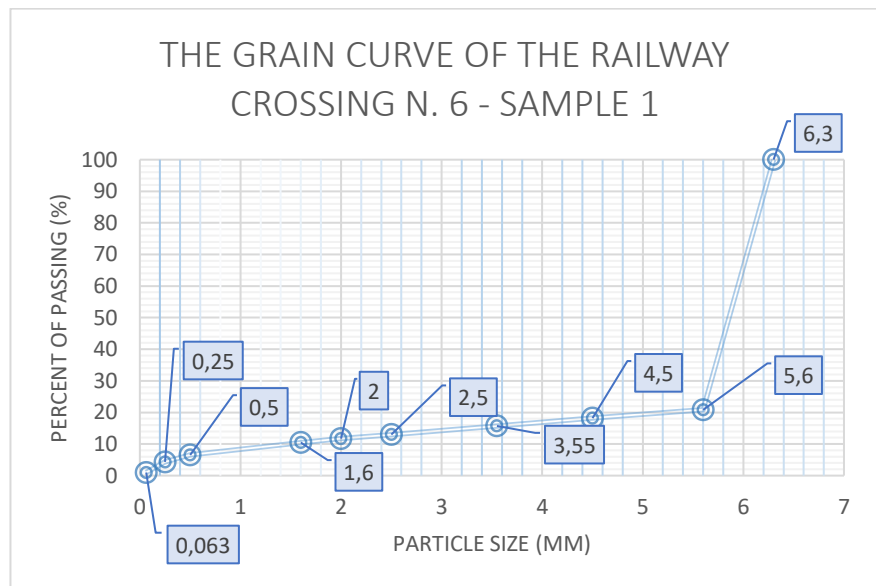


Figure 58 - The grain curve of the railway crossing n. 6 - sample 1

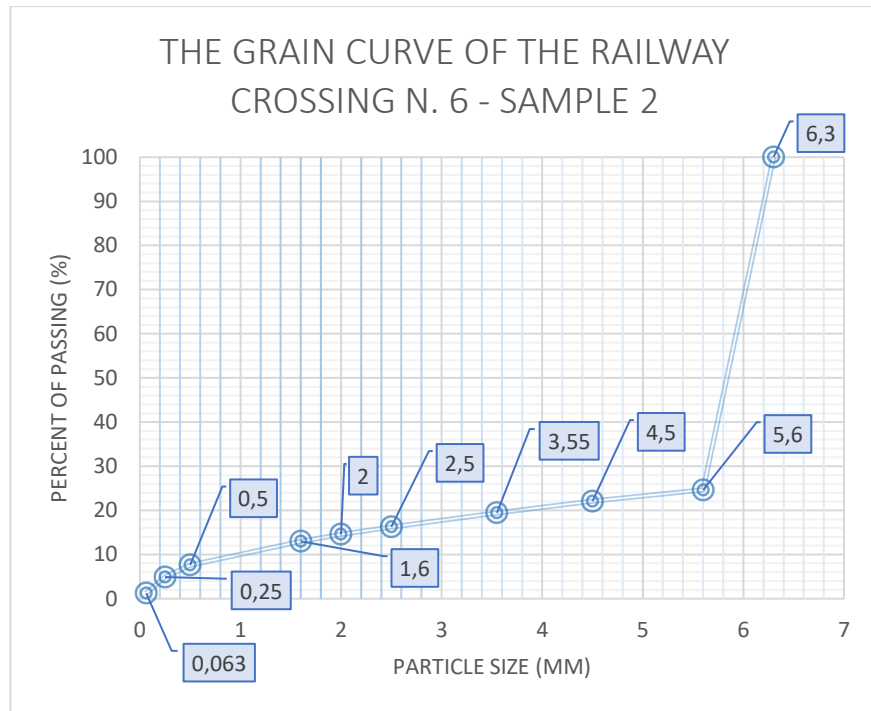


Figure 59 - The grain curve of the railway crossing n. 6 - sample 2

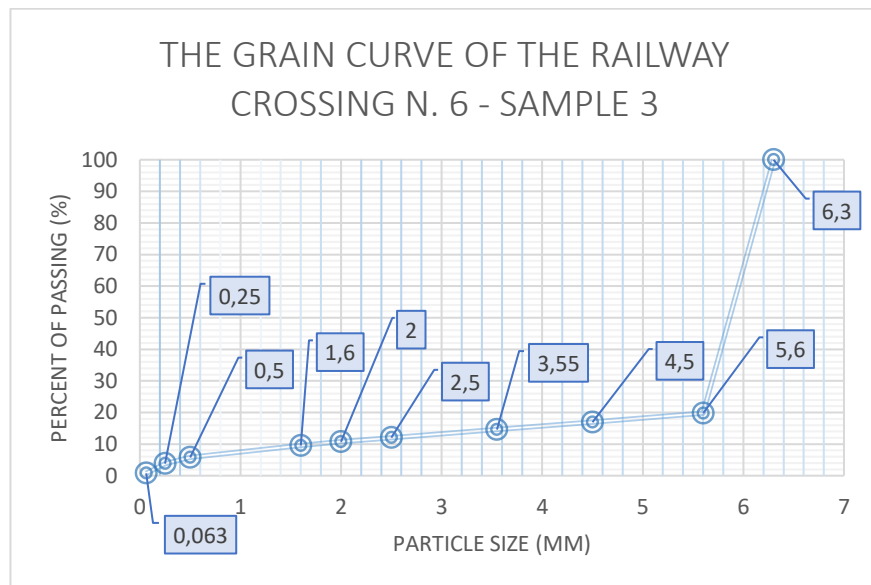


Figure 60 - The grain curve of the railway crossing n. 6 - sample 3

5. Surveyed GPR data (DVD) – excluding SŽDC data